Potential-Driven Surface Stress of a Cantilever-Based Sensor

Thesis by

Ann-Lauriene Haag

Department of Physics

McGill University, Canada

July 2016

Thesis submitted to McGill University in

partial fulfillment of the requirements of the degree of

Doctor of Philosophy

Dedicated to my mom

Ulrike Maria Haag

*30 May 1958 - † 24 October 2014

Acknowledgments

First and foremost, I would like to thank my supervisor Peter Grutter for his support and guidance throughout my PhD. During my Masters in 2009, he invited me to his lab for a 4-month project. His continuous support has lead to many great opportunities during my career for which I am very grateful.

I would like to give a very big thank you to the whole Grutter research group and former members for their valuable input during many discussion, as well as for being my close friends. Thanks Antoine for translating my abstract into french. A special thanks goes to Yoichi Miyahara for technical support, Yoshihiko Nagai for valuable feedback for all DNA-related experiments and Robert Gagnon for teaching me how to use the gold evaporator and the XPS.

To all my friends at McGill who made my time here amazing. I hope we will keep a long-standing friendship and will venture on many more hiking trips together.

I gratefully acknowledge funding resources for financial support. During my PhD I was funded by NSERC through the CREATE-Integrated Sensor System Fellowship program for two years. Afterwards, the Swiss National Science Foundation awarded me a Doc.Mobility Fellowship.

Lastly, I would like thank my mom who always reminded me that I can achieve everything. Many thanks to my brother, Tobias, who teaches me the valuable lesson of how to get things done one step at a time, his wife Lisa and their son Hieronymus who keeps me cheered up. My grandmother, Ilse Holland who is always there for me. And most of all my encouraging, supportive and loving husband, Zeno Schumacher who has been a major part in guiding me through my PhD and life. Thank you!

Ann-Lauriene Haag

McGill University

April 2016

Statement of Originality

The author, Ann-Lauriene Haag, claims the following elements of this thesis to be considered original scholarship and distinct contribution to knowledge:

- Characterization of different cleaning protocols for the intrinsic cleaning of a gold-coated electrode. X-Ray photoelectron spectroscopy (X-Ray) and cyclic voltommagrams are recorded to verify the effectiveness of the cleaning protocols. [Published: Haag, A.-L. et. al. *EPJ. Techn. Instrum.*, **2**, 1, 1-12, 2015]

- Long-term surface stress measurements to investigate the shelf-life properties of cantilever-based sensors. It is found that the surface stress deviates in the time frame of hours. This finding is essential for the development of real-life sensors. [Published: Haag, A.-L. et. al. *EPJ. Techn. Instrum.*, **2**, 1, 1-12, 2015]

- Development of a selective *in situ* modification protocol for biosensing applications. The surface of a gold electrode is held under potential control to enhance adsorption, inhibit adsorption and hold the surface at a given state. For the first time, a selective modification protocol for submonolayer coverages is presented. [Manuscript submitted: Haag, A.-L. et. al. *IOP Nanotechnology*, 2016]

- Quantitative measurement of the difference in surface stress change and current density for weak (perchlorate) and strong (chloride) adsorbing ions on a gold-coated cantilever. [Manuscript in Preparation: Haag, A.-L. et. al. 2016]

- In-depth analysis of the evolution of the surface stress - charge coefficient of a gold-coated cantilever. We have found that the sensitivity is larger for shorter applied potential pulses when the Debye length is shorter. Additionally, large absolute surface stress changes are measured for higher ion concentrations. [Manuscript in Preparation: Haag, A.-L. et. al. 2016]

Contribution of co-Authors

This thesis is a manuscript-based composition. One paper is published [1] and two papers are in preparation.

Chapter 3 is based on the following published manuscript:

Characterization of a gold coated cantilever surface for biosensing applications

Haag, A.-L., Nagai, Y., Lennox, R. B., Grutter, P.

EPJ. Techn. Instrum, **2**, 1, 1-12

I performed all the experiments and data analysis. Y. Nagai prepared the oligonucleotide samples. R.B. Lennox and P. Grutter assisted in writing the manuscript. P. Grutter supervised the project

Chapter 4 is based on the following manuscript:

Selective *in-situ* potential-assisted SAM formation on multi electrode arrays

Haag, A.-L., Toader, V., Lennox, R. B., Grutter, P.

submitted to *IOP Nanotechnology*

I performed all the experiments and data analysis. V. Toader prepared the ferrocene alkanehtiol samples. R.B. Lennox and P. Grutter assisted in writing the manuscript. P. Grutter supervised the project.

Chapter 5 is based on the following manuscript:

Sensitivity measurements of cantilever-based surface stress sensors

Haag, A.-L., Schumacher, Z. , Grutter, P.

to be submitted.

I performed all the experiments and data analysis. Z. Schumacher helped designing the experiment. All authors assisted in writing the manuscript. P. Grutter supervised the project.

Abstract

Biochemical sensors have a wide range of applications in medical diagnosis, drug discovery and even food quality monitoring. It is crucial to be able to detect very small concentrations of molecules in a sample with a high selectivity. Here, a cantilever-based sensor to measure changes in the surface stress due to binding or adsorption of molecules is used. This gold-coated cantilever acts as a working electrode and is electrically connected through a potentiostat to a counter and reference electrode in solution. This electrochemical set-up allows the performance of potential-driven measurements. The binding of oligonucleotides to the surface is measured through changes in the surface stress signal.

Next, an electrochemical technique to functionalize an array of cantilevers reliably with different probes *in-situ* is presented. This is achieved by controlling the applied potential of the individual electrodes and distinguishing between three key potentials. The first potential promotes the chemisorption of an alkanethiol to the gold surface. The second keeps the electrode in a reductive desorption state and inhibits alkanethiol adsorption. Lastly, a holding potential keeps an already formed modification in a stable state to prevent cross-contamination. To demonstrate this concept, two different electrochemically-addressable ferrocenyl alkanethiols are chemisorbed onto independent but adjacent gold electrodes under potential control.

Finally, to understand the sensitivity of these cantilever systems, the correlation between surface stress change and charge density is investigated. A linear correlation is found and by applying fast potential pulses of up to 0.1ms, the evolution of this correlation is probed. Higher sensitivities are measured for shorter applied pulses. These short pulses probe only the first few layer of the double layer. Additionally, a local increase in ion concentration is observed which also leads to higher sensitivities. This technique could enable the label-free detection of charges along a molecule in proximity of the electrode.

Résumé

Les capteurs biochimiques ont un large éventail d'applications dans le domaine du diagnostic médical, du développement de médicament et même du contrôle de qualité des aliments. Il est important d'être capable de détecter de très petites concentrations de molécules dans un échantillon avec une grande sélectivité. Dans cette thèse, un cantilever de microscope à force atomique est utilisé comme capteur biochimique en mesurant un changement de sa tension de surface dû à la liaison ou l'adsorption de molécules. Ce cantilever recouvert d'une mince couche d'or agit comme une électrode de travail en étant connectée à une électrode de référence et une électrode auxiliaire par l'entremise d'un potentiostat. Ce montage électrochimique permet d'effectuer des mesures sous l'effet d'un potentiel. La liaison d'oligonucléotides à la surface est mesurée par un changement dans le signal de tension de surface.

Ensuite, une technique électrochimique pour changer la fonctionnalité d'un ensemble de cantilevers avec différentes sondes in-situ est présentée. Cela est réalisé en contrôlant le potentiel appliqué à chacune des électrodes et en distinguant trois valeurs de potentiel clés. Le premier potentiel promeut la chimisorption d'alcanethiol sur la surface d'or. Le deuxième maintient l'électrode dans une réaction d'oxydoréduction de désorption qui de surcroît empêche l'adsorption additionnelle d'alcanethiol. Finalement, un potentiel de maintien garde un cantilever déjà modifié dans un état stable en le protégeant de la contamination croisée. Pour démonter la viabilité de cette idée, deux ferrocenyl alcanethiols adressables électrochimiquement sont chimisorbés sur des électrodes d'or distinctes mais adjacentes.

Finalement, pour comprendre l'origine de la sensibilité de ces capteurs biochimiques basés sur le cantilever, la corrélation entre le changement de tension de surface et la densité de charge est étudiée. Une corrélation linéaire est mesurée et en appliquant des impulsions rapides de potentiel allant jusqu'à 0.1ms, l'évolution de cette corrélation est explorée. Une

plus grande sensibilité est mesurée pour des impulsions de plus courte durée. Ces courtes impulsions ne sondent seulement que quelque unes des premières couches de la double-couche électrique. De plus, une augmentation locale de la concentration d'ion est observée. Cela contribue également à augmenter la sensibilité. Cette technique pourrait permettre la détection de charge le long d'une molécule à proximité de l'électrode sans nécessiter d'étiquette.

Contents

1

Introduction

Developing new generations of sensors for a diverse spectrum of samples is a demanding research area. Several sensors have been in use for more than a decade, especially in the field of biology, like the lateral flow pregnancy test and sensors to measure the glucose level in diabetics [2, 3]. However, the demand for a new generation of biosensors that can analyze samples fast, without the need of pre-treatment and can deliver testing for multiple analytes at once is high [4–6]. It is crucial to deliver fast and reliable results while reducing processing time and costs. Biosensors need to detect very small concentrations of molecules in a small volume of sample, therefore a high selectivity is crucial to detect only the specific target [7]. Developing those sensors requires not only a decreasing sensor size to be able to reach ever smaller detection limits, but also to make these sensors more selective to limit analyte 'cross-talking' [8, 9].

In recent years, several nano and micromechanical structures have been described as possible biosensor platforms [10–14]. These include nanomechanical cantilevers [15–19], resonators [20, 21], and optomechanical structures [22, 23]. The most common detection principles in these mechanical sensors due to biological binding effects are changes in surface stress [24–28] and mass [29–32].

In this thesis, the focus is on cantilever-based sensors typically made of silicon. The most common use of cantilevers is in Atomic Force Microscopy (AFM), where they are used to transduce a force to a measurable deflection [33]. Here, a tip less cantilever is used as a sensor. Three main operational sensing modes are used: dynamic, bimetallic and static mode (figure 1.1) [17, 19, 34, 35]. In the dynamic mode, the cantilever is driven at the resonance frequency f_0 and a change in the frequency due to mass (e.g. binding of molecules) is measured. In the bimetallic mode, one side of the cantilever is coated with a metal (e.g. gold). The system acts as a bimetall and is sensitive to temperature change. Exothermic reactions happening on the surface result in an increase of the temperature and therefore a deflection of the cantilever. This can for example be used for the detection of explosives [36]. In the last mode, the static mode, a metal-coated cantilever is sensitive to changes in the surface stress upon binding of molecules. This results in a measurable change in deflection. A variation of this static mode is used in this thesis.

Most experiments using the static mode require the use of a reference cantilever to eliminate any parasitic effect such as temperature changes, concentration changes, unwanted binding of molecules, etc. In these measurements, at least two cantilevers are needed, one acting as a chemically inactive reference and the other one as the sensor. Once the measurement is performed, the signal coming from the reference cantilever is subtracted from the sensing cantilever, thus rejecting all common noise. Cantilever biosensors have been used for the detection of a vast variety of biological targets such as DNA [1, 37, 37–45], antigens [46], proteins [47, 48], bacteria [49–51] and viruses [52].

In this thesis, a potential-driven surface stress measurement is used. A three-electrode electrochemical system, with the cantilever connected as the working electrode, is used to

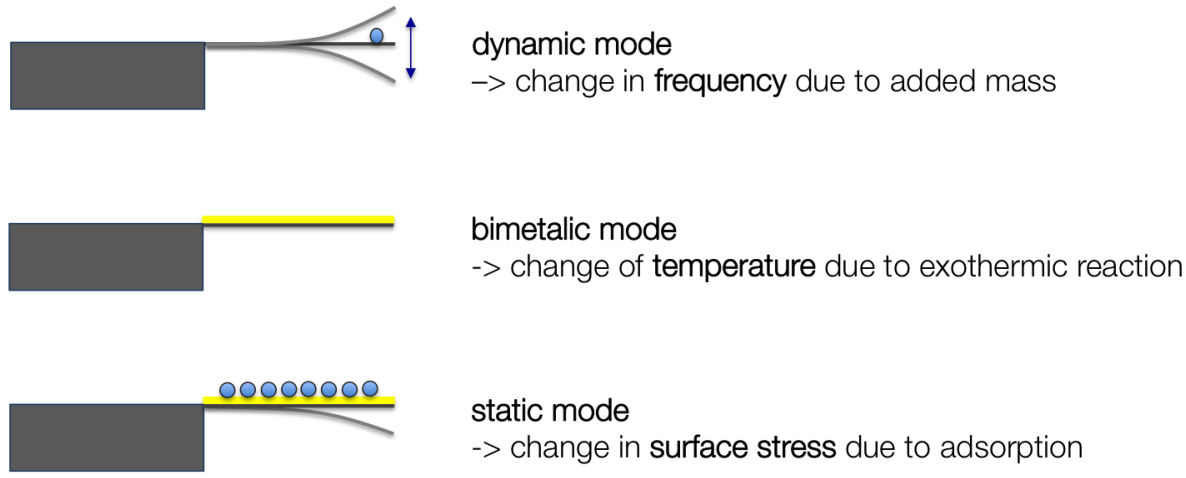

Figure 1.1: Different modes of operation for cantilever-based sensing techniques. The dynamic mode measures a frequency change upon a change of mass. For the bimetallic mode, a metal (e.g. gold) is coated on one side of the cantilever. Changes in temperature due to exothermic reactions can then be measured by the deflection of the cantilever. In the static mode, changes in the surface stress are measured due to adsorption of ions.

apply potentials to the surface of the cantilever. By applying a potential to the electrode, specific ions will be directed to the surface and cause a measurable change in the surface stress. This will not only eliminate the need of a reference cantilever as absolute surface stress changes upon a potential step are measured. It will also actively drive analytes and ions to the surface, thus overcoming diffusion limits and reducing measurement times. This leads to a drastic increase in surface stress signal [1, 25, 42] over conventional surface stress measurements. In addition, the electrochemical liquid cell setup can clean the sensor *in situ* so that well-defined conditions are applicable for all experiments. Cleaning is done by cycling the potential applied to the gold electrode between -0.8V and 1.4V, vs. Ag/AgCl (sat. KCl) until a reproducible cyclic voltamogram is achieved. This technique will reduce and oxidize the gold surface and therefore remove any contaminants residing on the surface.

In general, a clean gold electrode shows a redistribution of the electronic charge on the surface because the bond charge is missing a neighbor and therefore it is expected to redistribute into the space between the atoms, see figure 1.2. This bond-charge model was introduced by Ibach [53, 54]. An increase in the attractive interaction between the neighbor atoms at the surface will lead to a tensile surface stress. By notation, a tensile stress results in an upward bending of the metal, this is indicated by positive surface stress values. Compressive surface stress has a negative sign and will result in a downward bending of the cantilever.

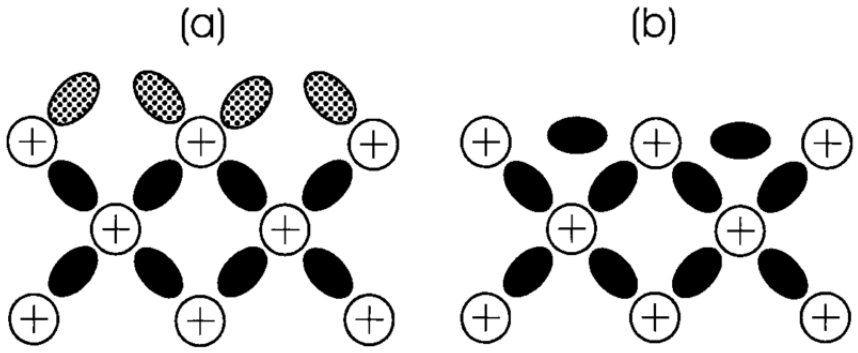

Figure 1.2: Redistribution of the charge density of a clean metal surface due to the missing neighbor at the surface. In (a), the charge distribution for a surface is shown and in (b), the charge distribution into the space of the atoms is demonstrated (adapted from [55]

By applying a potential, e.g. a positive step to the gold-coated cantilever surface in a solution of sodium chloride (NaCl), the negatively charged chloride ions are directed onto the surface. The chloride ions will modify the electronic charge distribution of the gold surface and this results in a large compressive surface stress [25]. The surface stress amplitude generated by the adsorption of ions is proportional to the available gold area. The more ions adsorb onto the surface, the larger the measured surface stress change [1]. Having an

alkanethiol (e.g. a C_6 chain with a thiol (S-H) linker) attached to the gold surface will lead to additional contributions to the surface stress due to the electronic repulsion of the Au^+S^- dipole.

Even though cantilever-based sensors were first described over 20 years ago, there is no viable commercial product on the market yet. However, a lot of fascinating science has come out of cantilever-based sensors, as mentioned above. Several reasons can be found for this. The lack of a detailed understanding of the origin of signals being, in my point-of-view, the most critical one. Especially in medical diagnostics, the false positive rate needs to be as low as possible. If the origin of the sensors signal is not fully understood, such false positive rates can not be ruled out. Most scientific work as been focused on proof of concept rather than large scale integration. Moreover, application-relevant issues such as shelf life and robust protocols distinguishing targets from false responses have received very little attention. This thesis aims to address some of these fundamental issues.

1.1 Outline of Thesis

In the following an outline of this thesis is presented. Note that chapter 3 - 5 are based on published and to be submitted manuscripts.

In chapter 2, the experimental methods used throughout this thesis will be described. The surface stress measurement setup as well as the electrochemical setup are explained and what information we can get from these methods. A theoretical introduction into the origin of surface stress as well as the electrochemical methods are shown. Additionally, characteristic surface stress changes of modified gold surfaces are presented.

Chapter 3 is based on a peer-reviewed published manuscript [1]. The paper characterizes our cantilever gold surface for biosensing applications. A potential step between ±0.2V is applied to the gold-coated cantilever surface in solution. This potential step will induce a surface stress change of the cantilever due to chloride ions adsorbing onto the surface. Additionally, the oligonucleotide that is modified onto the surface will contribute to the surface stress change by the repulsive forces between the negatively charged backbone of the oligonucleotide. At negative potentials, the oligonucleotide repels from the surface and lies down during positive potentials [56, 57]. This dynamic behavior will lead to a characteristic surface stress change pattern [42]. Since surface stress is proportional to the available gold area it is crucial to have a reliable and clean surface preparation. In this chapter three main challenges are analyzed: 1. How to achieve high surface stress signals by ensuring a reliable cleanliness of the electrode surface. X-ray photoelectron spectroscopy measurements were performed to test the effectiveness of different cleaning protocols and verify the cleanliness of our electrochemical cleaning protocol. 2. Improving the signal-to-noise ratio of oligonucleotide sensing by applying a multi-step functionalization protocol to achieve optimal probe density and 3. Characterization of long-term measurements to discuss sensor shelf life.

Chapter 4 demonstrates a technique to selectively modify two gold-electrodes in proximity with different ferrocene moieties with submonolayer coverage. The chapter is based on a manuscript submitted to *IOP Nanotechnology* in May 2016. One of the interesting issues of any type of sensor is to be able to analyze different probes simultaneously and efficiently. The current protocol to modify a biosensors with different probes include microcontact printing [58, 59], dip-pen nanolithography [60] and modified ink-jet printing[61, 62]. These techniques are all done externally, require additional machines and are not compatible with an integrated, automatized system. A technique to selectively modify electrodes *in-situ* with

two ferrocene moieties, Fc-C_{11}-SH and Fc-CO-C_{11}-SH is presented by controlling the surface potential. Three key potentials are distinguished that enhance adsorption E_{ads}, stabilize a modified layer E_{hold} and cause desorption E_{des}. The main advantage of this functionalization technique is the integrated nature of it. For the first time, the selective modification in the submonolayer regime is achieved using potential-assisted modification. Submonolayer coverages are needed to increase surface stress signals for surface stress based sensors [42, 63, 64].

Chapter 5 is based on a manuscript in preparation. A more detailed analysis of the temporal surface stress evolution for potential-driven adsorption of ions is discussed. This manuscript investigates the relevant time scales for ion adsorption by applying short (as low as 0.1ms) potential pulses to the gold-coated cantilever electrode in solution. By varying the potential pulse width, characteristic time scales for the double layer formation and ion diffusion can be probed. This is demonstrated for weak (perchlorate ClO_4^-) and strong (chloride Cl^-) adsorbing ions. Surface stress changes are simultaneously recorded with the current response using a three-electrode system. A characteristic surface stress - charge density coefficient ξ is determined for a polycrystalline gold-coated cantilever electrode for the two solutions. Enhancement in sensitivity is found for short potential pulses indicating that the cantilever sensor is more sensitive to changes happening in a thin double layer.

Lastly, a conclusion that summarizes the key aspects of this thesis and an outlook shows the potential of the project through different proposed ideas.

2

Methods and Theoretical Background

2.1 Experimental Setup

The experimental apparatus (aside from electrical control) is shown in figure 2.1. Two main parts are found in the setup: 1. Electrochemical cell featuring a three-electrode setup and a fluid cell and 2. A beam deflection measurement system featuring a laser that is aligned onto a gold-coated cantilever surface and a position sensitive photodiode that measures the change in deflection.

To control voltage potentials applied during electrochemical measurements, a potentiostat is connected to the three-electrode system. The position sensitive photodiode is connected to a voltage-to-current amplifier and fed into a National Instruments data acquisition card.

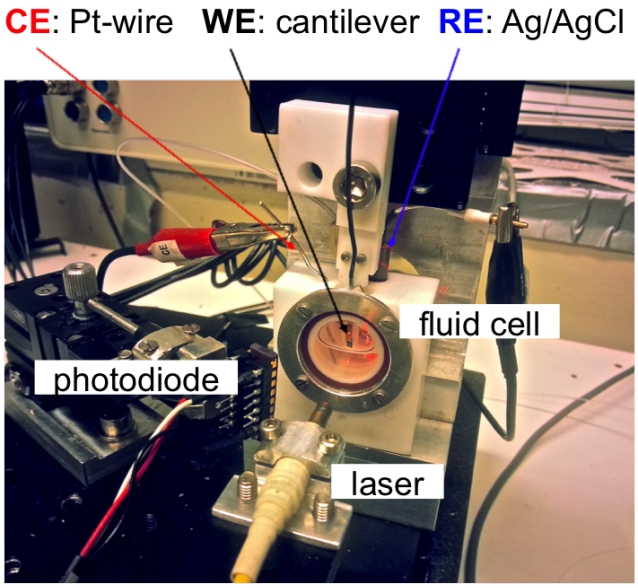

Figure 2.1: Experimental setup showing the two essential parts: electrochemistry and beam deflection. A standard three-electrode system is used to perform electrochemical measurements. A counter, working and reference electrode (CE, WE, RE) are immersed in the liquid cell. To measure the deflection of a cantilever, a laser is directed onto the cantilever and the reflected beam can be monitored with a position sensitive photodiode.

2.1.1 Electrochemical Fluid Cell

A custom-made Teflon fluid cell is used for all electrochemical measurements. Teflon (Polytetrafluoroethylene) is chosen as a material because of its compatibility towards electrochemical solutions. The cell can hold a volume of up to 4 ml and has openings at the top to attach a counter electrode, a reference electrode and a custom-made cantilever Teflon holder. In order to have optical access to the cantilever, a round opening can be found in the front and back. This opening is sealed with an O-ring and a glass window and is screwed together (see figure 2.1).

2.1.2 Beam Deflection System

The experimental apparatus includes a two-laser beam deflection setup. Two cantilevers can be placed inside the fluid cell and are each positioned at an angle of 15 ° (see figure 2.2). Two identical lasers are aligned to the tip of the cantilever and deflected onto a position sensitive photodiode (1L10, On-Track Photonics, Inc., USA). For all measurements described here, a tip-less cantilever (CSC-38 Mikromash, USA) with three levers is used. To reliably align the laser, it is aligned onto the second longest cantilever arm (on the left) and moved off the lever until the reflection vanishes. Next, the laser is moved along the positive x-direction onto the longest lever.

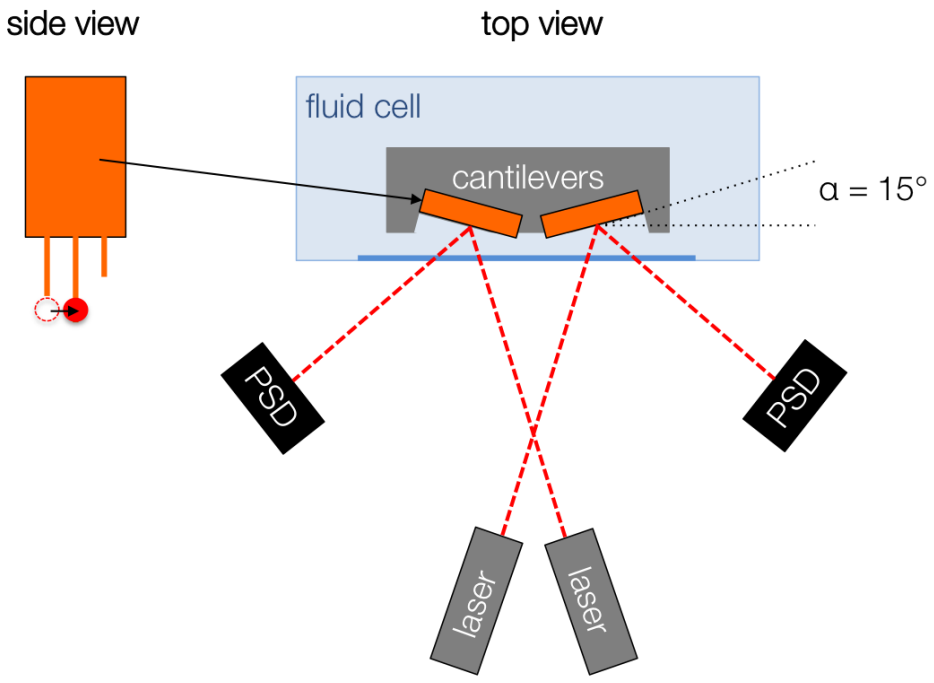

Figure 2.2: Schematics of the beam deflection setup for a two-cantilever system. The optical beam deflection, as well as the liquid cell from the top is shown. The side view of the laser alignment on the cantilever is shown on the left.

The laser is focused to a spot size of approximately 25 µm. As explained above, the alignment of the laser onto the cantilever is done wit the help of the second longest cantilever. This allows for a reproducible alignment of the laser onto the cantilever for each experiment, as shown in figure 2.3.

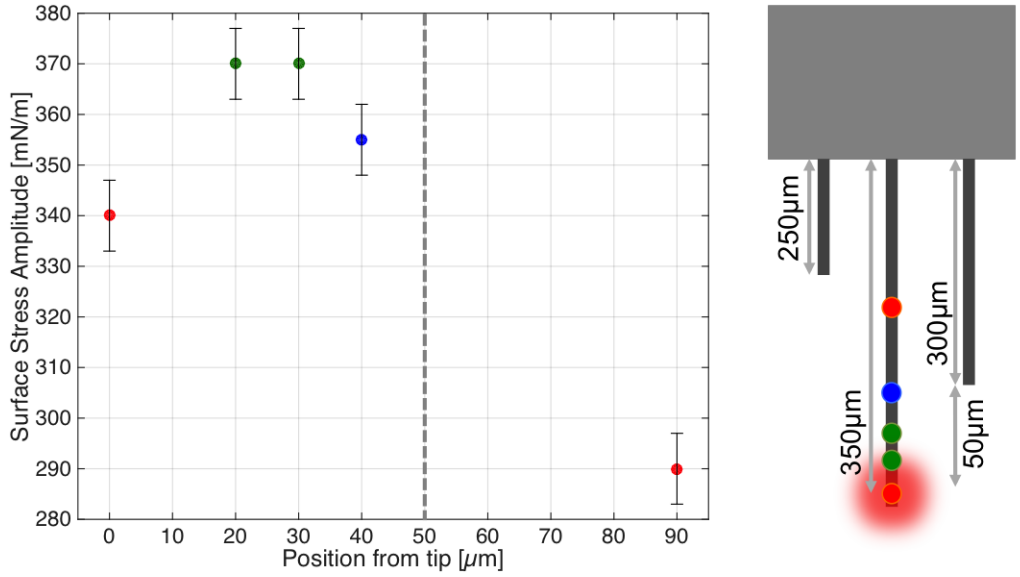

Figure 2.3: Position dependence of the beam spot on the cantilever to the measured surface stress amplitude for a ±0.2 V (vs. Ag/AgCl (sat. KCl)) potential step. Red dots indicate positions that are not optimal and green dots show optimal laser beam positions.

The cantilever holder is mounted on a micro manipulator plate. A series of surface stress amplitude measurements in 0.1 M NaCl for an applied potential step between ±0.2 V (vs. Ag/AgCl (sat. KCl)), are recorded. The position of the laser beam is moved along the longest cantilever. The optimal positions are indicated by the *green* dots. These are the positions that are achieved with the above described technique and result in surface stress amplitudes in the order of 370 mN/m. The *blue* laser position is slightly above the optimal position and a decrease in amplitude to 355 mN/m is measured. The *red* positions are at the

very edge of the cantilever (0 µm) giving a surface stress amplitude of 340 mN/m or if the laser beam is further away from the tip (here 90 µm), the surface stress amplitude decreases to 290 mN/m.

2.1.3 Electrochemical Setup

To perform electrochemical measurements, a three-electrode configuration is utilized. A working electrode (WE), a counter electrode (CE) and a reference electrode (RE) are needed. In the experiments shown in this thesis, a gold-evaporated surface is connected as a working electrode. The counter electrode is made of a Platinum wire and a silver / silver chloride (Ag/AgCl) (sat. KCl) reference electrode is used for the reference.

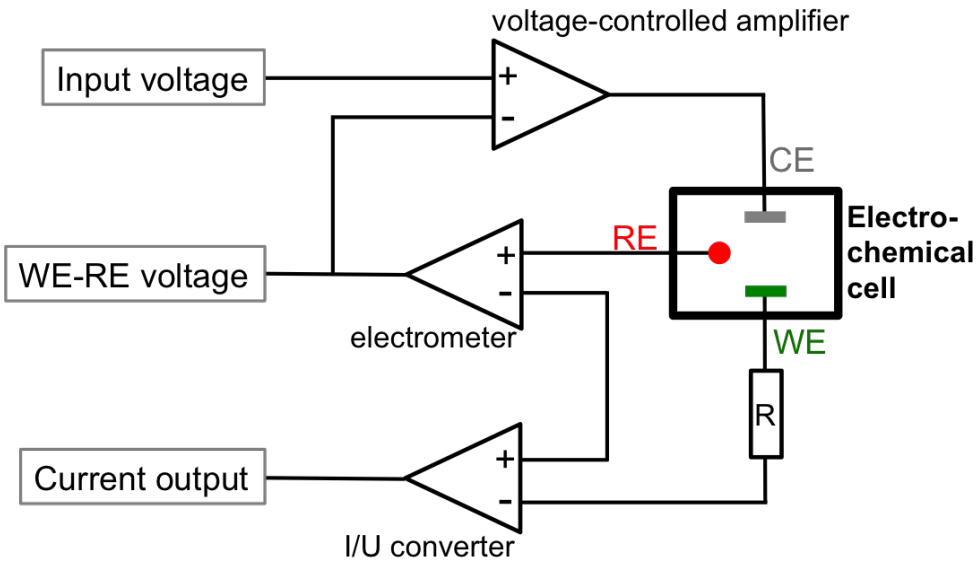

Figure 2.4: Circuit diagram of a potentiostat with a three-electrode setting. The input voltage is applied to the counter electrode (CE). The signal between the CE to the working electrode (WE), is directed to a current-to-voltage converter. No current is flowing through the reference electrode (RE).

These three electrodes are connected via a potentiostat (1030A, CH Instruments, USA) to apply a defined potential to the WE with respect to the RE and to measure the current between the WE and the CE, as shown in figure 2.4. The reference electrode has a fixed internal potential, therefore we note that the potential at the WE is with respect to the RE. Current does not flow through the RE at any point and only the electric charges on the working electrode are observed. If a negative potential is applied, the energy of the electrons is raised and a current can flow from the electrode through the solution to the CE (reduction current). For positive potentials the flow is from the solution to the WE (oxidation current).

All following electrochemical data is shown with respect to the Ag/AgCl (sat. KCl) reference electrode. This electrode exhibits the following internal reaction:

$$AgCl(s) + e^- \rightleftharpoons Ag(s) + Cl^- \tag{2.1}$$

The standard electrode potential for this reference electrode in a saturated KCl solution is $E^0 = 0.197$ V. Potential conversions into other reference electrodes used in the literature, like the standard hydrogen electrode (SHE) and the standard calomel electrode (SCE) are shown in figure 2.5.

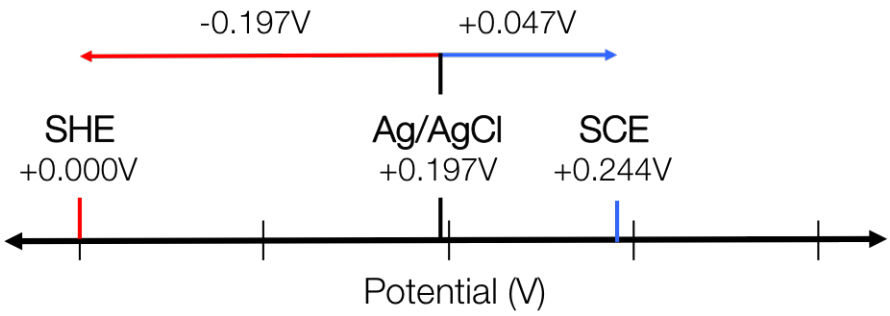

Figure 2.5: Conversion of a the standard potential of a Ag/AgCl (sat. KCl) reference electrode into other commonly used electrodes, i.e. standard hydrogen electrode (SHE) and standard calomel electrode (SCE).

To convert Ag/AgCl (sat. KCl) reference measurements into SHE measurements, one has to subtract the potentials values by -0.197 V. For conversion into SCE, potential values have to be added by +0.047 V [65].

2.2 Electrochemistry

2.2.1 Double Layer

If a metal electrode is in contact with an electrolyte, a solid-liquid interface is established. At this interface, a double layer builds up over time. In the 19^{th} century, Helmholtz [66] was the first one to think about this metal/electrode surface. He proposed a model of two layers carrying opposite charge separated by a distance of molecular order (see figure 2.6 A) [65]. The model can be described as a parallel-plate capacitor with a charge density q and a voltage drop V:

$$q = \frac{\epsilon\epsilon_0}{d}V \tag{2.2}$$

where d is the distance between the two plates, ϵ is the dielectric constant of the medium and ϵ_0 the vacuum permittivity. From here, one can define the differential capacitance C_d of the model.

$$C_d = \frac{\partial q}{\partial V} = \frac{\epsilon\epsilon_0}{d} \tag{2.3}$$

This model was later modified to include a diffusive layer of charge with the largest charge density near the electrode and decreasing charge density over distance away from the electrode, see figure 2.6 B and is referred to as the Gouy-Chapman model [65].

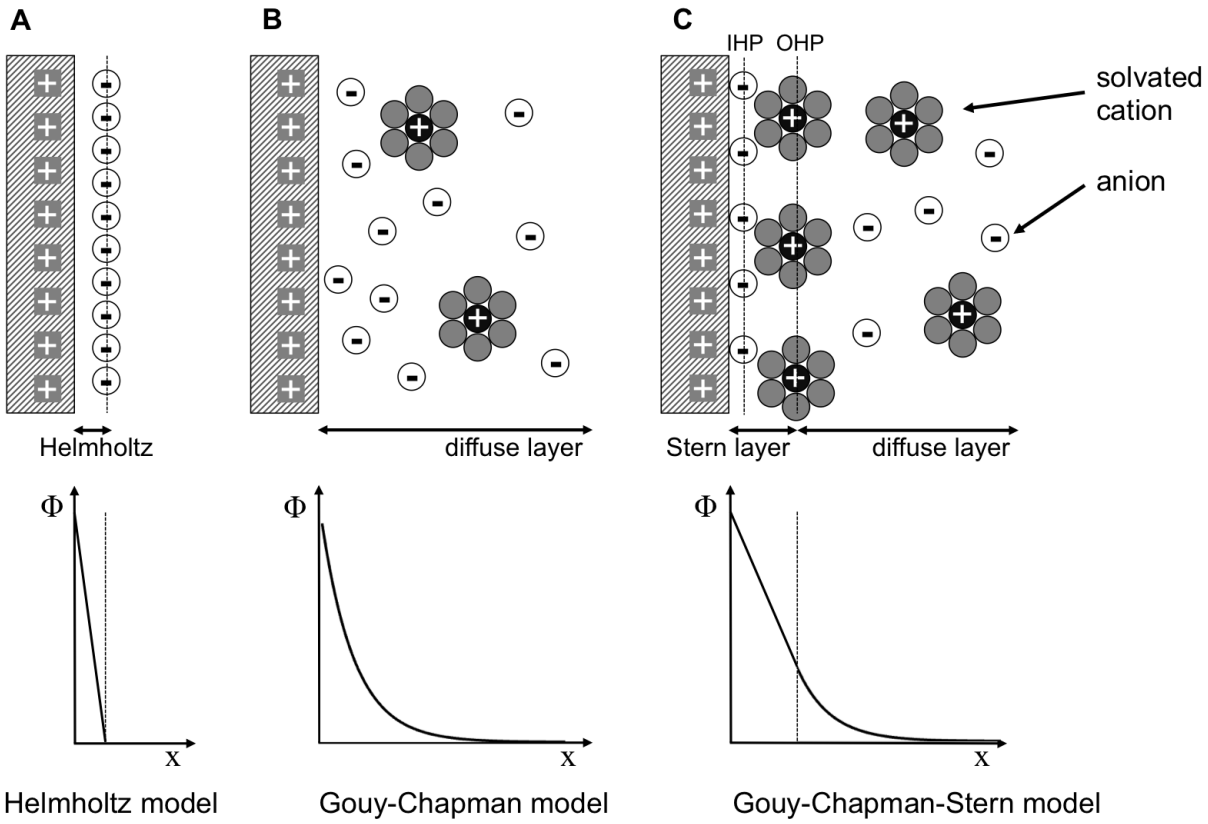

Figure 2.6: Evolution of the concept of the double layer formation. A positively charged electrode is in contact with an electrolyte. The potential vs. distance profile is shown for each model. In **A** the Helmholtz model is shown. In **B**, the diffuse layer is introduced to the Gouy-Chapman model. In **C** both concepts are combined resulting into the Gouy-Chapman-Stern model. In here, the Stern and diffuse layer together built the electrical double layer (EDL). The Inner Helmholtz Plane (IHP) as well as the Outer Helmholtz Plane (OHP) is indicated. Outside of the EDL, the bulk layer is present.

The double layer capacitance should rise for the diffusive double layer. If the electrode is highly charged, a more compact diffusive layer is created and C_d is increased. Assuming a 1:1 electrolyte, $\phi = 0$ far away from the electrode and $(d\phi/dx) = 0$, the Poisson-Boltzmann distribution describes the Gouy-Chapman model:

$$\frac{d^2\phi}{dx^2} = \frac{2k_BT}{\epsilon\epsilon_0}\Sigma\rho_i^o\left[exp\left(\frac{-e\phi}{k_BT} - 1\right)\right] \tag{2.4}$$

where ϕ is the electric potential, k_B the Boltzmann constant, ρ_i^o the inital concentration of ion species i and T the temperature. An analytical solution to equation (2.4) is the Gouy-Chapman solution:

$$\phi = \frac{2k_BT}{e}ln\left[\frac{1+\gamma e^{-\kappa x}}{1-\gamma e^{-\kappa x}}\right] \tag{2.5}$$

with

$$\gamma = tanh\left(\frac{e\phi_0}{4k_BT}\right) \tag{2.6}$$

and

$$\kappa = \sqrt{\frac{2e^2\rho_0}{\epsilon\epsilon_0 k_BT}} \tag{2.7}$$

For the Gouy-Chapman model, the potential profile decays over a distance away from the surface. If the metal potential ϕ_0 is large, a compact diffuse layer is generated and the potential drop is sharp. However, if ϕ_0 is smaller, a gradual decrease in potential is observed. As for the Gouy-Chapman model, a differential capacitance C_d can be defined by:

$$C_d = \frac{d\sigma^M}{d\phi_0} = \sqrt{\frac{2e^2\epsilon\epsilon_0\rho^0}{k_BT}}cosh\left(\frac{e\phi_0}{2k_BT}\right) \tag{2.8}$$

where σ^M is the total charge density of the metal.

From κ, one can define the Debye length λ_d which defines how far the electrostatic effects for a charge reaches into the solution, as:

$$\lambda_D = \frac{1}{\kappa} \tag{2.9}$$

As can be seen from equation (2.8) C_d can increase without limits with increasing ϕ_0. This is due the fact that the ions are being treated as point charges that can approach the surface infinitiously closely. To solve this problem, Stern [67] proposed a plane so that the center of the ion is at one ionic radius distance away from the electrode, called the *Inner Helmholtz Plane* (IHP). A second plane, the *Outer Helmholtz Plane* (OHP) contains the IHP as well as a layer of solvent close to the electrode. These two planes are described as the Stern layer, see figure 2.6. As for the potential profile, within the Stern layer, a linear decrease is observed and for x >OHP, the same potential decay as for the Gouy-Chapman model is observed.

The potential profile in the additional diffusive layer (outside OHP), is given by:

$$\frac{tanh(ze\phi/4k_BT)}{tanh(ze\phi_2/4k_BT)} = e^{-\kappa(x-x_2)} \tag{2.10}$$

with ϕ_2 the potential at x_2 (the position of the OHP). The overall Gouy-Chapman-Stern potential is then a combination of the Helmholtz and the Gouy-Chapman potential defined as:

$$\phi_0 = \phi_2 - \left(\frac{d\phi}{dx}\right)_{x=x_2} x_2 \tag{2.11}$$

Finally, the differential capacitance for this model can be described by 2.12. For simplicity, the inverse of the capacitance is shown. The capacitance is a series of two capacitances. The first coming from the Helmholtz layer which is the capacitance at the OHP (first term) and the second one comes from the diffusive layer, outside of OHP (second term).

$$\frac{1}{C_d} = \frac{x_2}{\epsilon\epsilon_0} + \frac{1}{(2\epsilon\epsilon_0 z^2 e^2 \rho_0/k_BT)^{1/2} cosh(ze\phi_0/2k_BT)} \tag{2.12}$$

In chapter 5, the relationship between double layer and surface stress is studied in more detail. A method to modify the thickness of the Debye length is presented.

2.2.2 Potential-Controlled Measurements

In many of our experiments, we apply a step potential to our cantilever system through the potentiostat and measure the resulting current response. There are many electrochemical techniques, but here we will focus on two: Cyclic Voltammetry (CV) and Chronoamperometry (CA). In a CV, the potential is sweeped linearly between two potential values and the resulting current vs. voltage profile is recorded. In general, a CV shows current peaks at specific voltages that correspond to reduction and oxidation reactions happening on the electrode. In addition, in our system, a CV is used to electrochemically clean the gold-coated electrode, see section 2.2.3. In CA, the potential is stepped between two values and the current vs. time is measured [65].

For Chronoamperometry measurements, the resulting current response can be described by two equations. The first contribution of the current response comes from the double layer charging (i_{ch}) and can be expressed by:

$$i_{ch} = \frac{\Delta E}{R_s} exp\left(-\frac{t}{R_s C_d}\right) \tag{2.13}$$

where ΔE is the potential step value, R_s the serial resistance and C_d the double layer capacitance, as described in section 2.2.1. The charging of the double layer has a time constant $\tau = R_s C_d$ which is defined as the time where the initial current value defined as E/R_s decreased to 37 %. The current resulting from the double layer charging decays exponentially. This charging current can be explained by an RC circuit.

If faradaic processes are present in solution, e.g. a redox molecule, a second current term is added (i_f). This faradaic current is expressed by the Cottrell equation:

$$i_f = \frac{nFA\rho_j^0\sqrt{D_j}}{\sqrt{\pi t}} \tag{2.14}$$

where n is the number of electrons being transferred in the redox reaction, F is the Faraday constant, A the area of the electrode, ρ_j^0 the initial concentration of ion species j and D_j the diffusion constant of ion j. This current decays with $t^{-1/2}$.

2.2.3 Electrochemical Cleaning

The electrochemical system attached to the fluid cell has two distinct purposes: First, it is used to clean and electrochemically characterize the surface of the gold coated cantilever. Second, it is used to apply a controlled, time-dependent potential to the cantilever to induce repetitive surface stress changes.

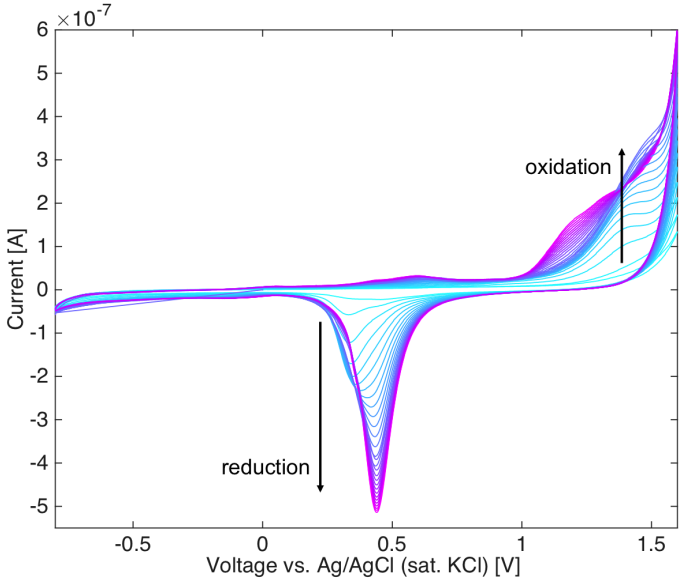

Figure 2.7: Cyclic voltammogram in 50 mM $KClO_4$ between -0.8 and 1.6 V, vs. Ag/AgCl (sat. KCl) to electrochemically clean a gold surface. The characteristic gold reduction peak at 0.4 V as well as the oxidation peaks at 1.4 V increase over time, indicating a cleaning of the surface.

The first one serves as an intrinsic cleaning step of our gold surface. Prior to all experiments, this cleaning is performed. For this, a cyclic voltammogram (CV) between -0.8 and 1.4 V (vs. Ag/AgCl (sat. KCl)) in 50 mM $KClO_4$ at a scan rate of 20 mV/sec is recorded until a repetitive voltammogram is obtained. The $KClO_4$ solution is degassed for 30 min before using to remove any oxygen. The gold surface is oxidized at anodic potentials at above 1.0 V and the formed gold oxide is removed during the reduction scan and lifts off any contaminants. In figure 2.7 a contaminated gold surface is cleaned and the resulting CV cycles over time are shown. A strong increase of the gold reduction peak is observed at around 0.4 V and an increase of the oxidation peaks are observed between 1.2-1.6 V indicating a removal of contaminants.

2.3 Potential-induced Surface Stress

A metal-coated cantilever electrode in contact with a solution will experience surface stress changes. This is due to the fact that the surface atoms of the electrode are missing a neighbor and their charge needs to redistribute between the atoms (see figure 1.2). Our system allows us to apply a potential to the cantilever to drive ions to the surface. This will induce a change in surface stress as the ions recover the redistribution of charge on the surface. For the duration of the applied potential, a double layer will build up until all charges in the bulk are in equilibrium, as described in section 2.2.1. For most of the experiments discussed here, a square-wave potential between a negative and a positive bias is applied to the gold electrode surface. If the gold electrode is in a solution of e.g. sodium chloride (NaCl), adsorption of chloride ions occurs at cathodic potentials and desorption occurs at anodic potentials.

This potential-driven adsorption and desorption of ions causes a change in the surface charge density on the surface and therefore a change in the deflection of the cantilever. As

described in section 2.1.2, this deflection can be recorded by a position sensitive diode.

In figure 2.8, a schematic of a typical surface stress measurement is shown. A square-wave potential is applied to the surface of the gold electrode and the resulting converted surface stress signal is recorded over time. The shape of the surface stress response gives rise to much information. For a clean gold-electrode in contact with an electrolyte, the resulting surface stress curve should resemble a square-wave pattern similar to the input signal. This is because ions will diffuse towards the surface and build up a double layer. The time frame for this process depends on the applied potential and the concentration of the solution and is in the order of sec or even minutes for surface stress. Chapter 5 will show an in-depth analysis of the time response of the surface stress. However, as will be shown in section 2.4, this surface stress pattern changes if molecules are attached to the surface. The amplitude of the surface stress change depends on how many ions can interact with the surface and is therefore largest for clean surfaces [1]. Contaminations will lower the electrochemical surface area of the electrode and result in a decrease of surface stress.

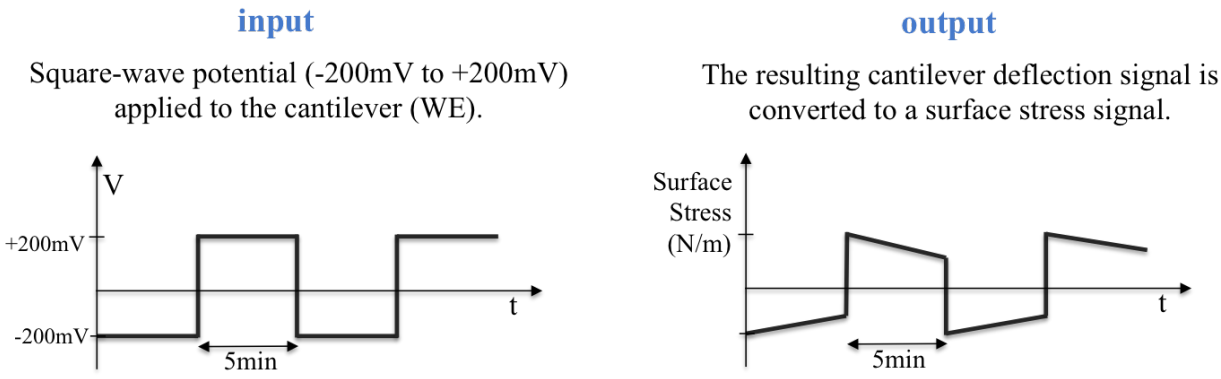

Figure 2.8: Schematics of a typical surface stress measurement. A square-wave potential is applied to the surface of the cantilever causing a change in the surface stress. This deflection is recorded using a position sensitive diode and the voltage output is converted into a surface stress signal.

2.3.1 Surface Stress of a Cantilever

To understand the surface stress changes of a metal electrode that is in contact with an electrolyte some basic concepts are explained in this section. The first important relationship is shown by the Shuttleworth equation which relates the surface stress σ with the surface free energy γ by:

$$\sigma_{ij} = \gamma\delta_{ij} + \frac{\partial\gamma}{\partial\epsilon_{ij}} \tag{2.15}$$

where δ is the Kronecker delta and $\partial\epsilon_{ij}$ is the surface strain described by $\partial\epsilon = \frac{dA}{A}$ with $A = A_0 exp(\epsilon)$ [68]. The surface free energy γ is defined by the reversible work per unit area (dw/dA) and is a measure of the energy that is required to move an atom from the bulk to the electrode surface. The last term in equation (2.15) is 0 for liquid electrodes as they can not maintain a strain. Canceling the last term results in the well-known electrocapillary equation.

The surface stress σ is the quantity of interest here. By definition, a compressive surface stress causes the stressed surface to expand, whereas a tensile stress causes the stressed surface to contract. Tensile stress is described by a positive and compressive stress by a negative surface stress value. For all experiments in this thesis, absolute surface stress values are reported, as changes are measured.

The classic Lippmann equation which describes the change of interfacial tension γ of a liquid electrode upon a change in the electric field E and relates this to the charge q as follows:

$$\frac{d\gamma}{dE} = -q \tag{2.16}$$

The classical Lippmann equation is only derived for liquid-liquid interfaces. With the advent of the use of solid electrodes in contact with electrolyte, there has been much work on finding relations of the surface stress of solid electrodes.

A more generalized Lippmann equation (or Couchman(-Davidson)) [69] equation can be derived as:

$$\frac{d\gamma}{dE} = -q + (\sigma_{ij} - \gamma\delta_{ij})\frac{d\epsilon}{dE} \tag{2.17}$$

The last term is zero for liquid electrodes. For solid electrodes however it was not well understood how much the last term contributes to the stress [70]. Couchman and Davidson argued that this term can be neglected for solid electrodes as well, so that the same equation can be used for solid and liquid electrodes [69, 71]. Therefore, we can conclude that the surface energy γ can be determined by the change in charge q upon a change in potential E, see equation 2.16 [72]. In chapter 5, this relationship for non-equilibrium potential conditions will be further discussed.

2.3.2 Conversion of Deflection to Surface Stress

With standard beam deflection methods, we can monitor the deflection of the cantilever due to changes in the surface stress. The change in the cantilever bending Δz can then be converted into surface stress change $\Delta\sigma$ using Stoney's [73] formula described by:

$$\Delta\sigma = \frac{Et^2}{3(1-\nu)l^2}\Delta z \tag{2.18}$$

with E the elastic modulus of the cantilever, ν the Poisson ratio, l the cantilever length, w the cantilever with and t the cantilever thickness. The spring constant k of the cantilever can be calculated using Hooke's law:

$$k = \frac{F}{\delta} = \frac{Ewt^3}{4l^3} \tag{2.19}$$

Solving equation (2.19) for E and putting it into equation (2.18) gives us the conversion of beam deflection into surface stress for our cantilever system:

$$\Delta\sigma = \frac{4kl}{3wt(1-\nu)}\Delta z \tag{2.20}$$

With this conversion the recorded voltage change from the linear photodiode is converted into our surface stress signal. Note that here only surface stress changes are recorded.

2.4 Modified Gold Surfaces

Gold is a perfect material for biological sensors as biomolecules can easily be attached to the surface via a thiol bond. Gold-thiol linkers are widely used to attach any kind of molecules in a plug-and-play configuration.

There is a clear correlation between available gold area and induced surface stress amplitude change [1]. A cleaner electrode surface will lead to a larger change in the surface stress upon applying a potential. Ions will be specifically directed towards the electrode and cause a change in the surface stress. The larger the number of available gold sites to interact with, the larger the surface stress change. If part of the surface is blocked by a surface modification like alkanethiols (or other contaminants), the surface stress decreases. Assuming a full coverage of alkanethiols on the gold surface, limited ions can interact with the surface and the surface stress change decreases.

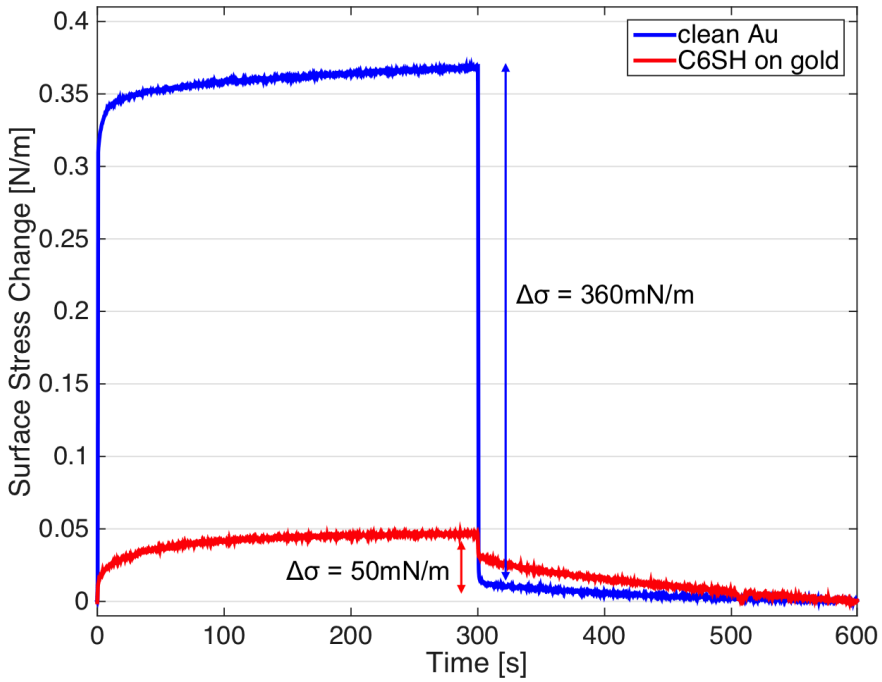

Figure 2.9: Surface stress response of a clean gold electrode (blue) and a C_6SH-modified gold electrode (red). From 0-300 sec, a positive bias of +200 mV (vs. Ag/AgCl (sat. KCl)) and from 300-600 sec -200 mV is applied to the gold-coated cantilever.

This principle is shown in figure 2.9. A potential step from -200 mV (0-300 sec) to +200 mV (300-600 sec) is applied to a gold-coated cantilever in Tris-HCl 10 mM NaCl 50 mM. In this case, the chloride ions will interact with the surface and cause a change in the surface stress. For an electrochemically cleaned gold cantilever, the surface stress amplitude is large, here $\Delta\sigma$=360 mN/m (blue trace). After incubating the electrode in an alkanethiol solution (C_6SH) for 5 min, a decrease of the surface stress amplitude to $\Delta\sigma$=50 mN/m (red trace) is observed.

There are three main factors that contribute to a change in surface stress if biomolecules are attached to the surface via a thiol bond: 1. Lennard-Jones interactions between adsorbed molecules, 2. electrostatic interactions between Au-thiol bonds that are adjacent and 3.

redistribution of the surface atoms upon binding of molecules will change the electronic structure and leads to a change in surface stress [25, 44]. It has been shown by Godin et.al. [25] that the first factor (Lennard-Jones interactions) only contribute to a small compressive surface stress change in the order of 0.001 - 0.01 N/m. Coulombic interactions that are derived from neighboring Au-thiol contributes to about 0.01 - 0.1 N/m of the stress change. The biggest impact comes from specific adsorption to the electrode surface and leads to surface stress changes as big as 1 - 10 N/m. This specific adsorption will change the charge density of the gold electrode surface.

In this thesis, two main modification markers were attached to the gold electrode via a thiol bond: Oligonucleotides and ferrocene alkanethiols. In the subsequent chapters, these two modifications are further analyzed.

2.4.1 Oligonucleotide on Gold

Oligonucleotides are short strands of DNA. Deoxyribonucleic acid (DNA) is a molecule that carries our genetic information decoded in four different base-pairs, i.e. adenine (A), thymine (T), cytosine (C) and guanine (G). Each base-pair binds specifically to another base-pair through hydrogen bonds. A binds to T via two hydrogen bonds and G binds more strongly to C via three hydrogen bonds.

Here, we will examine a 25-mer oligonucleotides, i.e. an oligonucletoide with 25 base-pairs. These are attached to the gold electrode surface via a thiol bond. DNA is negatively charged due to the phosphate groups in the backbone of the structure, see figure 2.10. This negative charge plays an important rule when measuring the surface stress changes upon applying potentials to the gold electrode. If a positive bias is applied, the negatively charged DNA will be attracted to the surface and the DNA will lie down. On the other hand, for a negative bias, the oligonucleotide is repelled from the surface and stands up. This

method was intensively discussed by Rant et.al. [63, 74–76] and Barton et.al. [57, 77–79]. Characteristic surface stress patterns can be observed for single-stranded and double-stranded oligonucleotides.

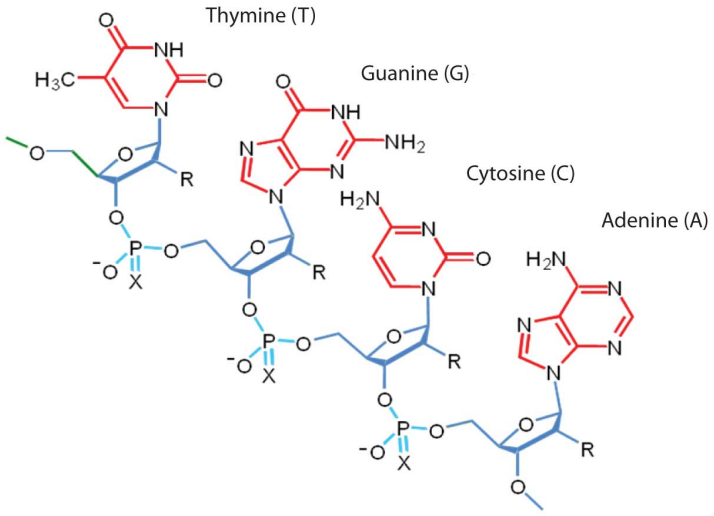

Figure 2.10: Single stranded DNA molecule showing the four different base pairs (Tyhmine, Guanine, Cytosine and Adenine) as well as the sugar and phosphate backbone. The phosphate backbone is negatively charged. (taken from: [80])

2.4.2 Ferrocene Alkanethiol on Gold

Ferrocene is an electrochemically active redox molecule that shows distinct redoxpeaks in a cyclic voltammetry. These redox-reaction peaks of are further seperated, the longer the alkanethiol chain length is. In theory, for a direct redox-reaction, the oxidation and reduction potentials are separated by 59.2/n mV (n = 1 for a 1-electron transfer reaction). However, the longer the chain length the larger the peak separation. The increased distance of the ferrocene group and the electrode reflects the decrease in electronic coupling between them [81]. The ferrocene redox reaction is shown in equation (2.21) and reflects a 1-electron

transfer reaction.

$$Fe^{2+} \leftrightarrow Fe^{3+} + e^{-} \tag{2.21}$$

Two different ferrocene molecules are being used in this work. For both molecules, a ferrocene group is attached to a C_{11}-alkanethiol with the difference that a carbonyl group is added to one of these molecules as shown in figure 2.11. As the alkyl chains have the same length, the peak separation is the same for both moieties. However, due to the carbonyl group, the position of the redox potential is shifted anodically by 250 mV [81–85]. Figure 2.12 shows the corresponding cyclic voltammogram for a Fc-modified (blue) and a Fc-CO-modified (red) gold electrode. The Fc-C_{11}-SH exhibits an oxidation peak at $E_p = 0.34$ V (vs. Ag/AgCl), whereas the Fc-CO-C_{11}-SH exhibits the redox peak at $E_p = 0.59$ V (vs. Ag/AgCl).

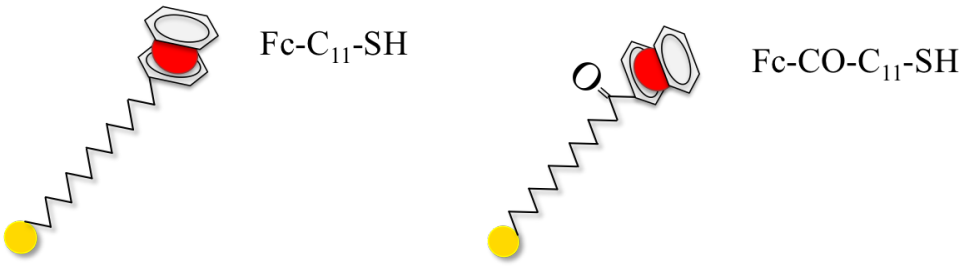

Figure 2.11: Two different ferrocene alkanethiol markers: 11-(Ferrocenyl)undecanethiol (Fc-C_{11}-SH) and 11-Ferrocenyl-carbonyl-undecanethiol (Fc-CO-C_{11}-SH). The sulfur is shown in yellow, and the iron center of the ferrocene is shown in red.

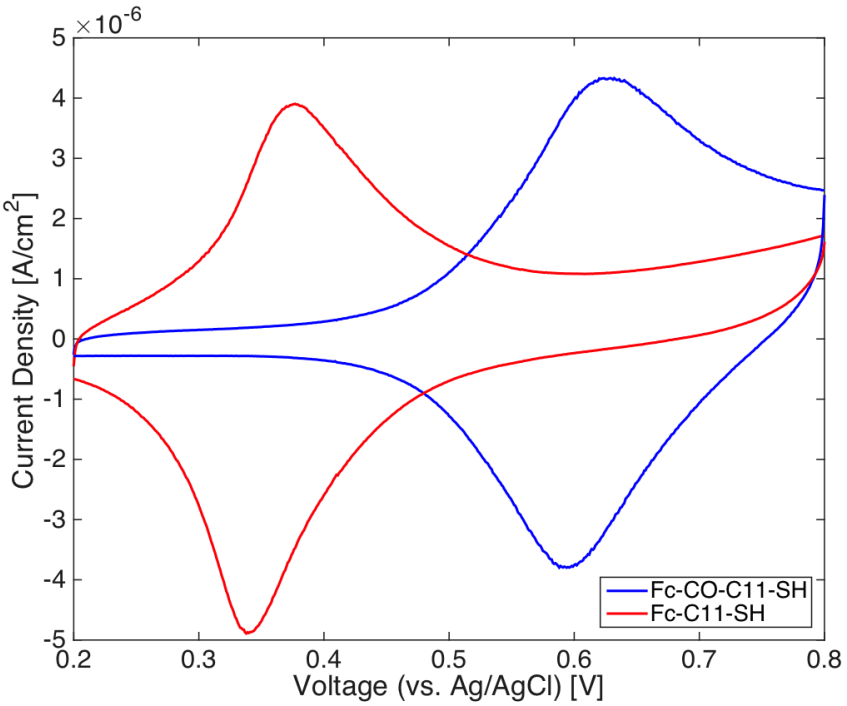

Figure 2.12: Cyclic voltammetry in $NaClO_4$ at 20 mV/sec (vs. Ag/AgCl (sat. KCl)) for a gold-coated electrode modified for 5 min with either Fc-CO-C_{11}-SH (blue) or Fc-C_{11}-SH (red). Distinct redox peaks are observed for each alkenyl ferrocene.

3

Characterization of a Gold-coated Cantilever

This section disscusses the characterization of our cantilever gold surface for biosensing applications and lis the fundament for all further chapters.

The chapter is based on the following published manuscript:
Haag, A.-L., Nagai, Y., Lennox, R.B. and Grutter, P. Characterization of a gold coated cantilever surface for biosensing applications. *EPJ Tech. Instrum.* **2**, 1-12 (2015).

3.1 Abstract

Cantilever based sensors are a promising tool for a very diverse spectrum of biological sensors. They have been used for the detection of proteins, DNA, antigens, bacteria viruses and many other biologically relevant targets. Although cantilever sensing has been described for over 20 years, there are still no viable commercial cantilever-based sensing products on the market. Several reasons can be found for this - a lack of detailed understanding of the origin of

signals being an important one. As a consequence application-relevant issues such as shelf life and robust protocols distinguishing targets from false responses have received very little attention.

Here, we will discuss a cantilever sensing platform combined with an electrochemical system. The detected surface stress signal is modulated by applying a square wave potential to a gold coated cantilever. The square wave potential induces adsorption and desorption onto the gold electrode surface as well as possible structural changes of the target and probe molecules on the cantilever surface resulting in a measurable surface stress change. What sets this approach apart from regular cantilever sensing is that the quantification and identification of observed signals due to target-probe interactions are not only a function of stress value (i.e. amplitude), but also of the temporal evolution of the stress response as a function of the rate and magnitude of the applied potential change, and the limits of the potential change.

This paper will discuss three issues that play an important role in future successful applications of cantilever-based sensing. First, we will discuss what is required to achieve a large surface stress signal to improve sensitivity. Second, a mechanism to achieve an optimal probe density is described that improves the signal-to-noise ratio and response times of the sensor. Lastly, lifetime and long term measurements are discussed.

3.2 Background

Nanomechanical structures can be used for label-free and low-cost biosensors that offer high sensitivities. In recent years, several nano and micromechanical structures have been described as possible biosensor platforms, such as nanomechanical cantilevers [15–18], resonators [20, 21], and optomechanical structures [22]. The most common detection principles due to biological binding effects are changes in surface stress [24, 25] and mass [32, 86].

Here we focus on a cantilever sensing platform that detects changes in surface stress. In our platform, a cantilever is coated with a gold layer that serves two purposes. First, this gold layer is used as a support structure of probe molecules bound to the surface typically using thiol linkers; this in principle gives the sensor specificity [87]. What is often not considered is the second role of this gold layer, as it can act as a very sensitive transducer that is located within nanometers of the probe molecules that sense the biological binding events [25, 88]. In our system, the surface potential of the gold coated cantilever is controlled and changed over time to induce changes of the surface coverage of the adsorbing ion. Changing the presence of any ionic or charged species near the surface leads to a large change of surface stress. This is based on the well established fact that surface stress is directly proportional to the surface charge density [89]. Surface concentration changes of charged species can be induced by applying an electrochemical potential which generates conformational changes of probe molecules.

Our approach to increasing the dynamic range of the stress signal is to drive the adsorption and desorption of ions to the cantilever surface, thus inducing a large measurable and characteristic surface stress change [42]. This movement of ions can be modulated as a function of time, allowing signal averaging techniques to be used. If clean gold surfaces are used, the resultant reproducible time dependent stress signals include information on the target-probe system, such as ion diffusion times and polymer dynamics. This information can be used for biochemical sensors or in fundamental studies (e.g. for the investigation of the folding dynamics of proteins). Reliable signal and thus target identification can be based on recognition of the complex time dependent stress patterns in addition to the information given by signal amplitudes.

In our experiments, we change the presence of ions near the surface by combining a

conventional cantilever stress sensing system with a standard three-electrode electrochemical system. All experiments are performed in buffer solution with the cantilever acting as a working electrode (WE), a platinum wire as the counter electrode (CE) and a Ag/AgCl (sat. KCl) electrode as the reference electrode (RE). The electrodes are connected through a potentiostat allowing a voltage to be applied between the working (cantilever) and the reference electrode thus measuring the current flowing between the working and the counter electrode (voltammetry) [65]. Upon application of a square wave potential to the gold coated cantilever between +/- 200 mV, chloride ions that are present in solution will ad-/desorb on the surface which leads to a change in surface charge density [70] and therefore to a change in surface stress [89]. In our system the stress-induced bending of the cantilever is measured by optical beam deflection methods and translated into a quantitative surface stress signal by using Stoney's formula [73] and appropriate calibrations [90, 91].

The electrochemical aspect of our sensor system serves two distinct purposes. First, it is used to clean and electrochemically characterize the surface of the gold coated cantilever. Secondly, it is used to apply a controlled, time dependent potential to the cantilever to induce repetitive surface stress changes. This first point is very important, as surface stress and surface stress changes are driven by surface charge density, which is a function of the cleanliness of a system [25]. Recalling that a clean metallic surface typically takes about 1 microsecond to be contaminated in air by absorbable organic molecules - hence the need for ultra high vacuum conditions (UHV) to investigate surface phenomena. Electrochemistry allows a systematic cleaning and characterization of surfaces in solution. Note that compared to the concentration of rest gas ('contaminations') in UHV, solutions are very seldom as pure - clean solution to background contaminations would need to be at a level of 1 part in 10^{13} to achieve similar lifetimes of clean surfaces in solution as in UHV.

An important insight is that the surface stress change on the cantilever is proportional to the available and accessible gold surface area. This can be used to measure and optimize the concentration of probes on a cantilever that leads to a decrease in the available gold surface area due to the target molecules covering part of the gold surface (see figure 3.1) [25]. On a clean gold coated surface, a large number of ions can interact with the surface resulting in a large surface stress change signal. If part of the surface is covered by molecules, in this case thiolated single-stranded oligonucleotide, fewer ions can access the surface leading to a smaller surface stress change. Covering the surface complete densely with a monolayer of molecules will hinder the ions to reach the surface and no large change in surface stress is observed. Residual (much smaller) stress changes can be due to steric hindrance and other effects. Our group has previously shown surface stress changes for aptamer functionalized gold surfaces. The aptamer undergoes a conformation change into a more compact state upon binding to its cognate ligand therefore increasing the available gold area, i.e. increased surface stress, compared to its relaxed state [42].

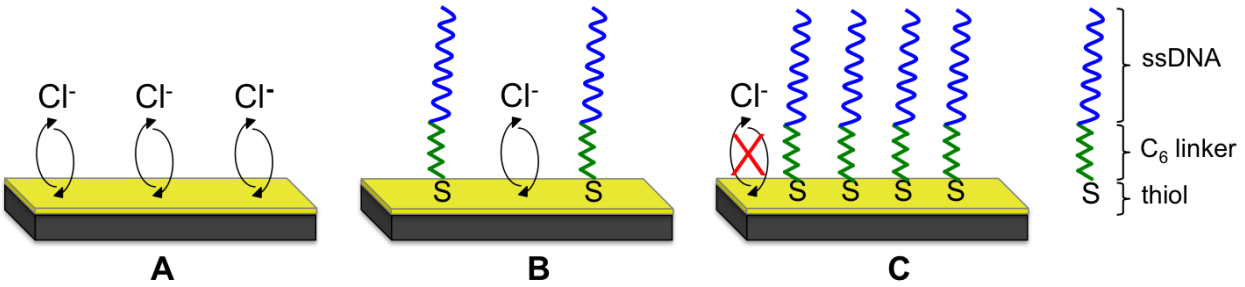

Figure 3.1: Potential induced adsorption/desorption of chloride ions on different functionalized gold surfaces. Schematics describe the relationship between surface stress change and available surface area. **A**, a bare and clean gold surface is shown. Chloride ions can freely interact with the whole surface and large surface stress changes are measured. Upon binding of some single-stranded oligonucleotide to the surface **B**, fewer ions can react with the surface leading to a smaller surface stress change. Once the layer is densely packed on the surface **C**, the surface stress change vanishes as no ions can reach the surface anymore.

In this paper we will discuss three issues that most nanomechanical based sensors are facing and present protocols to improve these issues. This will be the foundation for possible applications of biosensors applicable to real-life samples containing not only the analyte of interest, but many background 'contaminants'. These three challenges are: 1. How can large surface stress signals be achieved? Any contaminants on the surface will reduce the available surface area and therefore lead to smaller surface stress change. We will present an electrochemical cleaning protocol that results in a clean gold surface, leading to a large and quantitatively reproducible surface stress signal when surface charge densities change. 2. How can the signal-to-noise ratio be improved? An optimal probe density is required for good signal-to-noise ratios of the surface stress change. This is achieved by using a multi-step functionalization protocol recently described by Nagai et al. [42]. 3. How can sensors with long term stability and realistic shelf life be manufactured? For device applications one needs to know how the sensors performs during long term measurements in the analyte of interest. We will present long term measurements of our cantilever platform in solution and discuss our observations.

3.3 Methods

3.3.1 Oligonucleotide Preparation

All experiments were performed using a 25-mer thiolated single stranded oligonucleotide with a sequence of 5'-HS-SC6- TCGGATCTCACAGAATGGGATGGGC-3' (by IDT Technology, USA). The stock oligonucleotide solution was prepared by diluting to a concentration of 100 μM by in 40 μl of TE buffer (Tris-HCl 10 mM, 5 mM EDTA, pH=7.4). Prior to each experiment, the oligonucleotide is desalted by incubating in 25 mM TCEP (Fisher Scientific, USA) for 1 hr followed by a subsequent purification step using a NAP-5 column (GE Health-

care, UK). The desalting step breaks off the disulfide bond of the oligonucleotide making it reactive to the gold surface. The final oligonucleotide concentration for all experiment was set to 10 μM.

3.3.2 Cantilever Preparation

Silicon cantilevers (CSC38/tipless/no Al-coating, Mikromash) are solvent cleaned with acetone, isopropanol and methanol before thermal evaporation. A 2 nm thick titanium adhesion layer is evaporated onto the cantilever with a rate of 0.9 Å/s followed by 100 nm of gold at a rate of 1 Å/s at a pressure of $< 3\text{x}10^{-6}$ mBar and stored under ambient condition before use. To define the gold area that is exposed to the electrochemical setup, a thin layer of apiezon wax (Apiezon wax W, APWK, USA) that is dissolved in trichloroethylene (TCE) (Fisher Scientific, USA) is applied to the base of the cantilever leaving an area of 1.0 mm^2 exposed.

3.3.3 Electrochemical Cleaning

Argon is injected into potassium perchlorate (50 mM $KClO_4$) to remove any oxygen in solution. Subsequently, prior to each experiment the cantilever is electrochemically cleaned in 50 mM $KClO_4$ (Fisher Scientific, USA) by cycling the potential between -0.8 to 1.4 V at 20 mV/sec until a repeatable gold cyclic voltammogram peak is observed (CHI 1000, CH Instruments, USA). The cantilever is set up as the working electrode, a platinum wire (1 mm thick, Alfa Aesar, USA) is used as the counter electrode and a standard Ag/AgCl (sat. KCl) reference electrode (BASi, USA).

3.4 Results and Discussion

3.4.1 Electrochemical cleaning

We have tested different cleaning procedures by quantifying surface cleanliness electrochemically in situ and using surface science techniques ex situ. Based on results published by Fischer et al [92], we tested the following cleaning protocols: 1. Electrochemical sweep of the gold coated cantilever in 50 mM potassium hydroxide (KOH) from -0.2 to 1.2 V (vs. Ag/AgCl (sat. KCl)), 2. Electrochemical sweep in 50 mM potassium perchlorate ($KClO_4$) from -0.8 to 1.4 V (vs. Ag/AgCl (sat. KCl)) and 3. Piranha solution (Three parts concentrated sulfuric acid (H_2SO_4) and one part hydrogen peroxide (H_2O_2); note that great caution is necessary when using piranha solution) treatment of the cantilever for 5 min. We find that the $KClO_4$ and KOH^- mediated processes result in the cleanest surface as monitored using ex situ X-ray photoelectron spectroscopy (XPS) and in situ cyclic voltammetry. The atomic percent surface composition measured from XPS results of the survey scan for the piranha cleaning method results in 40.2 % gold, 33.6 % carbon and 26.1 % oxygen. A huge improvement of these values, i.e. higher gold percentage can be seen for the KOH sweep as well as the $KClO_4$ sweep. For KOH the composition is 65.3 % gold, 30.0 % carbon and 4.74 % oxygen, which is very comparable to the values for the $KClO_4$ sweep with 61.7 % gold, 33.8 % carbon and 4.5 % oxygen. The $KClO_4$ sweep is chosen to be the primary cleaning step for all further experiments, as this is a standard media for electrochemical cleaning of gold. Additionally, perchlorate has a very small affinity for gold and will not adsorb onto the gold surface.

In detail, with this method the cantilever is electrochemically cleaned in 50 mM $KClO_4$ by sweeping the applied potential in solution from -0.8 to 1.4 V (vs. Ag/AgCl (sat. KCl)).

Sweeping the potential from -0.8 to 1.4 V oxidizes the gold surface, whereas the reverse step, going from 1.4 to -0.8 V reduces the resulting gold oxide. This cleaning step serves to intrinsically remove contaminants from the surface. The cyclic voltammogram (current vs. potential, CV) scan is performed at 20 mV/sec and is continuously repeated until a reproducible CV of gold is achieved, indicating the removal of any contaminates. In figure 3.2 A, a CV from a bare clean gold evaporated cantilever is shown. Multiple peaks that overlap are observed between 0.9 to 1.2 V, which correspond to the oxidation of gold. A significant sharp reduction peak is observed at 0.35 V. Figure 3.2 B shows a cleaning process in action. The CV spectrum has two additional peaks at 0.35 V and 0.15 V consistent with chloride on the gold surface. Over the course of six full potential cycles, the chloride redox peaks vanish, leaving a clean bare gold surface.

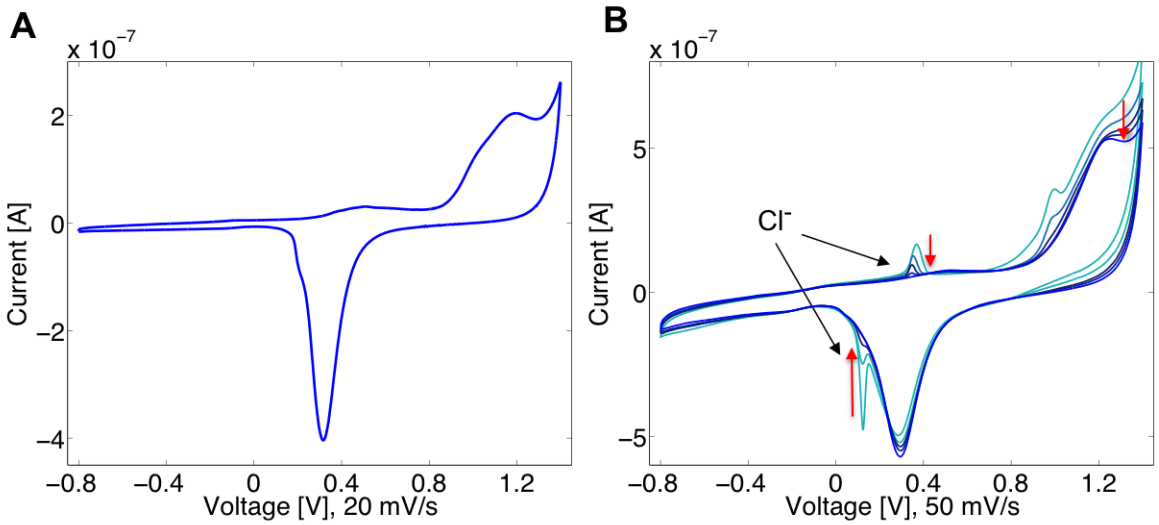

Figure 3.2: Cyclic voltammogram in 50 mM $KClO_4$ (vs. Ag/AgCl (sat. KCl)). **A**, the standard gold spectrum is shown at 20 mV/sec indicating a clean gold surface. **B**, a chloride contaminated surface is electrochemically cleaned. After six full potential sweeps, the chloride peaks vanish and a clear distinct gold reduction peak is observed.

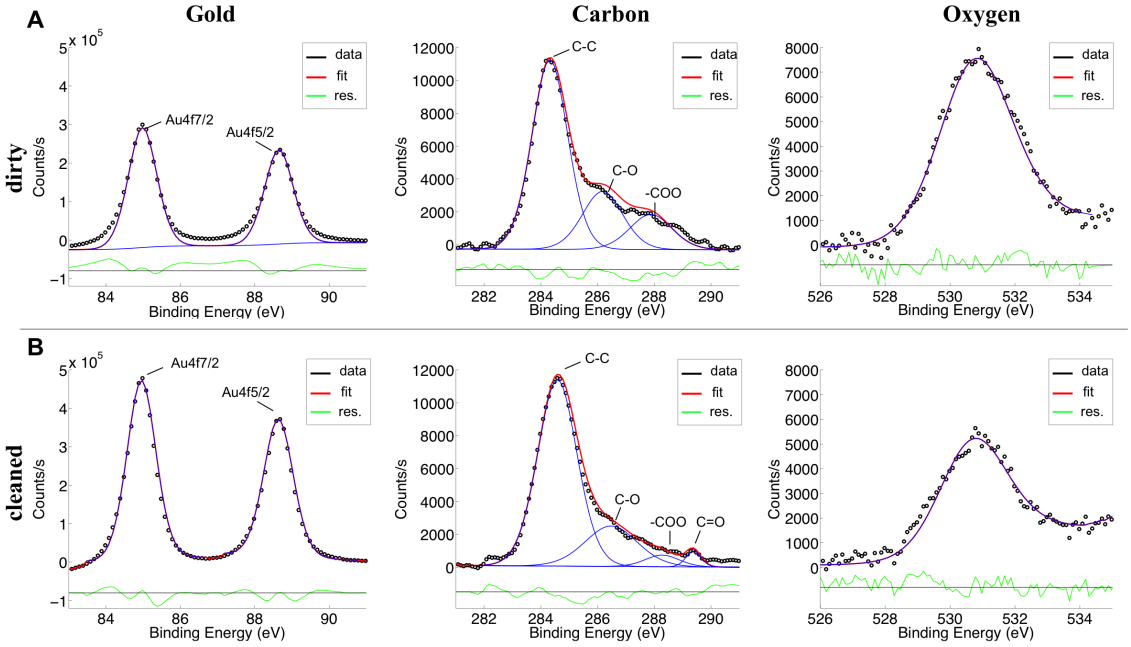

Figure 3.3: Uncleaned and cleaned gold coated samples to test effectiveness of electrochemical cleaning protocol with XPS. X-Ray Photoelectron Spectroscopy (XPS) data are shown for the Au4f, C1s and O1s peaks for uncleaned (**A**) and cleaned (**B**) gold samples. The percent surface composition for the uncleaned gold surface is 43.7 % gold, 41.2 % carbon and 9.4 % oxygen based on the survey scan. The gold peak can be increased to 61.7 % by electrochemically cleaning the surface. Additionally, carbon and oxygen are decreased to 33.8 % and 4.5 % respectively.

To further verify the effectiveness of the chosen cleaning protocol, X-ray photoelectron spectroscopy (K-Alpha X-Ray Photoelectron Spectrometer system, Thermo Scientific, USA) was performed on evaporated gold surface on a silicon substrate. In figure 3.3, the individual high-resolution spectra of Au4f, C1s and O1s are shown for two different samples: (A) gold sample that has not been cleaned, and (B) an electrochemically cleaned gold sample. Both samples are made from a piece of a silicon wafer with a thermally evaporated 2 nm titanium

adhesion layer followed by thermal deposition of 100 nm gold. The samples were stored under ambient condition for 1 week. Prior to the experiment, one sample is rinsed with MilliQ water and blow-dried using a nitrogen stream (uncleaned), the other sample is electrochemically cleaned using 50 mM $KClO_4$ and dried with nitrogen (cleaned).

The atomic percent surface composition of the uncleaned sample is measured to be 43.7 % gold, 41.2 % carbon and 9.4 % oxygen based on the survey scan. In figure 3.3 B, the electrochemically cleaned sample is shown. The time between the cleaning and measuring the sample with XPS was about 30 min. The overall composition of the surface was 61.7 % gold, 33.8 % carbon and 4.5 % oxygen. Compared to the dirty sample, a relative increase of about 40 % was observed for the gold peak and a relative decrease of 20 % and 50 % for the carbon and oxygen peak contamination was observed. Higher measured levels of gold on the surface means there is less contamination surface, demonstrating the effectiveness of the electrochemical cleaning protocol. The remaining oxygen and carbon peaks result from exposing the sample to air for 30 min prior to measuring the surface composition and cannot be avoided. This was verified by sputter cleaning a gold sample in UHV until a clean Auger spectrum was acquired, then exposing it to air for 20 minutes. The surface composition measured by the survey scan resulted in 66.1 % gold, 31.8 % carbon and 2.2 % oxygen.

An important feature of the intrinsic electrochemical cleaning protocol is the ability to revert the sensor surface to its base state in situ by removing the oligonucleotide functionalization layer. A cantilever that is functionalized with 10 uM 25-mer thiolated oligonucleotide was measured with XPS and the %at composition for gold, nitrogen and phosphorus is 11.1 %, 11.64 % and 5.97 %. A clear phosphorus peak in the XPS spectra indicates successful oligonucleotide functionalization, see figure 3.4 A. Subsequently, a sample functionalized under the same conditions is electrochemically cleaned with 50 mM $KClO_4$ to remove the oligonucleotide. XPS of the oligonucleotide functionalized and electrochemically cleaned sample is shown in figure 3.4 B. The atomic percentage (%at) composition for gold, nitrogen

and phosphorus is measured as 45.86 %, 9.73 % and 0 % (not measurable). The clear removal of the phosphorous peak indicated the removal of the oligonucleotide functionalization layer from the surface. Subsequently, a more thorough electrochemical cleaning can be done.

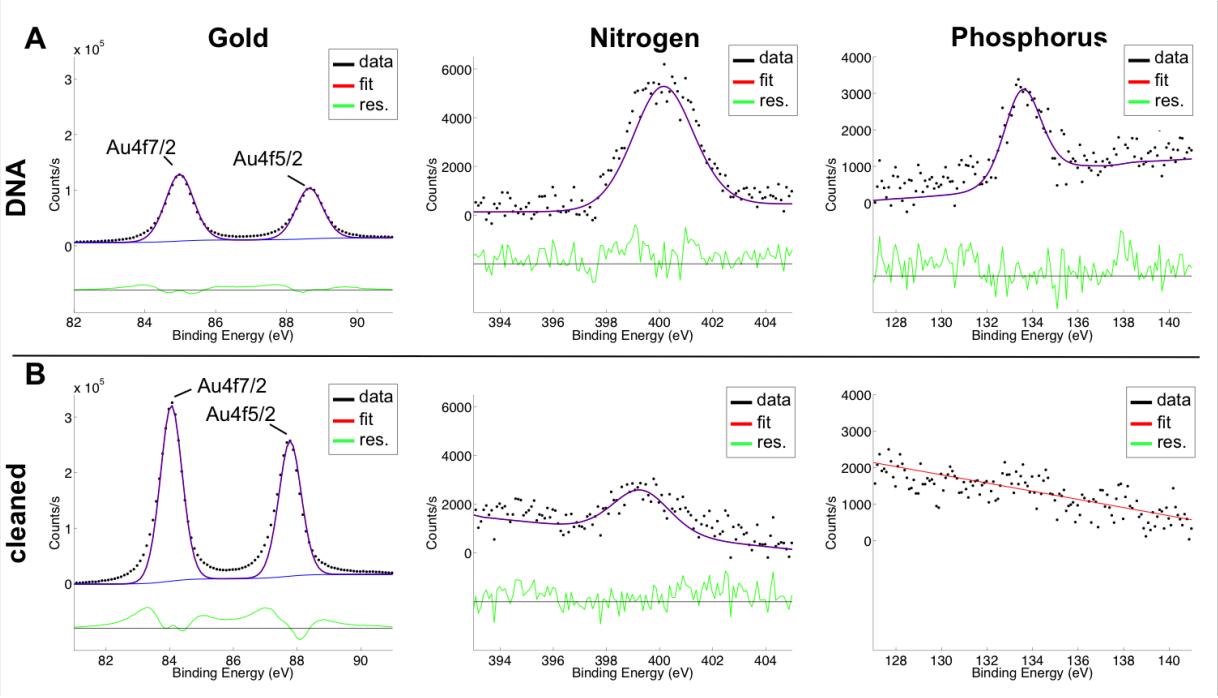

Figure 3.4: XPS measurements of the electrochemical removal of an oligonucleotide functionalization layer on the gold sample. X-Ray Photoelectron Spectroscopy (XPS) data are shown for the Au4f, N1s and P2p peaks for oligonucleotide functionalized (**A**) and electrochemically cleaned (**B**) gold samples. A clear increase in the gold peak as well as a clear removal of the phosphate peak of the cleaned sample can be seen.

3.4.2 Surface Stress Measurements

A large signal-to-noise ratio can be achieved by precisely controlling the probe density on the surface. If the surface is completely covered with the molecule of interest, ions cannot interact with the surface, and only very small surface stress changes are measured. Additionally,

a complete coverage of the surface by probe molecules is detrimental to a fast response time of the sensor, as many target molecules will not be able to interact with the probe molecules. Therefore, it is crucial to achieve an optimal probe density to maximize the signal-to-noise ratio of the measurements. Our group has developed a multistep oligonucleotide functionalization protocol that enables for systematic control of the functionalization density and thus leads to high quality sensor functionalization with good reproducibilities. After the electrochemical cantilever cleaning described above, a surface stress pattern is recorded for 30 min during application of a square wave potential between +/- 200 mV with a 10 min period. Afterwards, the cantilever is incubated in a 10 uM thiolated single stranded oligonucleotide solution for 5 min and another surface stress pattern is recorded. This step is repeated until the desired coverage is achieved. This can be controlled by first monitoring the decrease in surface stress amplitude due to the increased probe coverage and therefore a decreased availability in gold area and then evaluating the surface stress pattern change due to comparative adsorption of chloride ions in solution and the negatively charged oligonucleotide phosphate backbone [93]. The effective density of the oligonucleotide layer can be determined by using 12-ferrocenyl-1-dodecanethiol ($Fc(CH_2)_{12}SH$) to label unfunctionalized areas of the gold surface. The net area associated with unfunctionalized gold is determined from the integrated area of the electrochemically active ferrocene label. This process was previously shown by Nagai et al [42], details are described below.

From an applications point of view achieving a reproducible sensor response is highly desirable. In our system this translates into the necessity of achieving a reproducible probe surface coverage. The surface probe density can be characterized by measuring the chloride-induced stress changes of the cantilever (all experiments are performed in Tris-HCl 10 mM NaCl 50 mM pH 7.4 buffer (TN buffer)). To drive adsorption and desorption of chloride ions to the cantilever gold surface, a square-wave potential is switched between -200 and +200 mV,

with a 10 min period. As a result of the square wave potential, the cantilever will undergo characteristic bending due to the induced surface stress change. In figure 3.5, the surface stress change patterns for a gold surface that is clean (blue), partially functionalized with single stranded thiolated oligonucleotide (red) and 6-mercapto-1-hexanol (MCH) (green) versus time are shown. These three cases demonstrate the relationship between surface stress change and available gold surface area very well. The surface stress change for clean gold results in a large signal with an amplitude of $\sigma = 350$ mN/m. Furthermore, it shows a response pattern that is in phase and similar in shape to the applied square wave potential. This is because chloride ions are essentially immediately driven to/from the surface; surface charge density (leading to a change in surface stress) thus follows the profile of the applied potential.

Upon functionalization of the cantilever gold surface with 25-mer thiolated single stranded oligonucleotide with a packing density of roughly 9 % as described in [42], the surface stress amplitude decreases and the response pattern starts to deviate from that of the applied square potential. The trace shows an upward slope trend for regions where +200 mV is applied and a downward slope for regions where -200 mV is applied. The amplitude decreases from 350 mN/m to 80 mN/m compared to the clean gold surface. This supports the fact that if less gold surface is available for the chloride ions to adsorb to, the smaller the surface stress change will be. The oligonucleotide covers a part of the surface and makes it less accessible for chloride ions to adsorb/desorb at the applied potentials. The change in shape of the response curve is due to changes in the structure of single-stranded oligonucleotide when potential is applied and results from interactions between the charged oligonucleotide phosphate backbone and the gold surface and hydration shell dynamics. Quantitative modeling of these various phenomena and their interplay is presently being investigated. What is clear at this stage is that the detailed shape of the stress response curve allows determination of the probe surface coverage.

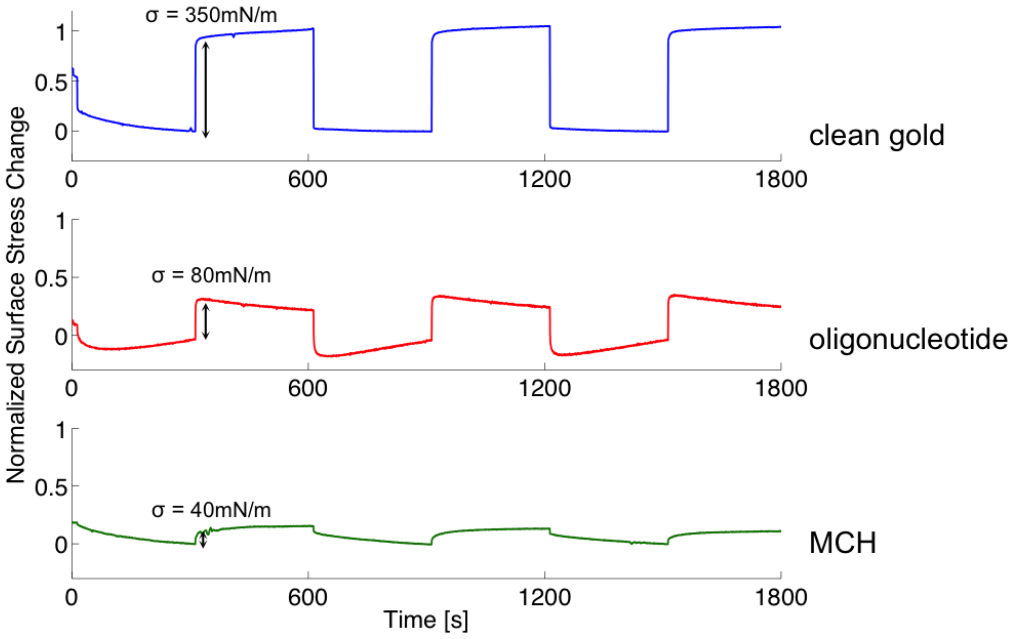

Figure 3.5: Surface stress change on a clean compared to functionalized gold coated cantilevers. Surface stress change pattern of the cantilever as a response to an applied square wave potential at +/-200 mV with a 10 min period. The blue trace shows the response of a clean gold evaporated surface measuring a large surface stress change of σ=350 mN/m. Upon functionalization with single-stranded oligonucleotide (red trace), the surface stress change decreases to σ=80 mN/m. Covering the surface with 6-mercapto-1-hexanol (MCH) (green trace) leads to a low surface stress change of σ=40 mN/m.

To further demonstrate this principle, another sample was functionalized with MCH, a short thiolated C6 linker for 5 min. MCH binds strongly to the gold surface resulting in a densely packed layer. Ion adsorption is blocked and the capacitance of the electrode is reduced [94]. The surface stress change pattern shows an even stronger deviation from the shape of the applied potential and a further decrease in stress amplitude to values such as

40 mN/m. Note that the pattern change provides a potentially more robust signal to detect hybridization than the amplitude, which can vary depending on the number and type of defects in the self-assembled monolayer [83].

In summary, we point out two key observations. This first is that the amplitude of the surface stress change at the switching potential decreases, the more the gold surface is blocked by any molecules, allowing fewer chloride ions to ad-/desorb onto the surface. The absolute value of the amplitude is a function of the initial gold cleanliness. Contaminants in the solution that competitively bind to the clean gold surface (e.g. bromide in a chloride solution) and potential-induced conformational changes in the probe molecules also affect the signal amplitude. Reproducible large absolute signal values can be achieved by suitable gold cleaning protocols as described above.

The second key point is that the surface stress pattern is characteristic of the nature of the surface bound molecules (either of the probe functionalization layer or the probe-target complex). The former can be used to (re-)generate well defined probe functionalization layers in situ. The latter allows for the determination of the presence of target molecules as recently demonstrated by Nagai et al. [42], who reported on the pattern shape change due to oligonucleotide hybridization and aptamer-protein interactions of optimized sensing layers. The change in the pattern can be attributed to the negatively charged phosphate backbone of the DNA and mechanical property changes upon hybridization. A negative applied potential will repel the DNA from the surface leaving the DNA in a standing up position [79]. Over time, a double layer will build up that screens the DNA charge which results in a relaxation of the DNA into its neutral state. This is reflected in the slope change in the surface stress change pattern observed at -200 mV. At positive potentials, the DNA is attracted to the gold surface and is lying down. The relaxation of this position is visible in

the slope change of the surface stress change pattern. In passing, we note that by varying the temporal period of the applied potential, conformation dynamics can be studied, potentially allowing label free fundamental experimental insights into important topics such as protein folding.

3.4.3 Long-term Measurements

An important question is how long the sensor response remains stable. Because cantilever based sensors are very sensitive, their response is expected to drift and change as a function of time, concentration of contaminants, etc. We have performed long-term stability recordings in the TN buffer used for our oligonucleotide and aptamer protein measurements. The cantilever was electrochemically cleaned in 50 mM $KClO_4$, rinsed with MilliQ water and placed in buffer. No oligonucleotide functionalization was performed. A square wave potential between +/- 200 mV with a period of 10 min is applied to the cantilever for 14 hrs (84 cycles). The surface stress change of the cantilever was recorded over time, as shown in figure 3.6. Overall, the surface stress amplitude decreases from 150 mN/m to 100 mN/m after 4 hrs, to 60 mN/m after 10 hrs, and finally less than 50 mN/m after 14 hrs. Additionally, a pattern change is observed. The slope of the pattern at +200 mV changes from a positive to a negative trend after 8 hrs. A similar change is observed for the slope at -200 mV changing from a negative to a positive trend after 11 hrs. A zoom into three different regions of the curve after 1, 9.5 and 13 hrs is shown in the figure 3.6. The overall decrease in amplitude is attributed to chemisorbed ions on the surface leading to a decrease in the available gold area. A CV was recorded in 50 mM $KClO_4$ before and after the long-term measurement. The charge increases by 85 %, indicating an increase in the capacitance, assuming that the active area has remained constant. The experiment starts by applying a potential of -200 mV and ends 14 hours later at +200 mV after 84 cycles. Generally, one observes that the sensor

remains stable for 10 hrs in TN buffer before competitive chemisorption takes place leading to an unreliable measurement. This is likely a function of the purity of the buffer components and water used to prepare the buffer solution. With the intrinsic electrochemical cleaning setup, the cantilever can be restored to its original state, i.e. a clean gold surface *in situ*.

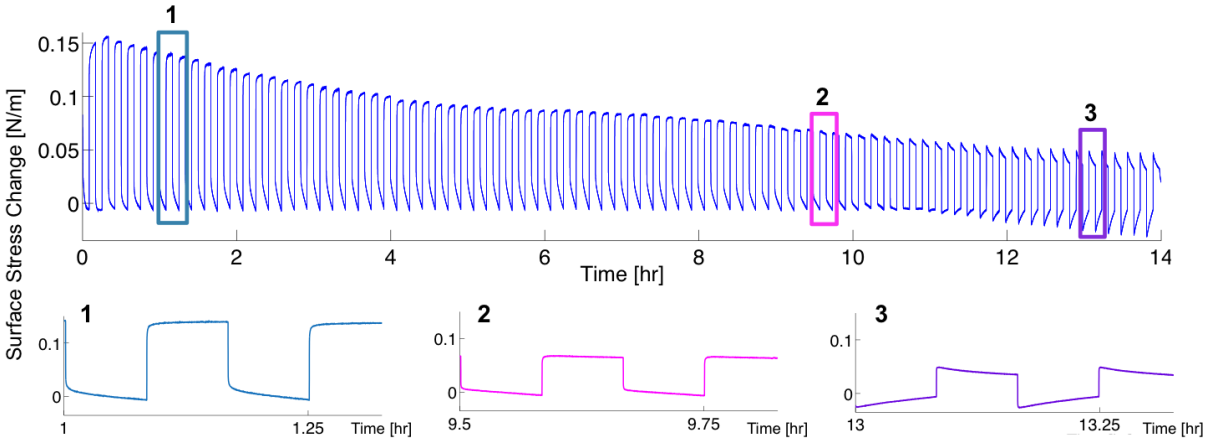

Figure 3.6: Longterm surface stress measurement of gold coated cantilever in buffer. Longterm surface stress of a gold coated cantilever in TN buffer recorded for 14 hrs. A square wave potential between +/-200 mV with a period of 10 min was applied to the cantilever. A zoom of three sections are shown and labeled as 1, 2 and 3. At (**1**) a large surface stress change is measured. After around 9.5 hours (**2**), the pattern starts to change resulting in a negative slope for +200 mV and a positive slope for -200 mV, clearly visible after 13 hrs (**3**). Furthermore, the overall surface stress change amplitude decreases indicating that that ions chemisorb onto the surface over time covering part of the gold surface.

3.5 Conclusion

We have addressed and discussed three issues that are fundamental to successful cantilever biosensor integration and relevant for many other sensor platforms and applications. First, in sensors where the signal relies on surface charge changes such as in chemFETS or cantilever

based sensors, a clean chemical functionalization layer support surface is crucial in order to obtain large signals. Here we report an electrochemical cleaning method of the gold surface often used to support the thiolated probe molecules by sweeping a potential that is applied to the sensor surface between -0.8 and 1.4 V in 50 mM $KClO_4$ until a reproducible cyclic voltammogram is obtained. XPS data verifies the effectiveness of this cleaning method. The advantage of this method is that the sensor can be cleaned intrinsically without the use of any harsh chemicals that might harm the sensor integration environment. This cleaning step will remove the functionalization layer of the sensor restoring it to its original state. Second, we demonstrate how to achieve a high signal-to-noise ratio by carefully controlling the probe coverage of the sensor. A multistep functionalization protocol is described relying on characteristic changes in the stress response as a function of probe density to in situ electrochemical stimulation. This systematically provides a higher quality layer and a better control of the surface coverage, leading to higher signal-to-noise ratios and to a reproducible, predictable sensor response. Surface stress change measurements on a clean gold surface, oligonucleotide and MCH modified gold cantilever surfaces are described. In all experiments described here, a square wave potential between $\pm$200 mV is applied to the cantilever in TN buffer. These experiments confirm that the surface stress change is proportional to the available gold area. Additionally, the surface stress change pattern gives detailed information about conformational changes on the surface upon applying a potential. Lastly, long term stability measurements are shown in buffer indicating the sensor lifetime to be about 10 hrs. The origin of this limitation is currently being investigated. After 10 hrs, a electrochemical cleaning step is necessary to recover the surface to its initial high sensitivity state.

4

Selective *in situ* Modification

With the knowledge about the importance of cantilever cleaning and probe coverage described in the previous chapter, a technique to selectively modify two gold-electrodes with different ferrocene moieties with submonolayer coverage is demonstrated in this section. Potential-control of the gold electrode surface is utilized to control the functionalization steps.

The chapter is based on the following submitted manuscript:
Haag, A.-L., Lennox, R.B and Grutter, P. Selective in situ potential-assisted SAM formation on multi electrode arrays. *IOP Nanotechnology* (2016).

4.1 Abstract

The selective modification of individual components in a biosensor array is challenging. To address this challenge, we present a generalizable approach to selectively modify and characterize individual gold surfaces in an array, in an *in situ* manner. This is achieved by controlling the applied potential of the individual sensors in an array, each acting as a

working electrode in solution. The extent of adsorption and desorption of the derivatizing molecules is thus controlled. To demonstrate this concept, two different self-assembled monoloayer (SAM)-forming electrochemically-addressable ω-ferrocenyl alkanethiols (C_{11}) are chemisorbed onto independent but adjacent gold electrodes. At applied potentials (vs. Ag/AgCl (sat. KCl)) cathodic relative to the adsorption potential of the alkylthiol, the ferrocene alkanethiol does not adsorb onto the surface and the electrode remains underivatized. However, applying modest positive potentials relative to the adsorption potential leads to extensive coverage within 10 min. The resulting SAM remains in a stable state while under these modest anodic potentials. In this state, the existing SAM does not significantly desorb nor do new ferrocenylalkythiols adsorb. Using three characteristic potentials allows for controlled submonolayer probe coverage of the individual componenents of gold electrode arrays *in situ*. These three potentials are characteristically different for different adsorbates. Characterization of the ferrocene-modified electrodes via cyclic voltammetry demonstrates that each ferrocene marker is exclusively adsorbed to the electrode it was directed to.

4.2 Introduction

Multiplexed biosensing arrays are of great interest as they allow for the rapid and selective detection of many analytes in a complex mixture. Controlling the functionalization of the individual components of the array is however complex, and when achieved is generally performed in a serial fashion using additional apparatus [95]. Techniques used to modify one sensor in the presence of many others include microcontact printing [58, 59], dip-pen nanolithography [60] and modified ink-jet printing [61, 62]. Here we present a technique to functionalize the individual components in an array of gold electrodes with different functionalities by using selective potential-assisted electrochemical deposition and inhibition of deposition. Two different electroactive ferrocene markers (Fc-C_{11} and Fc- CO-C_{11}) attached

at the ω-position to a C_{11}-alkyl thiol are used to demonstrate this concept.

The adsorption of alkanethiols on single crystal and polycrystalline gold have been shown to be potential-dependent [96–100]. A modest positive potential (e.g. >200 mV vs. Ag/AgCl) can increase the rate of adsorption of alkanethiols on polycrystalline gold so that excellent coverage can be achieved within minutes [96, 101, 102]. Applying a potential during SAM formation results in a well-defined SAM in terms of coverage. On the other hand cathodic potentials (<-200 mV vs. Ag/AgCl) inhibit the rate of chemisorption of alkythiols on polycrystalline gold and indeed at potentials <-600 mV to <-1100 mV (depending on chain length [103] and crystallographic orientation [104]), chemisorbed alkythiols are reductively desorbed [100, 105–107]. The relevant reactions are described in equation 4.1

$$RS - Au + e^- \longrightarrow Au(0) + RS^- \tag{4.1}$$

for the case of reductive desorption and

$$RSH + Au \longrightarrow RSAu + H^+ + e^- \tag{4.2}$$

for the case of oxidative adsorption.

The electrochemical removal (stripping) of functional monolayers followed by full coverage selective adsorption of a second molecule has been demonstrated [82, 108]. Collman *et al.* [82] functionalized two adjacent gold electrodes with the same adsorbate. Subsequent reductive desorption at one electrode removed the chemisorbed thiol. Exposure to a second adsorbate results in derivatizion of only the SAM-stripped electrode, as the other electrode remains unchanged under the experimental conditions. This approach works on the principle of selective reductive desorption of a SAM to allow for introduction of a second adsorbate.

This process requires complete monolayer functionalization at each step, as otherwise cross-functionalization and binary SAMs will result.

In some cases, a partially coated sensor surface is desired [1, 42, 63]. Peterson *et al.* [64] have shown that surface-tethered single stranded DNA, when in a low surface density regime, is desired as probe hybridization proceeds with relatively fast kinetics. In comparison, high probe surface density ($\theta = 0.6$) leads to a decrease in both hybridization efficiency and relatively slower kinetics. Many other studies show that sub-monolayer coverage of tethered DNA probes leads to optimal hybridization efficiencies for DNA binding on gold [94, 109], on gold nanowires [110], or for protein binding [111]. Nagai *et al.* [42], using microcantilever sensors, demonstrated that maximal surface stress changes between single stranded oligonucleotides and hybridized probes are achieved at a probe density of ca. $\theta = 0.3$ in the absence of other adsorbates. There is, to our knowledge, no potential-assisted method described in the literature which results in the selective *in situ* modification of multiple electrodes with submonolayer coverage.

Here we present a method to produce submonolayer adsorbate coverage on two different but spatially proximal gold electrodes *in situ* with different electroactive ferrocene alkanethiols. This is achieved by controlling the applied potential of the gold samples during modification using three distinct potentials: E_{ads} (adsorption), E_{des} (desorption) and E_{hold} (holding). The potential at E_{ads} promotes the chemisorption of an alkanethiol on the gold surface. The potential E_{des} maintains the electrode in the reductive desorption state and inhibits alkanethiol adsorption from occuring. Lastly, E_{hold} is an intermediate potential that is not reductive enough to desorb an already formed monolayer but is not sufficiently anodic to promote the adsorption of new alkanethiols via an electrochemically-promoted exchange reaction.

It is important to note that Ma et.al. [96] and Paik et.al. [101] have demonstrated that reproducible SAM formation can occur over time scales of a few minutes by using potential-assisted deposition. This technique enables the multiple electrode experiments described here. In the absence of potential-assisted deposition, desorption and holding rates at open cirucit are both very slow and irreproducible. The long incubation times necessary for SAM formation without potential assistance will also lead to considerable exchange reactions at the first-formed SAM. The functionalization technique described here yields submonolayer coverage on a gold surface, *in situ* modification, and is scalable in that any number of electrode sensor surfaces can be functionalized with different molecules with the use of a multipotentiostat.

4.3 Experimental Section

4.3.1 Materials

11-(ferrocenyl)undecanethiol (Sigma Aldrich, USA) was dissolved in absolute ethanol to a concentration of 1 mM. 11-(ferrocenyl)-carbonyl undecanethiol was synthesized as per literature methods (see supporting information). Alkanethiol SAM formation involves the use of a 1:1 solution of 11- (ferrocenyl)undecanethiol (Fc-C_{11}-SH) and 11-(ferrocenyl)-carbonyl undecanethiol (Fc-CO-C_{11}-SH) in 100 mM $LiClO_4$ (absolute ethanol). Electrochemical cleaning was performed in a 50 mM $KClO_4$ solution. All other cyclic voltammograms were recorded in 100 mM $NaClO_4$. The following reagents were purchased and used without further purification: potassium perchlorate (>99 %, Sigma Aldrich, USA), lithium perchlorate (>95 %, Sigma Aldrich, USA), sodium perchlorate (>98 %, Sigma Aldrich, USA) and absolute ethanol (>99.8 %, Sigma Aldrich, USA).

4.3.2 Gold Surface Preparation

Silicon wafers were diced into small (0.5 x 1 cm) pieces and solvent-cleaned with acetone, isopropanol and methanol before sequential thermal evaporation of Ti and Au was performed. A 2 nm Ti adhesion layer was evaporated at a constant rate of 0.9 Å/s followed by a 100 nm thick Au layer at a constant rate of 1 Å/s (pressure $< 1\text{x}10^{-6}$ mBar, room temperature). Samples were stored under ambient conditions until needed. To define the electrochemical active area of the exposed gold in solution, a thin layer of Eccobond 286 (Emerson & Cuming, USA) is applied to the base of the gold surface leaving an exposed macroscopic area of $\sim$1.0 mm^2 .

4.3.3 Electrochemical Cleaning

All samples were electrochemically cleaned prior to each experiment. Samples were cycled between -0.8 and 1.4 V (vs. Ag/AgCl (sat. KCl)) in 50 mM $KClO_4$ at a scan rate of 20 mV/sec until a repetitive voltammogram was obtained. The gold electrode served as the working electrode, a platinum wire (1 mm diameter, Alfa Aesar, USA) as the counter electrode, a standard Ag/AgCl (sat. KCl) reference electrode (BASi, USA) as the reference. Electrochemical measurements were performed using a CHI 1030A (CH Instruments, USA) potentiostat. For all experiments two gold electrodes are recorded simultaneously by using each electrode as a separate working electrode sharing one counter and one reference electrode (Bipotentiostat).

4.3.4 Measurement of Ferrocene Coverage

The area of the gold electrode was determined from the gold oxide reductive stripping peak in the cyclic voltamogram performed from -0.8 to 1.4 V. The quantity of surface oxide

formed during the anodic excursion is determined by integrating the gold oxide reduction peak in the cathodic scan, Q_{red}. Assuming a standard charge value of Q_{std}=400 μC/cm^2 for polycrystalline gold [112], the microscopic surface area can be calculated by:

$$A = \frac{Q_{red}}{Q_{st}} \tag{4.3}$$

The geometric surface area is determined for each gold electrode via optical methods. The ratio of the electrochemical surface area to the geometric area yields roughness factor values of 1.1 to 1.6 for the electrodes used in this study.

Ferrocenylalkythiol coverage was determined by integrating the ferrocene-associated oxidation peak in the CV obtained in 100 mM $NaClO_4$. The surface coverage Γ of the electroactive ferrocene group is given by:

$$\Gamma = \frac{Q}{nFA} \tag{4.4}$$

with Q = charge obtained by integrating the current peak, n is the number of electrons transferred ($n = 1$ for the ferrocene couple), F the Faraday constant, and A is the electrochemical surface area of the gold electrode. To determine the fractional surface coverage of the ferrocene-modified alkanethiol on the gold electrode, the theoretical maximal coverage of 4.5 x 10^{-10} mol/cm^2 (equivalent to 2.7 x 10^{14} molecules/cm^2) is divided by the calculated coverage [113]. The theoretical maximal coverage is calculated by assuming a spherical ferrrocne with diameter of 6.6 Å, hexagonally close-packed [114].

4.3.5 SAM Formation

The gold surfaces were selectively modified with the two different ferrocene derivatives by varying the applied potential as described in detailed below. Modification was performed in

either 1 mM Fc-CO-C_{11}-SH or Fc-C_{11}-SH (1:1) with 100 mM $NaClO_4$ solutions for 10 min at a constant applied potential. After electrodeposition, the surfaces were rinsed with ethanol and Milli-Q water before a CV was recorded in 100 mM $NaClO_4$ from 0.2 to 0.8 V (vs. Ag/AgCl (sat. KCl)).

4.4 Results and Discussion

4.4.1 Determination of Required Applied Potentials

The first step toward a successful potential-assisted modification is to determine the ferrocenylalkythiol coverage as a function of the applied potential. Prior to each experiment, the evaporated gold electrodes are electrochemically cleaned before exposing them to the ferrocene derivitive [1]. To measure the extent of potential-dependent adsorption, the gold electrode was exposed to a 2 ml of 1 mM Fc-C_{11}-SH / 100 mM $LiClO_4$ solution while applying cathodic potentials (vs. Ag/AgCl (sat. KCl)) from -1.4 to -0.9 V for 10 min at each potential. After each incubation step, the sample was rinsed with ethanol and Milli-Q water before a CV was recorded in 100 mM $NaClO_4$ at 20 mV/sec. The resulting ferrocene oxidation peak was integrated to calculate the ferrocene surface coverage (equation 4.4). Results are plotted as a function of applied potential in figure 4.1 A. No apparent ferrocene derivative signal is observed for potentials <-0.9 V. Potentials of <-0.9 V (red area) thus serve to maintain a gold electrode free of chemisorbed ferrocenylalkanethiol. Application of a potential of 0.3 V (vs. Ag/AgCl (sat. KCl)) to a clean gold electrode results in Fc-C_{11}-SH of > 50 % after 10 min incubation.

The second step involves determining the potential range over which the ferrocenylalkylthiol SAMs are stable in regards to both desorption and thiol-for-thiol exchange. To

measure the desorption potential of the ferrocene alkanethiol, the modified surface was exposed to the ferrocenyl solution (1 mM) while changing the potential from -0.3 to -0.8 V. The corresponding ferrocene coverage is shown in figure 4.1 B. To compare the coverage of different experiments, the full layer is set to 100 % and the decrease of coverage with respect to the full layer is expressed as a percent of total coverage. Starting at -0.3V, the ferrocene surface coverage decreases indicating that gold-thiol bond is destabilized and the ferrocenylalkylhiol desorbs from the surface. The holding potential, described as the potential where an existing SAM ($0 < \theta < 1$) is held to be stable towards additional alkythiol adsorption or desorption for the time necessary to modify another electrode and is determined to be >-0.6 V.

This potential-dependent ferrocene coverage establishes the three operational potentials of interest to this study: E_{ads}, E_{desorb} and E_{hold}. E_{ads} (>0.3 V) is the potential at which adsorption of the C_{11}-alkanethiol occurs. E_{desorb} is the potential at which alkanethiol adsorption onto a clean gold electrode is not measurable (<-0.9 V). E_{hold} (-0.6 V) is in the potential range at which a pre-formed C_{11} alkylthiol SAM is held to prevent further thiol desorption, adsorption and exchange. These potential ranges provide limits with which to selectively functionalize two different alkylthiol ferrocene markers onto different gold electrodes which are present in solution.

4.4.2 Potential-driven Modification Protocol

These three potential regimes allow one to control the functionalization of two proximal electrodes with two different species. Two different ferrocene derivatives, Fc-CO-C_{11}-SH and Fc-C_{11}-SH demonstrate the effectiveness of the selective functionalization protocol based on desorption and adsorption. The two probes have the same alkyl chain length (C_{11}) and the same chain terminus (thiol), yet one has an added carbonyl group to the ferrocene moiety.

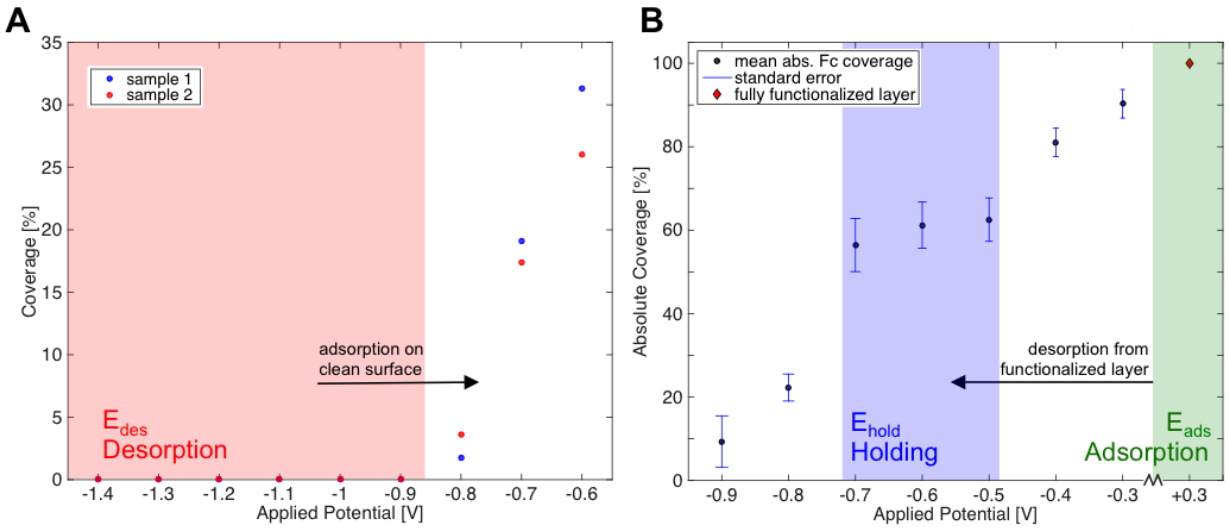

Figure 4.1: Ferrocene coverage depending on the applied potential to the gold electrode. The electrode was immersed in 1 mM Fc-C_{11}-SH, 100 mM $NaClO_4$ for 10 min while applying various potentials. After each incubation at a specific potential, the electrode was rinsed and a CV was recorded in 100 mM $NaClO_4$ at 20 mV/sec, vs. Ag/AgCl (sat. KCl). The oxidation peak is integrated to calculate the ferrocene surface coverage, using equation 4.4. **A** shows the adsorption of Fc-C_{11}-SH onto a clean surface with increasing applied potentials. In **B**, a fully-functionalized electrode is systematically desorped by applying a step-wise decreasing potential. At least three data points were included for the calculation of the mean in **B**.

This carbonyl shifts the corresponding redox potential anodically by 250 mV with respect to the Fc-C_{11}-SH [81, 83–85]. The Fc-C_{11}-SH exhibits an oxidation peak at $E_p = 0.34$ V (vs. Ag/AgCl), whereas the Fc-CO-C_{11}-SH exhibits the redox peak at $E_p = 0.59$ V (vs. Ag/AgCl). If a mixed SAM is formed on one electrode, two distinct peaks are observed. In a two working electrode configuration, each gold electrode is subjected to an electrochemical cleaning process in 50 mM $NaClO_4$ (vs. Ag/AgCl (sat. KCl)) by cycling the applied potential between -0.8 and 1.4 V until a reproducible cyclic voltammogram with distinct gold oxidation and reduction peaks is observed. The electrochemically active surface area is

determined by integration of the anodic peak current.

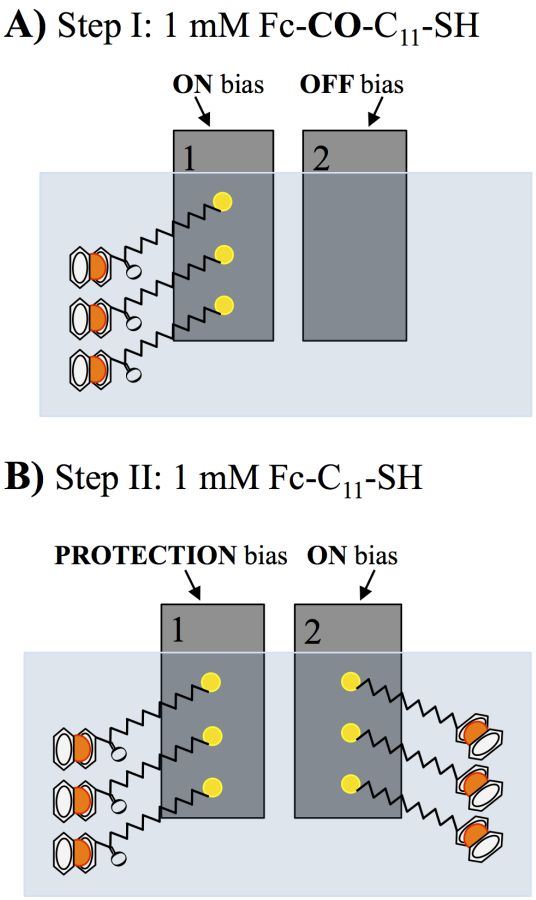

Figure 4.2: Scheme showing the two-step selective in situ surface modification on two gold electrodes. **A)** Both electrodes are immersed in 1 mM Fc-CO-C_{11}-SH, 100 mM $NaClO_4$ for 10 min. Different potentials are applied to two electrodes, so that the alkanethiol is only deposited onto electrode 1. **B)** The solution is changed to the second adsorbate, 1 mM Fc-C_{11}-SH, 100 mM $NaClO_4$ and the two electrodes are immersed for 10 min while the applied potentials targets the probe to the second electrode exclusively.

These two different ferrocenes are used to experimentally demonstrate the two-step protocol of selective functionalization of the electrode shown in Figure 4.2. In the first step,

both gold electrodes are simultaneously exposed to the same probe by immersion into a liquid cell filled with a total of 2 ml 1 mM Fc-CO-C_{11}-SH, 100 mM $LiClO_4$ for 10 min. During the functionalization process, electrode 1 is held at 0.3 V (E_{ads}), whereas electrode 2 is held at -1.4 V (E_{desorb}). After incubation, the electrodes are rinsed with ethanol and Milli-Q water and placed in a fresh liquid cell filled with 2 ml 100 mM $NaClO_4$. Cyclic voltammetry verifies the extent of derivatization. Both electrodes are rinsed with ethanol at the completion of the functionalization process. In a second step, both electrodes are placed in the same solution containing the second adsorbate (2 ml, 1 mM Fc-C_{11}-SH, 100 mM $LiClO_4$) for 10 min at specific potentials. During the functionalization, electrode 1 is held at -0.6 V (E_{hold}) and electrode 2 is held at +0.3 V (E_{ads}) to modify it with the second ferrocene probe.

The resulting cyclic voltammogram recorded simultaneously on each gold electrode after the second modification step is shown in Figure 4.3. Electrode 1 (blue) is modified with Fc-CO-C_{11}-SH and Electrode 2 (red) is modified with Fc-C_{11}-SH. Oxidation peaks at E_p = 0.59 V (Fc-CO-C_{11}-SH) and E_p = 0.34 V (Fc-C_{11}-SH) provide for the determination of the respective ferrocene coverage. For the Fc-CO-C_{11}-SH treated electrode 1, the overall surface coverage is 43.4 ± 0.4 %, corresponding to an alkanethiol density of 1.951 x 10^{-10} ± 0.016 x 10^{-10} mol/cm^2. On the other hand, electrode 2 treated with Fc-C_{11}-SH has a coverage of 32.7 ± 0.3 % (density: 1.474 x 10^{-10} ± 0.015 x 10^{-10} mol/cm^2).

4.4.3 Cross-coverage

Measurable quantities of Fc-C_{11} are observed on the Fc-CO-C_{11}-derivatized electrode. These peaks result from a competitive deposition of an undesired alkylferrocene in the presence of a derivative. Integration of the oxidation peak allows one to quantify cross-coverage. For electrode 1 (modified with Fc-CO-C_{11}-SH) the coverage by Fc-C_{11}-SH is only 1.1 ± 0.2 %

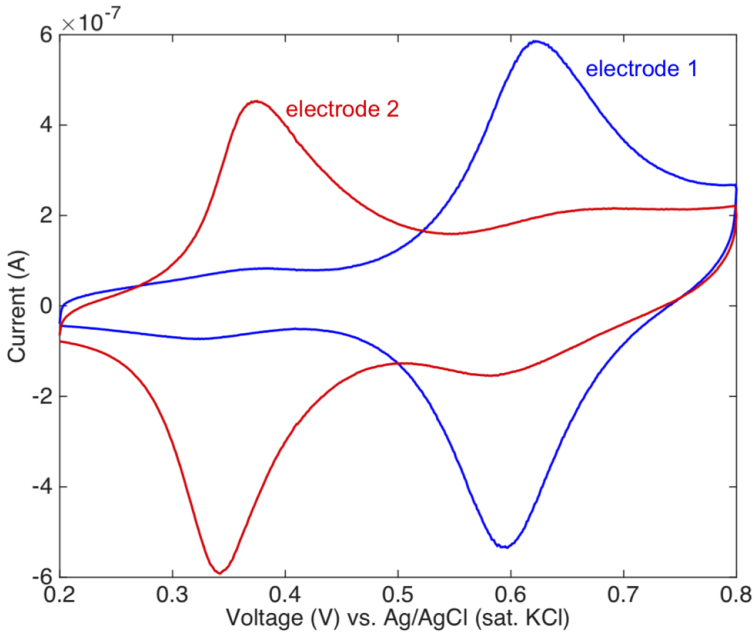

Figure 4.3: Cyclic voltammogram recorded simultaneously for both electrodes in 100 mM $NaClO_4$ (vs. Ag/AgCl (sat. KCl) at 20 mV/sec. The peak centered at $E_p = 0.34$ V corresponds to the Fc-C_{11} peak and the peak at $E_p = 0.59$ V corresponds to the Fc-CO-C_{11}.

(density: 4.727 x $10^{-12} \pm 0.748$ x 10^{-12} mol/cm^2) and electrode 2 (modified with Fc-C_{11}-SH) shows a cross-coverage of 2.4 $\pm$ 0.2 % (density: 1.071 x $10^{-11} \pm 0.066$ x 10^{-11} mol/cm^2) with Fc-CO-C_{11}-SH. The coverage and cross-coverage values for three independent experiments are summarized in Figure 4.4. In column C, the previously analysed experiment is shown. A and B are carried out using the same protocol. The distribution in the coverage is suggested to come from the polycrystalline nature of the gold electrodes and the relatively short incubation time (10 min) of each step. The histogram shows that electrode 1 undergoes high Fc-CO-C_{11}-SH coverage whereas electrode 2 shows high Fc-C_{11}-SH modification. The cross-coverage at each electrode is less than 4 % in all experiments.

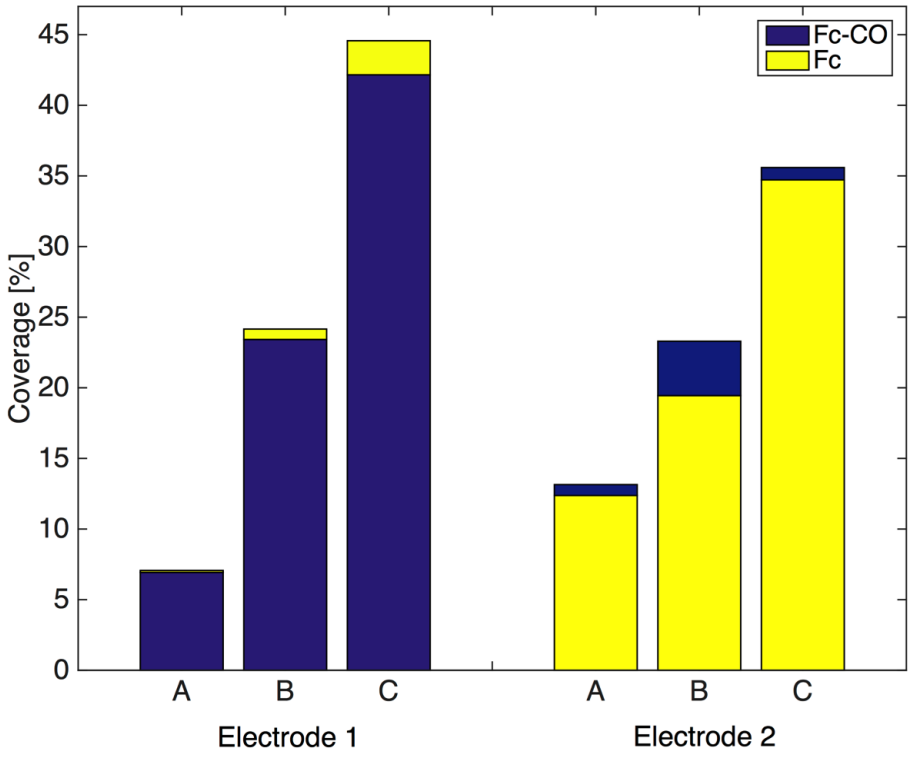

Figure 4.4: Cross-coverage for three different modification regimes (A-C). Electrode 1 is modified with Fc-CO-C_{11}-SH (+0.3 V) while a negative potential is applied to electrode 2. In the second step, electrode 2 is modified with Fc-C_{11}-SH (+0.3 V) while electrode 1 is held in the protective state (-0.6 V). The final surface coverage is plotted. A cross-coverage value of less than 4 % is achieved for all experiments.

Differentiation has to be made between the two cross-coverage values, as they have different origin. In case C, the cross-coverage value of 2.4 % of Fc-CO on electrode 2 results from the deposition on a clean electrode held at -1.4 V during the first step. The second contamination value is lesser (with a value of 1.1 % of Fc-C_{11}-SH on electrode 1) and results from the second modification step while the partially modified surface is being held at $E_{hold} = -0.6\,V$. Adsorption on a clean non-functionalized electrode can cause complications if more surfaces are being modified, as each modification step will increase the degree of

undesired adsorption. Due to the *in situ* electrochemical system, electrochemical cleaning can be performed on a set of non-functionalized arrays after every n-th modification. This step will ensure that minimal contamination on new blocked surfaces occurs. On the other hand, undesired adsorption during the holding potential of an electrode is believed to not increase significantly during further modification steps, as the adsorption kinetics are slower at higher coverage [115].

4.5 Conclusion

The work presented here describes an *in situ* method to selectively functionalize gold electrodes with different probes at submonolayer coverages. Application of specific potentials to the gold electrodes during SAM formation demonstrates that the extent of deposition of electrochemically active molecules can be controlled. All modification processes are done under potential-control to have a reproducible SAM formation that occurs within 10 min. SAM formation time scales are in the order of hours if modification is performed under open circuit conditions. In our study, two different gold electrodes were functionalized, each with an electrochemically distinct alkylferrocene adsorbate: Fc-CO-C_{11}-SH and Fc-C_{11}-SH. Potential-assisted SAM formation is achieved by distinguishing between three potentials: E_{ads} (+0.3 V) held at slightly cathodic potentials enhances the alkanethiol adsorption rate so that excellent coverage can be achieved within 10 min [96, 97]. E_{des} (-1.4 V) inhibits adsorption by maintaining the electrode in a reductive (alkylthiol) desorption state. Lastly, E_{hold} (-0.6 V) holds the state of a modified ferrocene alkanethiol electrode by hindering the adsorption of new alkanethiols vie electrochemically-promoted exchange reactions. The key potential here is E_{hold} which enables the functionalizion SAMs with submonolayer coverage. Cyclic voltammogram measurements in 100 mM $NaClO_4$ show two distinct electrochemical peaks indicating the successful selective modification on the two gold electrodes. From these

measurements, cross-coverage values of 4 % of the full coverage are determined.

Previous reports have only shown potential-assisted functionalization relying on a full SAM coverage. For a wide range of sensors however, a full coverage is not desired but a submonolayer coverage. The method presented here can selectively modify electrodes at submonolayer coverage by implementing a holding potential that keeps a functionalized electrode in its current state and prevents further adsorption or desorption within the time frames of the experiments. The technique can be applied *in situ* and is scalable so that a full array of gold electrode sensors can be modified and can thus be used for a wide variety of metal-based sensors.

5

Sensitivity Measurements

In this section, a more detailed analysis of the temporal evolution of the surface stress and current response for potential-driven adsorption of ions is discussed. By varying the potential pulse width, characteristic time scales for the double layer formation and ion diffusion can be probed.

The chapter is based on the following manuscript in preparation:
Haag, A.-L., Schumacher, Z and Grutter, P. Sensitivity measurements of cantilever-based surface stress sensors (2016).

5.1 Abstract

A gold-evaporated cantilever, as previously discussed, is used to simultaneously measure the change in surface stress as well as the current response during an applied potential step. In this electrochemical configuration, the cantilever acts as the working electrode, a platinum wire as the counter electrode and the Ag/AgCl (sat. KCl) electrode as the reference electrode. To study the time-dependent signal and the sensitivity of the system, the frequency of the

potential step applied to the cantilever is varied from 1 sec to 0.1 ms. First, a comparison between a strong adsorbing (chloride Cl^-) and a weak adsorbing ion (perchlorate ClO_4^-) in a 1 mM solution is presented. Next, the linear relationship between surface stress and charge density is measured for these fast potential steps. The slope of this fit is defined as the sensitivity of the system and is shown to increases for shorter potential pulses. Finally, the behavior of the surface stress and current for consecutive potential segments is studied.

5.1.1 Introduction

In recent years, several nano and micromechanical structures have been described as possible biosensor platforms [10–14]. Here we focus on cantilever-based sensors which have been used for the mechanical detection of a vast variety of biological targets such as DNA [1, 37, 37–45], antigens [46], proteins [47, 48], bacteria [49–51] and viruses [52]. The most common detection principles in these mechanical sensors due to biological binding effects are changes in surface stress [24–28] and mass [29–32]. For the sensing of oligonucleotides under potential-control, we have shown that the ion adsorption dominates the magnitude of the surface stress signal [42]. An important consequence of this is that the magnitude of the observed stress signal is proportional to the area of exposed clean gold [1]. Ions are directed to the surface by applying potential pulses and these accumulated charges cause a substantially larger measurable change in the surface stress [1, 25, 42] over conventional surface stress measurements at open-circuit potentials.

In this chapter, we apply a series of potential steps to the gold-coated cantilever surface with decreasing pulse width and the resulting surface stress change as well as the current response is simultaneously measured. The current can be integrated and normalized by the sensors area to determine the charge density and correlate it with the stress response.

It has been shown that the surface stress change is linearly related to the surface charge

density for Au(111) for different ion species [71, 88, 89] with a characteristic proportionality coefficient ξ defined by the slope of the plot of surface stress σ versus charge density q:

$$\xi = \frac{d\sigma}{dq} \tag{5.1}$$

The coefficient is a measure of the stress sensitivity of the cantilever sensor. A larger value corresponds to a larger slope which means that a small change in charge density corresponds to a large change in surface stress. Several studies have analyzed this coefficient on metal electrodes. In particular, Haiss et. al. [89] used a flame-annealed gold-coated glass cantilever and Ibach et. al. [71] used a macroscopic Au(111) single crystal cantilever to measure this parameter. Both studies measured the potential-induced deflection of the cantilever using Scanning Tunneling Microscopy (STM). Tabard-Cossa et. al. have shown the stress-charge relationship on a polycrystalline Au(111) microcantilever [88]. All measurements observed a negative surface stress - charge coefficient with reported ξ-values between -0.67 V and -2.0 V for chloride adsorption [88, 89, 116–122]. Several factors play a role in the variation of these values. These include but are not limited to cleanliness of the surface and surface treatment [88], different crystal orientation (single-crystal vs. polycrystalline) [117], investigated potential window [120], ion concentration [123] and measurement method. As pointed out in a recent study, the surface roughness of the metal electrode can change the coefficient value from -0.7 V (for rough surfaces) to -1.15 V (for smooth surfaces) [122]. None of these studies have investigated the temporal evolution of the coefficient and only operate in steady-state conditions. We show, for the first time, the behavior of the coefficient ξ on a gold-coated cantilever on decreasing potential step width in a 1mM NaCl and 1mM $NaClO_4$ solution.

5.1.2 Surface Stress Change and Charge Density

To understand how surface stress is related to charge density, some basic concepts are discussed. As briefly explained in section 2.3.1, the Lippmann equation relates the surface free energy γ with the charge density q by:

$$\frac{\partial \gamma}{\partial E} = -q \tag{5.2}$$

Assuming that the differential capacitance stays constant, equation 5.2 can be integrated to yield:

$$\gamma = -\int q dE \tag{5.3}$$

Using the relationship between charge density and capacitance ($d\sigma = CdE$), one can see from equation 5.3, that the surface free energy is proportional to C^2 and q^2. A parabolic dependence is therefore observed for a plot of the surface free energy vs. potential. For solid-liquid interfaces, however, the surface free energy can not be determined experimentally. A change in the surface stress can be measured over a change of applied potential. For solid-liquid interfaces, the generalized Lippmann equation was developed:

$$\frac{\partial \gamma}{\partial E} = -q + (\sigma_{ij} - \gamma \delta_{ij}) \left(\frac{\partial \epsilon_{ij}}{\partial E} \right) \tag{5.4}$$

with σ the surface stress, δ the Kronecker delta and ϵ the interfacial strain. For surfaces with a 3-fold or higher symmetry, the surface stress is isotropic and σ can be assumed to be scalar.

For liquid-liquid interfaces, the surface stress σ is equal to the surface free energy γ, so that equation 5.4 is reduced to the general Lippmann equation (see eqn. 5.2).

A measured surface stress change is related to the surface free energy by the Shuttleworth equation:

$$\sigma_{ij} = \gamma\delta_{ij} + \left(\frac{\partial\gamma}{\partial\epsilon_{ij}}\right) \tag{5.5}$$

with ϵ being the interfacial strain. For liquid-liquid interfaces, the last term on the right-hand side vanishes, as the atoms are free to flow to the surface upon a change in the surface strain. Therefore, the stress is equal to the surface free energy.

5.2 Fast-Potential Pulses

In this section, a more detailed analysis of the surface stress change and current response is shown. Understanding the evolution of surface stress and charge density signal for different ions allows quantitative insights into the dynamics of charge and ionic transfer in solution, a topic of great importance not only in sensing, but more importantly in energy and biological applications.

To measure the time-resolved surface stress and current signals, the length of the applied potential pulse is decreased. A potential pulse between +/- 0.1 V to 0.5 V with a defined pulse width (ranging from 1 sec to 0.1 ms) is applied to the gold-coated cantilever for 5 segments (figure 5.1A). The potential values are chosen so that no redox reaction in the solution or the gold occurs. The shortest pulse width (0.1 ms) is limited by the potentiostat setting used for these experiments (CHI 1030A, CH Instrument, USA). The cantilever is exposed to either 1 mM sodium chloride (NaCl) or 1 mM sodium perchlorate ($NaClO_4$) solution after an electrochemical cleaning [1]. Chloride and perchlorate ions will induce a change in the surface stress of the cantilever which can be monitored using standard beam deflection methods. A fast change in surface stress followed by a slower change is observed

until equilibrium is reached and schematically shown in figure 5.1 B. A compressive change in surface stress is observed for an applied potential greater than the potential of zero charge, $E >$ PZC. The first rise is correlated with the well-known double layer charging of the interface as observed in the current data. The slower change correlates to the diffusion of ions towards the surface until the electrode surface is screened and equilibrium conditions are established.The characteristic surface stress change amplitude A_n for each segment is defined as the distance between the last value of the first segment and the last value of the second segment. With the three-electrode configuration, the current vs. time response can be simultaneously measured (figure 5.1 C). A sharp current spike is first observed followed by a slower current decay until equilibrium conditions are reached. The sharp spike comes from the instantaneous change in potential and the subsequent instant drive of ions to the surface and has a time constant in the order of 10μs for an applied potential of 100 mV in a 1 mM solution [124]. More ions will then diffuse towards the electrode to form a complete double-layer. The potential here is low enough to inhibit electrochemical reactions (i.e. redox reactions), therefore, the current will fall back to zero after the double layer is formed and equilibrium conditions are established. The presence of faradaic processes (e.g. reduction/oxidation of gold) would lead to a constant current flow and the recorded current will not go back to zero. By decreasing the time of the applied potential pulse, larger I_{end} current values are recorded, because equilibrium conditions are not yet established. The recorded current can be integrated over time (and divided by the electrochemical area of the cantilever) to yield the charge density profile. The electrochemical area is determined by integrating the gold reduction peak of a cyclic voltammetry recorded in 50 mM $KClO_4$ and dividing this by the standard gold charge [112].

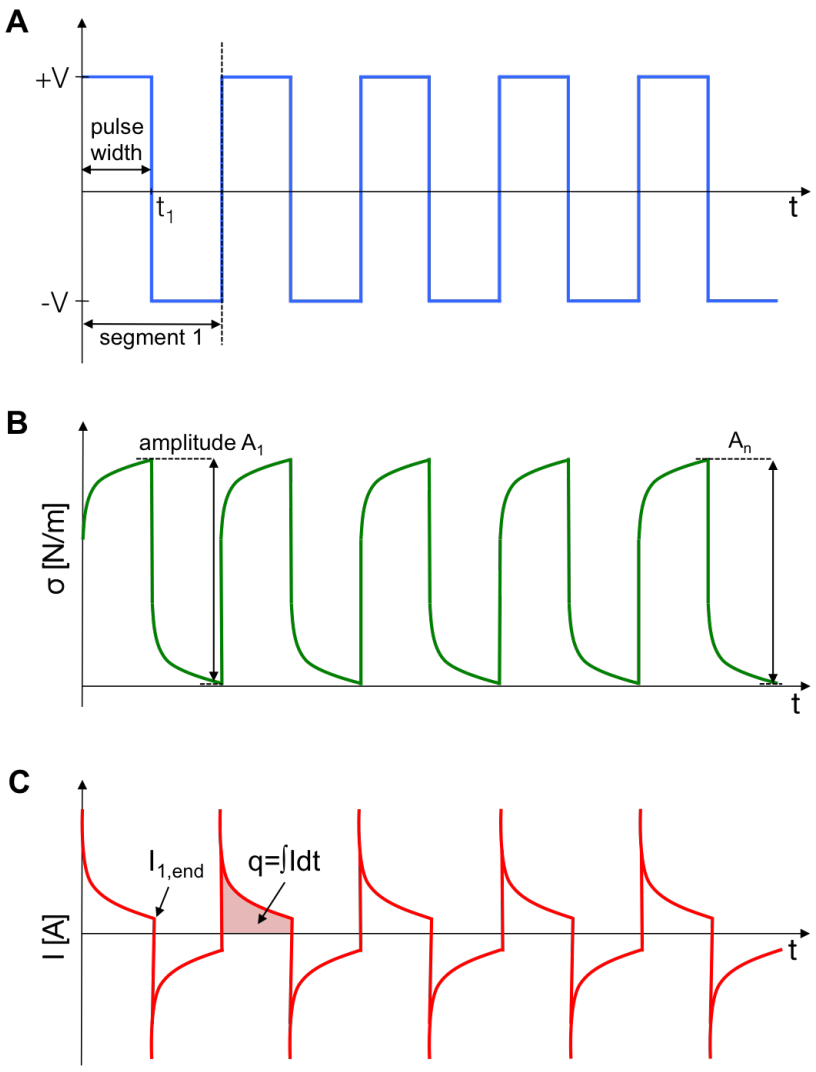

Figure 5.1: Schematics for fast potential switch measurement, showing the input voltage **A**, the surface stress response **B** and the current recording **C**

.

By varying the pulse width t_1, the change between equilibrium and transient conditions is monitored. The potential-dependent conditions are further studied by varying the applied potential between 0.1 V and 0.5 V. The surface stress increases with increased applied surface

potential, as more ions are directed to the surface inducing a larger surface stress signal.

If a potential step is applied to a system in solution, the current response is described by the Cottrell equation [65]. However, the Cottrell equation only describes the faradaic current which is observed after the initial double layer contribution. The initial current response is dominated by the charging current for the double layer formation and is expressed by:

$$i_{ch} = \frac{\Delta E}{R_s} exp\left(-\frac{t}{R_s C_d}\right) \tag{5.6}$$

with ΔE the potential step, R_s the serial resistance and C_d the double layer capacitance. The double layer capacitance C_d is described by the Gouy-Chapman-Stern model and is dependent on several parameter including the ion concentration ρ_0 and the electric potential ϕ. Both of these parameters are time-dependent and change over the course of the applied potential step. Therefore, this equation can only be solved numerically. Only recently have results been reported for saline solutions [124] and pure water [125]. For small gaps defined by $A >> d^2$, Marrow-Sato [126] derived the following equation so that the current, I, that is flowing due to an applied potential in a sodium chloride solution is described by:

$$I = \frac{A}{d}\left(e\int_0^d \left[\rho_{Na^+} W_{Na^+} - \rho_{Cl^-} W_{Cl^-} + D_{Na^+}\frac{\partial \rho_{Na^+}}{\partial x} - D_{Cl^-}\frac{\partial \rho_{Cl^-}}{\partial x}\right] dx + \epsilon_r \epsilon_0 \frac{\partial E}{\partial t}\right) \tag{5.7}$$

which is depended on the ion number density for sodium ions and chloride ions (ρ_{Na^+} and ρ_{Cl^-}), the ion drift velocities (W_{Na^+} and W_{Cl^-}) and the diffusion coefficients (D_{Na^+} and D_{Cl^-}). The ion drift velocity is the flow velocity that the ion has due to the applied potential field. This equation will result in the true total current flowing due to an applied voltage step.

In our experimental set-up the simplified Morrow-Sato shown in equation 5.7 is not valid, as small gaps are not present. The size of the electrode is much smaller than the distance between electrodes (in the order of cm). Therefore, it is not trivial to quantitatively

describe the current response without numerically solving the equation. In this paper, an experimental description of the current response due to short applied potentials is shown for chloride and perchlorate ions and correlated with surface stress measurements.

5.2.1 Materials and Methods

5.2.2 Gold Surface Preparation

Measurements are performed on a tipless silicon cantilever (CSC38, Mikromash, USA). The cantilevers are solvent cleaned (acetone, ethanol, isopropanol) before thermal evaporation of an adhesion layer of 2 nm Titanium followed by 100 nm of gold under ultra-high vacuum conditions. Evaporation rates for Titanium are set to 0.9 Å/s and 1 Å/s for gold (pressure $< 1\text{x}10^{-6}$ mBar, room temperature). Samples were stored under ambient conditions until needed. To define the electrochemically active area of the exposed gold in solution, a thin layer of Eccobond 286 (Emerson & Cuming, USA) is applied to the base of the gold-coated cantilever leaving a defined exposed area.

5.2.3 Electrochemical Cleaning

Prior to each experiment, the cantilevers are electrochemically cleaned by cycling the potential from -0.8 V to 1.4 V vs. Ag/AgCl (sat. KCl) in 50 mM $KClO_4$ at a scan rate of 20 mV/sec until a reproducible signal is observed. All electrochemical measurements are performed in a three-electrode configuration, with a platinum wire as the counter electrode (1 mm diameter, Alfa Aesar, USA), the cantilever as the working electrode and an Ag/AgCl (sat. KCl) reference electrode (BASi, USA) as the reference. Electrochemical measurements were performed using a CHI 1030A (CH Instruments, USA) potentiostat.

5.2.4 Surface Stress Measurements

After the electrochemical cleaning step, cantilevers are immersed into a 1 mM solution of either sodium chloride (NaCl) or sodium perchlorate ($NaClO_4$). All solution are purchased from Sigma-Aldrich (USA) and are prepared using Mili-Q water. Five potential pulses (segments) between ± 0.1 V to 0.5 V are applied to the cantilever. The potential pulses are varied from 1 sec to 0.1 ms. Surface stress changes are measured by standard beam-deflection methods. A laser is aligned to the cantilever so that a change in bending due to an applied potential can be measured with a position sensitive diode (PSD). By using Stoney's formula [73], the measured change in voltage of the photodiode can be converted into a surface stress change. Simultaneously, the current is measured using the potentiostat.

5.3 Results and Discussion

5.3.1 Weak versus Strong Adsorbing Ions

Current and surface stress measurements were done on a gold-coated cantilever in two different solutions: 1 mM $NaClO_4$ and 1 mM NaCl. The latter one contains strongly adsorbing chloride ions and the first one more weakly adsorbing perchlorate ions. Chloride, like other halides, is a quasi-spherical anion with its negative charge well distributed. It can therefore easily share its negative charge with an empty d-orbital from the gold surface to form a dipole. Perchlorate ions, however, have their negative charge not well distributed, because only one of the four oxygens is negatively charged. Interactions with gold are therefore less efficient. Chloride ions have an ionic radius (including the hydration shell) of 167 pm, whereas perchlorate ions are roughly twice as large at 309 pm [127]. This means fewer perchlorate ions can interact with the surface per unit area and that each perchlorate ion

interacts weaker with the gold surface than a chloride ion.

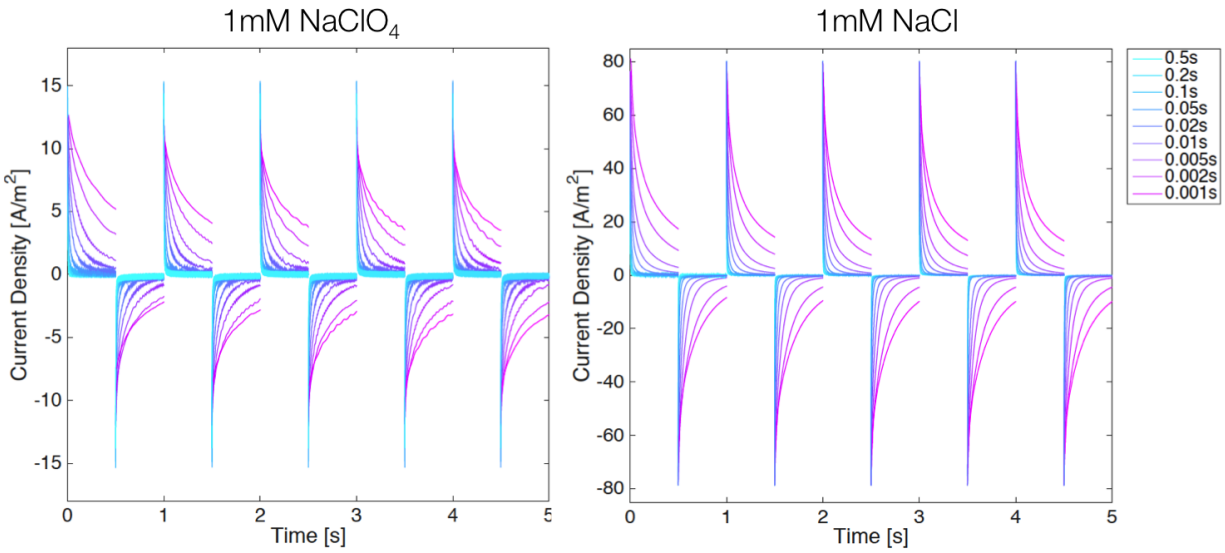

Figure 5.2: Current response for 1 mM $NaClO_4$ and NaCl for a potential pulse at ± 0.2 V vs. Ag/AgCl (sat. KCl). The current is plotted vs the segment meaning that each pulse width is stretched. The pulse width is varied from 0.5 s (light blue) to 0.001 s (pink). The x-axis is normalized to the segment length. Note the difference in the current axis for both plots.

For all measurements, 5 potential pulses between ± 0.2 V (vs. Ag/AgCl (sat. KCl)) are applied to the cantilever in a three-electrode configuration. The pulse width is then decreased from 0.5 s to 0.001 s. All current values are converted into current density by dividing the current with the electrochemical surface area of the electrode. In figure 5.2, the current response for all pulse widths are shown. For better clarity, all segments are stretched in the x-direction so that the length of the pulse is the same. Clearly, the maximum peak current value is smaller for $NaClO_4$ than for NaCl, 14 A/m^2 and 70 A/m^2. For longer pulse width, the current decays to values close to zero (light blue traces). However, for potential pulses shorter than 0.05 s current values higher than zero are measured. This is because the potential is switched before the current reaches equilibrium. This behavior is observed for

both solutions. .

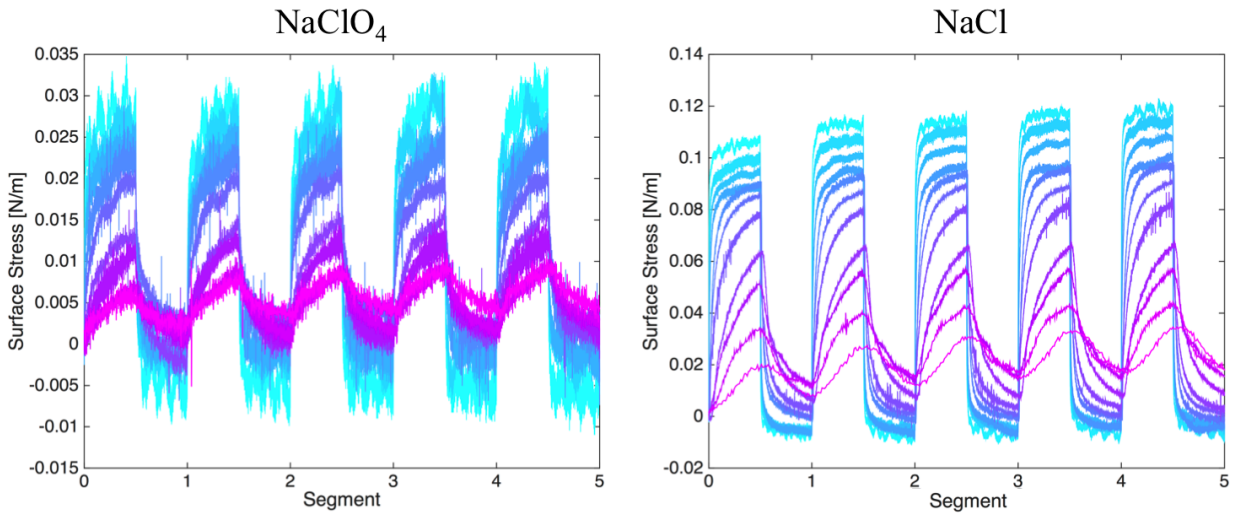

Figure 5.3: Surface stress response for 1 mM $NaClO_4$ and NaCl for a potential pulse at ± 0.2V (vs. Ag/AgCl (sat. KCl) with a width of 0.5 s (light blue) to 0.001 s (pink). The x-axis is normalized to the segment length.

The corresponding surface stress response for both solutions is shown in figure 5.3. Results for $NaClO_4$ show a maximum surface stress change amplitude of 35 mN/m for the longest pulse (0.5 s, light blue). This surface stress amplitude reduces to less than 7 mN/m for the shortest measured pulse (0.001 s, pink). As expected, for NaCl the surface stress change is larger and decreases from 120 mN/m to 18 mN/m. A roughly 3.5-times increase in surface stress is observed for the more strongly adsorbing chloride ions corresponding to a similar increase in the current peak (figure 5.2). Clearly, to achieve a large surface stress signal in potential-driven measurements a chloride-containing solution is the preferred choice [1].

To emphasize the correlation between the measured current density and surface stress change, the current value I_{end} for all segments at positive bias as well as the the surface stress

change amplitude are plotted for all pulse widths, see figure 5.4. The positive bias response is of greater interest, as it is responsible for the direction of chloride or perchlorate ions to the surface. Therefore, to compare weak vs. strong adsorbing anions, only the positive bias is plotted and discussed here.

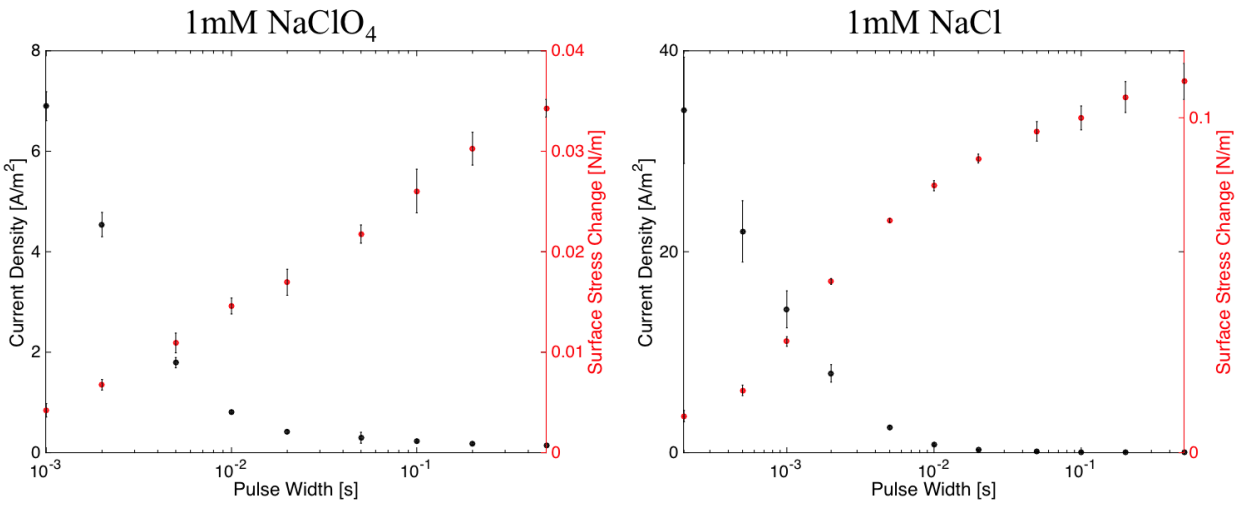

Figure 5.4: Current and surface stress change amplitude versus pulse width for all segments. The equilibrium current at the end of each positive potential step is plotted. The mean values of the surface stress and current for five consecutive segments along with the standard deviation is plotted.

For longer potential pulses (>0.2 sec), the current decays almost back to zero by the end of the pulse as demonstrated in figure 5.2. A drastic increase of this current is observed for shorter pulses. This increase is observed for NaCl and $NaClO_4$, however, overall current values are less for perchlorate ions as they interact more weakly with the surface. For the surface stress change, a continuous decrease for shorter potential pulses is observed. It seems that the current response reaches an equilibrium for longer pulses (near zero), whereas the stress is still changing. This is the case for both ions tested and due to the fact that the current does not completely decay back to zero, but rather still shows an equilibrium value

of around 100 nA for all longer potential pulses. This current comes from the chloride and perchlorate bulk diffusion. The surface stress is not only sensitive to the changes near the surface, but rather extends to changes in the bulk.

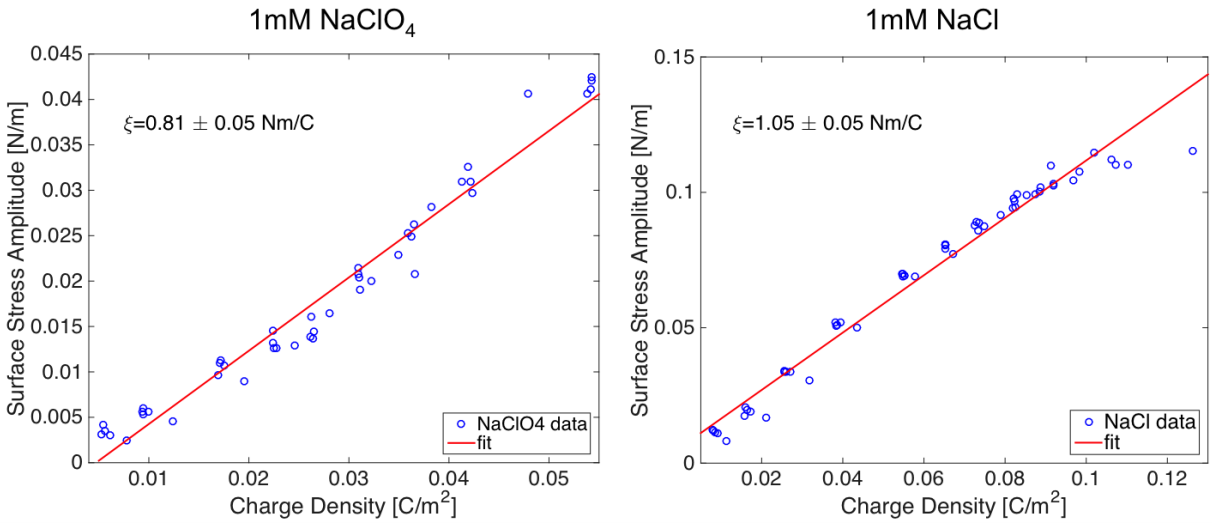

Figure 5.5: Surface stress amplitude and charge density for potentials at +0.2V (vs. Ag/AgCl (sat. KCl)) for 1mM $NaClO_4$ and 1mM NaCl. The data points for all potential pulses are plotted and a linear line in the form of $y = \chi * x$ is fitted.

To further investigate this, the current is integrated over time and divided by the electrochemical area of the cantilever so that the charge density can be plotted. The charge density is calculated for all positive potentials. In figure 5.5, the surface stress amplitude is plotted against the charge density to measure correlation. A strong linear dependence is found with a slope of 0.81 V $\pm$ 0.05 V for $NaClO_4$ and 1.05 V $\pm$ 0.05 V for NaCl. Note that values here are positive, due to the fact that absolute surface stress changes are measured. By analyzing the raw surface stress response, a negative compressive change is observed, leading to negative coefficient values. Although the current reaches an equilibrium value, the charge increases continuously as the pulse length is longer and more charge reaches the

surface of the electrode. The charge density response resembles the surface stress change amplitude very well. On first sight it seems that the surface stress is more sensitive to the ions for longer pulses, whereas the current does not give us any more information for longer pulses.

So far, the current and surface stress response for weak (perchlorate) and strong adsorbing ions (chloride) as well as the linear relationship between charge density and surface stress was discussed. A more detailed discussion about this linearity follows in the next section.

5.3.2 Linear Correlation Between Surface Stress and Charge Density

A closer look at the slope of the surface stress change - charge density coefficient leads to further insight into the dynamics of the system. As discussed above, this coefficient ξ is described by the slope of the plot and is a measure of how much the surface stress changes upon a change in charge density.

In the following, potential pulses from 0.1 V to 0.5 V are applied to the gold-coated cantilever electrode. The potential width is decreased from 1 sec to 0.1 sec, 0.01 sec and 0.001 sec and the resulting surface stress and charge density are simultaneously recorded. The cantilever surface stress change versus charge density plots for decreasing potential pulses in 1 mM NaCl are shown in figure 5.6. The mean and standard deviation for five independently performed experiments on different cantilevers are plotted and a linear fit in the form of $m * x$ is fit to the data. It is assumed, that at zero charge density, no surface stress is observed, therefore, no y-offset is applied.

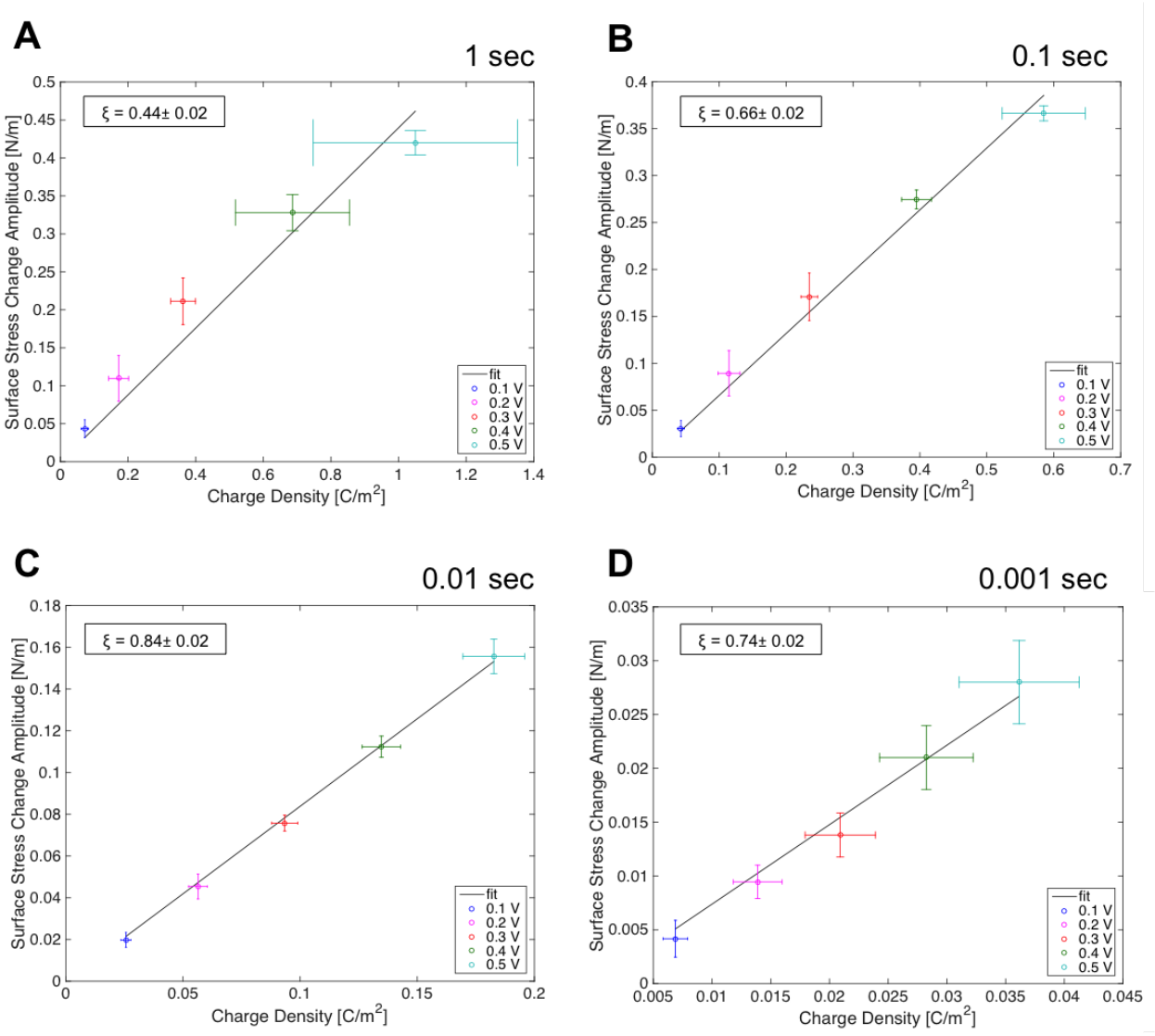

Figure 5.6: Surface stress change - charge coefficient for decreasing potential pulses (1, 0.1 sec, 0.01 sec and 0.001 sec) at potentials between 0.1 V and 0.5 V (vs. Ag/AgCl (sat. KCl)) in 1 mM NaCl. The potential-dependent surface stress and charge density mean and standard deviation for five different cantilevers are plotted.

An increase in the coefficient is seen for shorter pulses, from 0.44 V ± 0.02 V for 1 sec to 0.74 V ± 0.02 V for 0.001 sec. This increase in coefficient for shorter pulses results from

an increase in slope, as shown in figure 5.7. A larger slope means that a small change in charge results in a higher change of surface stress signal, indicating that the sensor is more sensitive to changes in charge for shorter pulses.

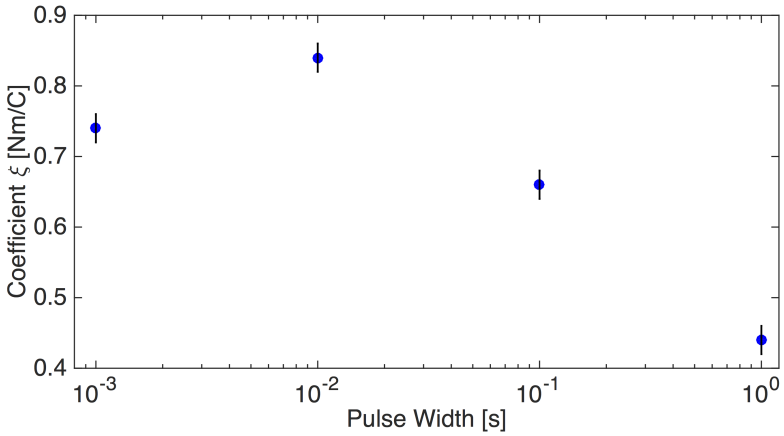

Figure 5.7: Coefficient ξ values for decreasing different potential pulses. A clear coefficient decrease is observed for longer pulses. The errorbars result from the error of the linear fit for five consecutive potentials.

One explanation for this effect could be that for shorter pulses the initial double layer charging is measured, which happens on a faster time scale. For these pulses at 0.001 sec, only the first few layers contribute to the cantilever measurement, showing that the sensitivity is higher for the first layers than for the bulk diffusion. As observed in figure 5.2, the current decays more rapidly first, followed by a slower response until the system reaches equilibrium. Therefore, for longer pulses, the additional diffusion of ions towards the surface is measured. In summary, the surface stress - charge coefficient ξ changes for faster potential pulses and is most sensitive to the initial charge than for the ion diffusion from the bulk.

5.3.3 Deviation of Surface Stress and Current

For now, we have only looked at the mean of all five potential segments. However, taking a closer look at the evolution of the signal within the same potential and pulse setting, an interesting behavior can be observed.

In the following figures, the time evolution of the current response for all segments is investigated in detail. In figure 5.8, the current response at +0.2 V for a variety of potentials pulses is shown. To better visualize the difference of the data, only the first 6 ms of the response is shown. The current trace is identical for all pulses during the first segment. However, looking at the last segment, a clear deviation of the current trace is observed.

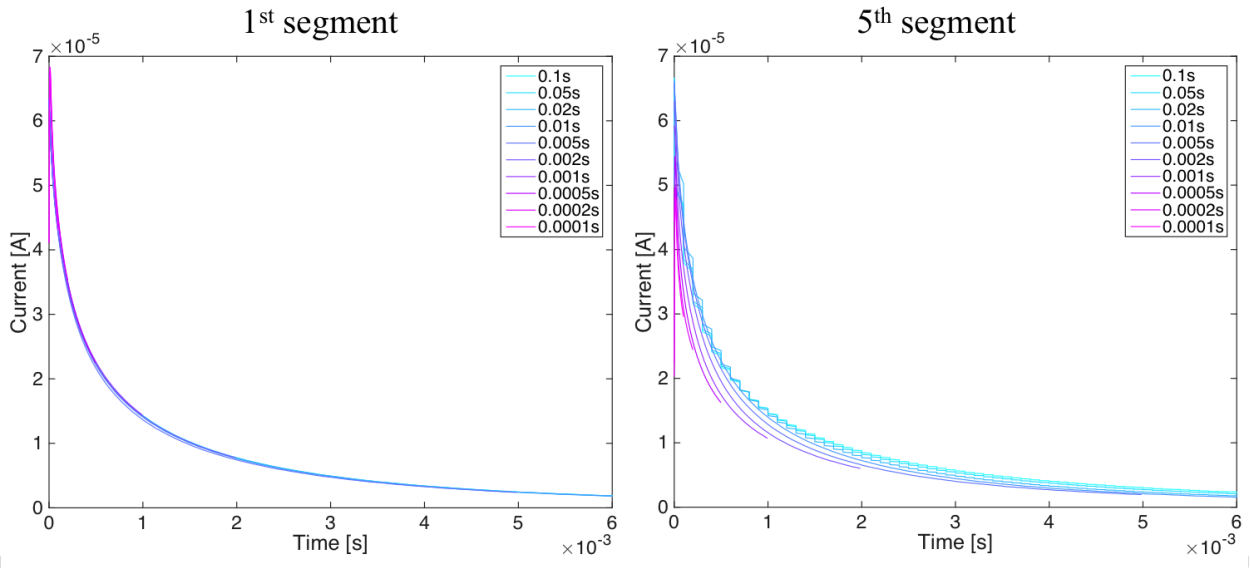

Figure 5.8: Current vs. time response for varying pulse width for first and fifth segment. The response at -0.2 V is shifted vertically for better presentation.

We assume that for shorter potential pulses non-equilibrium conditions are measured indicating that the double layer can not build up properly, therefore a shorter Debye length

is probed. For the first pulse, a chloride layer builds up at the electrode surface at positive bias. This layer will partially be removed at negative bias, before it is being established again during the second segment. Charges from the chloride ions that are not removed completely, will be taken over to the next segment resulting in higher current values for subsequent segments. The local chloride concentration is increased for each segment for shorter potential pulses. In the next section, the specific response of the surface stress - charge coefficient to these local changes is discussed.

As briefly shown in figure 5.6, a linear relationship between the surface stress amplitude and the charge density is observed. This linear relationship behaves differently within the five consecutive segments measured. The stress vs. charge density plot for two different potential pulses, 0.1 sec and 0.001 s (figure 5.9 for a cantilever response in 1 mM NaCl at potentials between $\pm$ 0.1 V and $\pm$ 0.5 V (vs. Ag/AgCl (sat. KCl)) is shown. The coefficient is plotted for each of the five segments by fitting a linear curve through the points, assuming that at zero charge, there will be zero surface stress response. For shorter pulses, the deviation of the coefficient within the same potential step is more pronounced than for longer pulses. The errors are from the fitting of the experimental data.

The coefficient is in units of Nm/C (or Volts) which can also be used to define the sensitivity of the cantilever response, as it is a measure of how much surface stress change is measured for a given change in charge. As shown by the fitting, the coefficient values (sensitivity) increases with segment number, from 0.46 V $\pm$ 0.06 V for the first segment to 0.96 V $\pm$ 0.17 V for the fifth segment for potential pulses of 0.001 sec. This increase can be explained by the carrying over of extra charge into higher segments. The current response does not reach equilibrium conditions, therefore, the double layer is not completely built up by the time the potential switches. Therefore, extra chloride ions will be transferred into the next segment. This increases the local concentration of chloride ions and less chloride from the bulk is needed for the new double layer build-up.

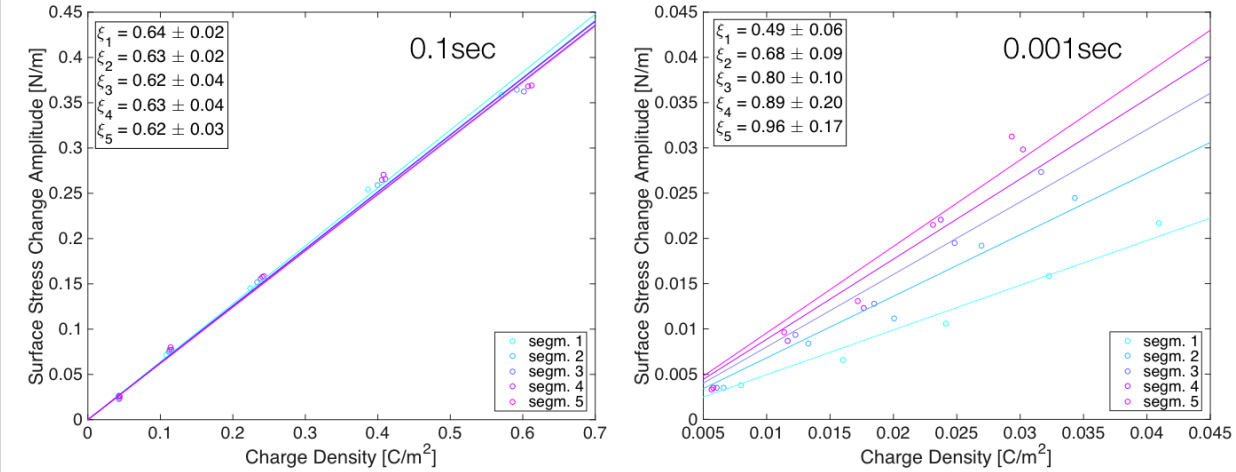

Figure 5.9: Surface stress change - charge coefficient for each of the five positive potential segments. In A, the response for a potential pulse of 0.1 sec is plotted and in B for 0.001 sec.

We thus interpret that the first segment probes a thicker doubler layer than the last segment. The double layer thickness is described by the Debye length λ_d as κ^{-1}:

$$\kappa^{-1} = \sqrt{\frac{\epsilon\epsilon_0 k_B T}{2e^2\rho_0}} \tag{5.8}$$

with ρ_0 the ion concentration, ϵ the dielectric constant of the medium and ϵ_0 the vacuum permittivity. The Debye length quantitatively describes the thickness of the diffuse layer and, therefore, how far into the solution a surface potential reaches. The Debye length in a 1 mM sodium chloride concentration is 96 Å. If the local concentration ρ_0 is increased for each segment, the Double layer thickness will be decreased. This is in line with the results shown in figure 5.6, where higher sensitivities are reached for shorter pulse as this probes a thinner layer.

5.3.4 Segment-specific Behaviour

To take a deeper look at this behavior, the results for three different potential pulses (0.1, 0.01 and 0.001 sec) for a potential range between ± 0.1 V and ± 0.5 V (vs. Ag/AgCl (sat.KCl)) are shown. In figure 5.10, the surface stress versus charge density plot for 1 mM NaCl (red) and 1 mM $NaClO_4$ (blue) are shown. The direction of the data within the segments is highlighted by an arrow pointing from the first to the fifth segment. The signal changes most prominently between the first and the second segment and then rapidly seems to reach a steady-state value.

It is expected that an increase in charge density results in an increase of surface stress change. However, this is only observed for NaCl at longer potential pulses. In contrast, for $NaClO_4$ and for short potential pulses (0.001s) a decrease in charge density and an increase in surface stress is observed for consecutive segments at the same potential. This can be explained by the fact that for short pulses, the system does not obey equilibrium conditions anymore and an incomplete double layer is built up. Therefore, for the next pulse, the different starting state leads to the observed different dynamics.

It is seen that for the 0.1 s pulses (figure 5.10 A) the correlation between stress and charge density is linear within all segments for NaCl (red). This is expected, as more charge will accumulate on the surface with each segment, and this results in a larger surface stress change. However, decreasing the potential pulse to 0.1 s and 0.001 s (figure 5.10) changes this relationship. Within one potential setting (e.g. 0.5 V at 0.001 sec), the charge density decreases with the segment number whereas the surface stress change increases. Here, the charge decreases due to the increased local chloride concentration, as the system does not obey equilibrium conditions. Because the double layer does not build up completely, chloride ions from previous segments, are being carried over into the next segment.

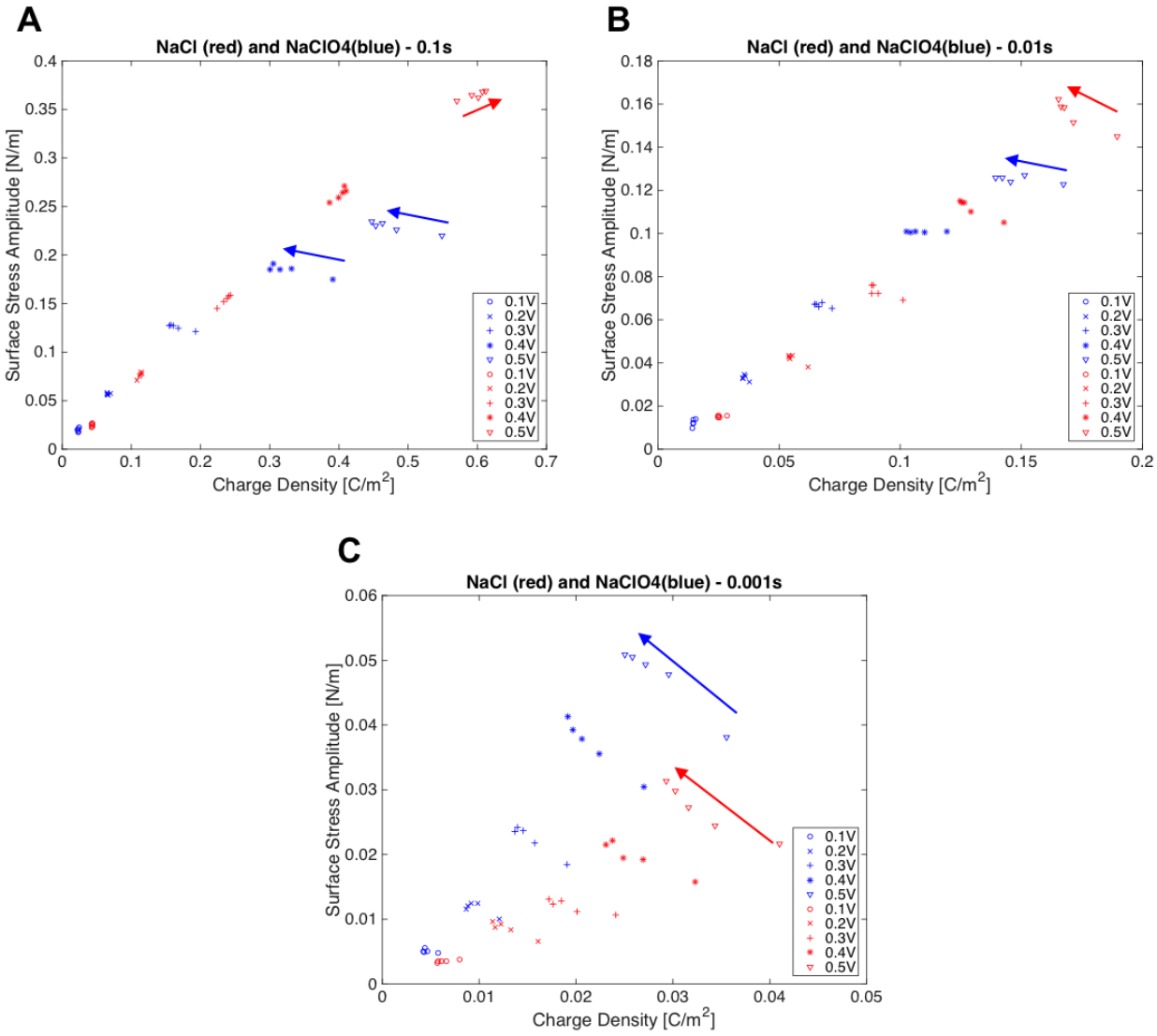

Figure 5.10: Surface stress change amplitude of the cantilever vs. the charge density measured from the current response for 1 mM NaCl (red) and 1 mM $NaClO_4$ (blue) for pulses of 0.1 s, 0.01 s and 0.001 s.

We assume that the increase in concentration changes the starting conditions of the pulse and therefore fewer ions are needed to build up the double layer for the next segment since

the double layer thickness is inversely proportional to the ion concentration. This leads to a decrease of current flow and thus charge density as observed in figure 5.10B and C. On the other, the increase of concentration near the surface leads to an increase in surface stress change. Therefore, for shorter potentials (<0.1 sec). the charge is inversely dependent on the surface stress ($q \propto 1/\sigma$) within consecutive segments. The effect within the segments is, however, dependent on the diffusion coefficient of the anion being probed. If the potential pulse is slow enough so that equilibrium conditions are met, a linear dependence between surface stress and charge is observed. This is the case for the chloride ions at longer potential pulses (0.1 s). However, the inversely proportional effect is observed for perchlorate ions, as the diffusion time for these ions is longer (1.79 x 10^{-9} m^2/s for $ClO4^-$ and 2.03 x 10^{-9} m^2/s for Cl^-) [128].

5.4 Conclusion

In summary, the time-dependent evolution of the surface stress and current signal of a gold-coated cantilever in a 1 mM NaCl and $NaClO_4$ solution is observed. Potential values between $\pm$ 0.1 V and $\pm$ 0.5 V (vs. Ag/AgCl (sat. KCl)) with decreasing potential width form 0.1 sec to 0.1 ms are applied to the gold-coated cantilever electrode. Larger surface stress and current values are recorded for the stronger adsorbing chloride anion than for the weaker adsorbing perchlorate. By comparing the charge density with the surface stress, a linear relationship is found which is in agreement with previous studies [88, 89, 116]. Decreasing the potential pulse up to 0.001 sec results in an increase of the surface stress-charge coefficient. A shorter pulse results in an incomplete double layer and therefore a thinner charge layer is probed. The coefficient is a measure of the sensitivity of the sensor, therefore, we conclude that for shorter pulses, a higher sensitivity is observed. The charge from this result in a higher change of surface stress than the compensating charge coming from the bulk diffusion

being measured for longer pulses.

By analyzing the coefficient response for five consecutively applied segments, a variation is observed. For 0.001 sec, the coefficient for the first segment is smaller than for the consecutive segments (0.46 ± 0.06 Nm/C for the first and 0.96 ± 0.17 Nm/C for the last segment). The coefficient reaches a steady state after more than five segments in the case of 0.001 sec and after three segments in the case of 0.01 sec. The local ion concentration increases due to the non-equilibrium conditions leading to a decrease in Debye length and, therefore, an increase in sensitivity. This is in agreement with the previously found increased sensitivity when a thinner layer is probed (faster potential pulses).

Lastly, it is shown that for fast pulses, the charge density appears to be inversely proportional to the surface stress change, $q \propto 1/\sigma$. As observed, the charge density decreases for increasing segments. This is assumed to be due to the extra chloride ions being transferred into the next segment. The extra ions increase the local concentration near the electrode and the charging current needs to be smaller, as less charge is needed to screen the electrode surface. This leads to a decrease in charge density with increasing segments. On the other hand, this increase in concentration leads to an increase in surface stress change as more ions contribute to the overall change in surface stress. Larger absolute surface stress values are measured due to the increased concentration.

As discussed above quantitatively describing this system is not trivial, as all parameters are time-dependent. However, by numerically solving the particular current response for these fast switching potentials, one can extract the changes in ion concentration for each segment, as well as the resulting change in double layer thickness. This calculation will help to further utilize this concept for biosensing applications. The charge response of a

biomolecule attached to the cantilever surface can be probed by reducing the applied pulse width and thus reducing the probed Debye length. It has been demonstrated that charges along an antigen can be probed by changing the concentration of the probing solution [129]. A local change in concentration can be achieved with fast potentials or in observing the response as a function of the segment number, as outlined above. Consecutively applied potentials could, therefore, measure the contribution of the charge and surface stress change along a molecule. The advantage of this method is that experiments can be performed very fast (within minutes) and are label-free. The biomolecules do not need to be labeled with e.g. a fluorescence molecule.

6

Conclusion

Understanding the origin and the evolution of surface stress signals are of great interest for biochemical sensors and for fundamental studies of adsorption on a metal surface. We have used a gold-coated cantilever to measure surface stress changes upon binding of molecules or adsorption of ions. In this thesis, a cantilever acting as a working electrode is electrically connected to a reference and a counter electrode in solution. The electrochemical setup serves multiple purposes. It is used to clean the electrode surface electrochemically as well as to apply potential pulses to the cantilever to drive ions to the surface and measure changes in the surface stress of the gold layer. The bond charges at the surface of a clean metal electrode are missing a neighboring atom and therefore, the electronic charge is redistributed and flows between the gold atoms at the surface. This redistribution of charges results in a tensile stress of the metal [53, 54]. Applying a positive potential to a gold-coated cantilever in a sodium chloride solution will lead to the accumulation of negatively charge chloride ions near the surface. These ions will modify the electronic charge distribution of the gold surface and generate large compressive surface stress changes. This potential-

induced surface stress is proportional to the available gold area and leads to larger surface stress values compared to measurement operated at the open-circuit potential, as ions are specifically directed to the surface. The bending of the cantilever is measured by standard beam deflection methods and a position sensitive photodiode (PSD).

In particular, in chapter 3 the fundamentals for increasing the signal-to-noise ratio by cleaning and a method to detect oligonucleotide binding on a cantilever by measuring the surface stress pattern is shown. Furthermore, it is demonstrated how important the cleanliness of the electrode surface is and a successful electrochemical *in-situ* cleaning protocol is presented. By sweeping the potential applied to the cantilever between -0.8 and 1.4 V in 50 mM $KClO_4$ (vs. Ag/AgCl (sat. KCl)) until a reproducible cyclic voltammogram is obtained, clean and well-defined surfaces are achieved that systematically lead to large surface stress changes. X-Ray Photoelectron Spectroscopy (XPS) measurements verify the effectiveness of the cleaning method. The advantage of this protocol is that the sensor can be cleaned *in situ* and is compatible with standard materials used in biosensors application (e.g. Polydimethylsiloxane (PDMS)). Most other methods use harsh chemicals that require the cantilever to be cleaned externally and are thus not compatible with sensor integration in a compact system. A large signal-to-noise ratio for SAM-modification on a cantilever can be achieved by carefully monitoring the probe coverage of the sensor. It is shown that optimal surface stress changes are obtained for submonolayer coverage [42, 130]. These experiments confirm that the surface stress change is proportional to the available gold area. If the surface is completely occupied e.g. a full layer of oligonucleotide probes or other contaminants, the surface stress signal vanishes, as no gold on the surface is available for the ions to interact with. Finally, long-term stability measurements were performed in a buffer solution of Tris-HCl 10 mM NaCl 50 mM and it is shown that after 10 hrs a deviation in the surface stress signal is observed and further cleaning steps are necessary.

In chapter 4, an *in situ* method to selectively functionalize gold electrodes with different probes at submonolayer coverage was presented. A scalable method to modify multiple adjacent electrodes with different probes is of great interest for metal-based sensors. For many surface stress-based sensors, submonolayer coverages are desired to optimize response time and signal-to-noise ratio [1, 42, 63, 64]. Our presented technique shows for the first time a selective *in situ* method that achieves submonolayer coverages. The method presented does not require external apparatus to functionalize the sensor array. The modification process is done under potential-control of the gold electrode, to achieve excellent coverage within minutes [96, 101, 102]. Two different gold electrodes were functionalized, each with an electrochemically distinct alkylferrocene adsorbate: Fc-CO-C_{11}-SH and Fc-C_{11}-SH. Three key potentials are distinguished: E_{ads} (+0.3 V) held at slightly cathodic potentials enhances the alkanethiol adsorption rate. E_{des} (-1.4 V) inhibits adsorption by maintaining the electrode in a reductive (alkylthiol) desorption state. Lastly, E_{hold} (-0.6 V) holds the state of a modified ferrocene alkanethiol electrode by hindering the adsorption of new alkanethiols via electrochemically-promoted exchange reactions. Cyclic voltammograms measured in 100 mM $NaClO_4$ are recorded to show the successful selective modification. Two distinct electrochemical peaks corresponding to either the Fc-CO-C_{11}-SH or the Fc-C_{11}-SH are measured on each electrode. Cross-coverage values are measured to be less than 4 % of the full coverage.

In the last chapter of this thesis, the linear relationship between surface stress and charge density was further studied. As shown in previous sections, by applying a potential step to a metal electrode in solution, ions will adsorb onto the surface and cause a compressive surface stress change. This surface stress will reach an equilibrium once a complete double layer is built up and all charges are screened. For now only equilibrium surface stress con-

ditions are measured to make sure that all surface reactions took place and large surface stress signals are achieved, see chapter 3. However, by applying short pulses of as low as 0.1ms, this equilibrium condition is not achieved anymore and the temporal evolution of the current and surface stress measurement can be studied. Here, the gold-coated cantilever is exposed to a solution of 1 mM $NaClO_4$ or 1 mM NaCl and a series of short potential pulses are applied. By comparing the surface stress change with the charge density, we have found that the cantilever sensor is more sensitive for shorter pulses. A shorter pulse means that the double layer does not fully build up and, therefore, a thinner double layer is generated. The slope of the surface stress against charge density plot is defined by the coefficient ξ and has units of Nm/C or V. The larger the slope the more sensitive the cantilever, as a smaller change in charge density results in a larger change in surface stress change. Additionally, by consecutively switching the potential applied to the gold-coated cantilever electrode on fast time scales, non-equilibrium conditions are generated. The potential is switched before the double layer fully screens the surface and extra ions are retained into the following potential segments. This results in a larger local ion concentration near the electrode surface and a decrease in double layer thickness as less charge is needed for screening. We found that higher sensitivities and a larger absolute surface stress due to the increased concentration is measured. This opens up a new field of label-free sensing for location-specific charges as emphasized in the outlook section.

7

Outlook and Proposed Experiments

This thesis provides insights into the fundamentals of understanding surface stress sensing of cantilever-based systems. What started as an application-driven project resulted into a more fundamental study of the generation and evolution of surface stress signals. The cantilever-based setup helps us to understand the fundamentals to design better biosensors. In the following, some ideas where this project can lead to and how other fields can benefit from the results of this thesis, are discussed.

Measuring Conformational Changes

With the surface stress patterns introduced in chapter 3 we can look at the dynamics of biomolecules attached to the gold-coated cantilever under potential control. As already shown, characteristic patterns can be seen for single stranded (ssDNA) and double stranded DNA (dsDNA) [1, 42]. Because of the negatively charged backbone of the DNA, it reacts to changes of the surface potential. At negative potential, it repels from the surface and for positive potential it is lying down. With this technique, differentiation can be made between

ssDNA and dsDNA, as ssDNA is more flexible and can therefore react faster to changes of the surface potential, whereas the more rigid dsDNA reacts slower. With this understanding conformational changes of molecules due to binding effects can be distinguished. For this aptamers which are single-stranded DNA or RNA molecules are of great interest, as they can bind to preselected targets including protein and peptides with a high affinity and specificity [131, 132]. They undergo conformational changes upon binding which can change the stiffness of the molecule. As explained above, the stiffness of a molecule results in different surface stress patterns. In addition, a more compact structure will have a larger footprint on the sensor, letting less ions interact with the surface and leading to smaller surface stress signals. Hence, conformational changes due to binding can be measured with surface stress.

Selective Modification Protocol

The selective *in situ* modification protocol presented in chapter 4 shows a technique to modify two different ferrocene moieties on two gold-coated electrodes. We have successfully shown for the first time an *in situ* method to achieve submonolayer coverage for the selective modification of two different ferrocene alkanethiols. This principle can be further extended to different thiolated molecules, e.g thiolated oligonucleotides. The required potentials should be in the same region as described in chapter 4, as a thiol is used for the attachment on gold. However, the additional charge on the oligonucleotide could result in additional effects. A complete potential and coverage analysis needs to be done, in order to understand these specific contributions. In addition, this protocol can be expanded to different functional groups, e.g. cyclic disulfide to better understand the Au-thiol bond, as this is not yet completely understood [133, 134]. Last but not least, an array of electrodes can be modified with this technique. It would be interesting to measure the cross-coverage value as a function of modification steps and at what point additional electrochemical cleaning is necessary. With this one can understand how scalable this technique is for real-life biosensors.

Sensitivity for Different Ions

Based on chapter 5, the determination of the cantilever sensitivity to a larger variety of ions can be studied. For now, the surface stress - charge coefficient ξ is measured in 1 mM NaCl and 1 mM $NaClO_4$. This measurement can be extended to different ions and concentrations for a specified potential window. Lipkowski et al. [70] showed that the Gibbs excess which defines the surface concentration changes by varying the potential for different ions, see figure 7.1. A larger Gibbs excess value results in more adsorption on a surface and therefore, a larger change in surface stress, as the charge is proportional to the surface stress. By fine-tuning this potential, adsorption of one ion can be favored whereas the adsorption of other ions can be inhibited. In addition, the individual surface stress contributions of contaminants at different potentials can be studied. This could help to understand the specific contribution of different ions for real-life biosensors that use a serum as their analyte. The serum contains not only the ion of interest but many more. Additionally, the adsorption strength on polycrystalline gold can be further studied and different metal coatings can be tested.

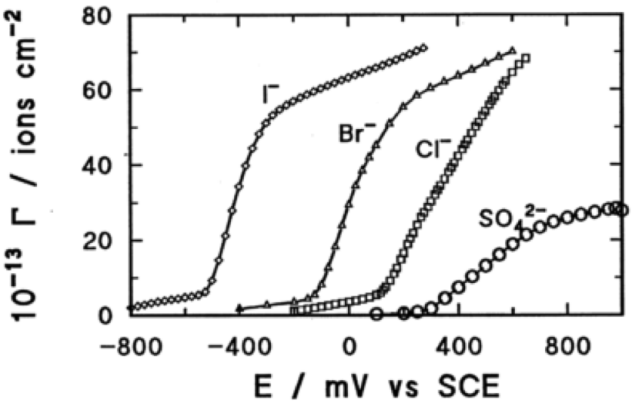

Figure 7.1: Gibbs excess for different ions at varying potentials (adapted from [70])

Lithium Iron Phosphate Battery

The charging and discharging principles of lithium iron phosphate ($LiFePO_4$) batteries are not yet completely understood. Understanding these principles, could lead to more efficient battery materials. In particular, the transport mechanics inside these materials could be studied with our cantilever-based surface stress sensors. By making a cantilever out of the $LiFePO_4$ material, the changes in surface stress due to an applied voltage can be studied. As shown in figure 7.2, the lithium iron phosphate has ion channels along its b-direction. Lithium ions can diffuse through these channels. If the cantilever is oriented so that these ion channels point towards the electrode surface, Lithium ions can be directed into these channels upon applying a negative potential. The dependence of the surface stress on the orientation of the ion channels to the surface could be studied.

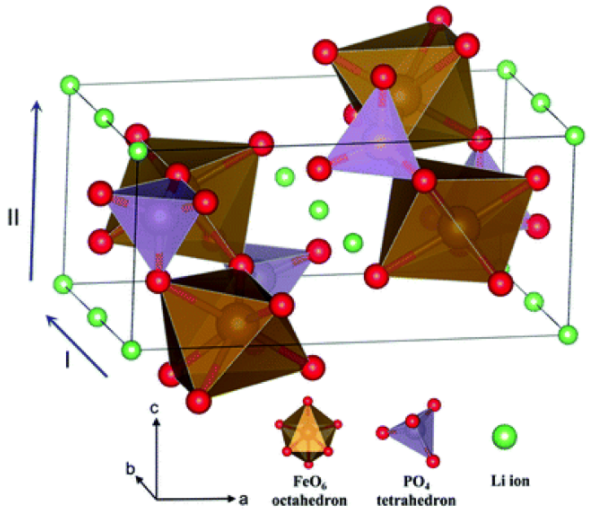

Figure 7.2: Structure of lithium iron phosphate ($LiFePO_4$) with the Lithium ion channels in the b-direction (adapted from [135]).

Numerically Solving Current Response

As shown in chapter 5, by applying fast potential pulses to an ionic solution, non-equilibrium conditions can be created. The double layer charging is not in equilibrium for short pulses. This results in changes of the local concentration as well as changes in the current response. Therefore, quantitatively describing this system is not trivial, as all parameters are time-dependent. However, by numerically solving the particular current response for these fast switching potentials, one can extract the changes in ion concentration for each segment, as well as the resulting change in double layer thickness. Furthermore, ion diffusion coefficients can be calculated. This will help to better design future experiments.

Spatially Resolving Biomolecules

By applying fast potential pulses to the cantilever system one can locally increase the ion concentration near the surface, as shown in chapter 5. This leads to an increase in sensitivity of the surface stress sensor and a decrease in the Debye length. The Debye length is inversely proportional to the concentration: the higher the concentration, the shorter the Debye length. By attaching an antigen or another small biomolecule to the surface of the cantilever, one could slowly probe the response along the axis of the molecule, by reducing the Debye length, as shown in figure 7.3.

It has been demonstrated that charges along an antigen can be probed by changing the concentration of the probing solution [136]. However, in this study the solution has to be changed, whereas we can change the concentration by applying fast potential pulses. As mentioned above, with the help of numerical solutions to this problem, one can fully understand by how much the concentration changes and, therefore, the Debye length.

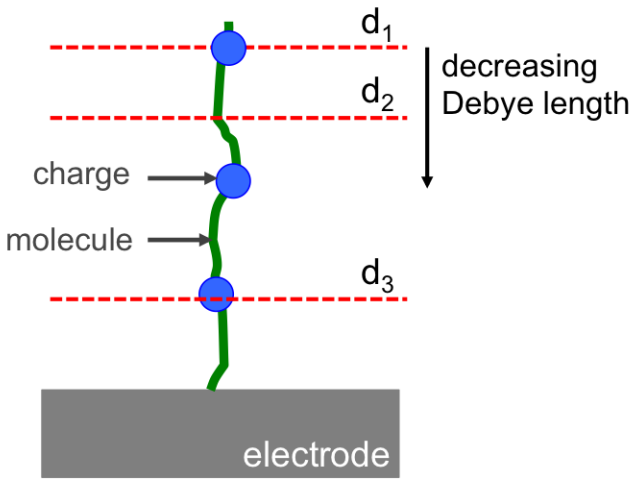

Figure 7.3: Schematics for the tuning of the Debye length due to an applied potential switch. Here a molecule (green) with charges at specific locations along the molecule (blue) is shown. The faster the potential switch, the shorter the probed Debye length.

In general, the Debye length is described by equation 5.8. A change in concentration from 1 mM to 2 mM will result in a 2.82 nm decrease in Debye length (from 9.62 nm to 6.80 nm). Consecutively applied potentials measure the contribution of the charge and surface stress change along the molecule. These charges could reside along the molecule, e.g. potassium ions that bind to oligonucleotides [137]. In this measurement, the duration of the first applied pulse defines the initial Debye length and the continuing short potential pulses reduce the probing length. The advantage of this method is that experiments can be performed very fast (within minutes) and are label-free. The biomolecules does not need to be labeled with e.g. a fluorescence molecule. Therefore, these measurements can be performed *in situ*.

8

Appendix

8.1 A-1: Timing Error in Potentiostat

For all electrochemical experiments, an 8-channel Bipotentiostat (CHI 1030A) from CH Instruments (Austin, TX, USA) is used. When using two (or more) channels simultaneously and applying a pulse width of 1 ms or lower, would result in a timing error. To test this error, a 1 ms pulse width chronoamperometry step potential between -0.2 V and +0.2 V is applied to a test-configuration. This configuration consists of two 320 ohm resistors with two working (WE), one counter (CE) and one reference electrode (RE) connected as shown in figure 8.1.

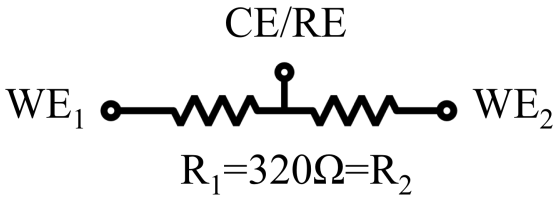

Figure 8.1: Resistor configuration for two working electrodes.

Current vs. time traces given by the poteniostat software as well as the raw current signal

taken from the rear back panel of the potential is recorded with an oscilloscope. Three cases were tested: **A.** 2 electrodes connected with sequential current measurement (black trace); **B.** 2 connected electrodes with simultaneously current measurement (blue trace) and **C.** 1 electrode connected (red trace).

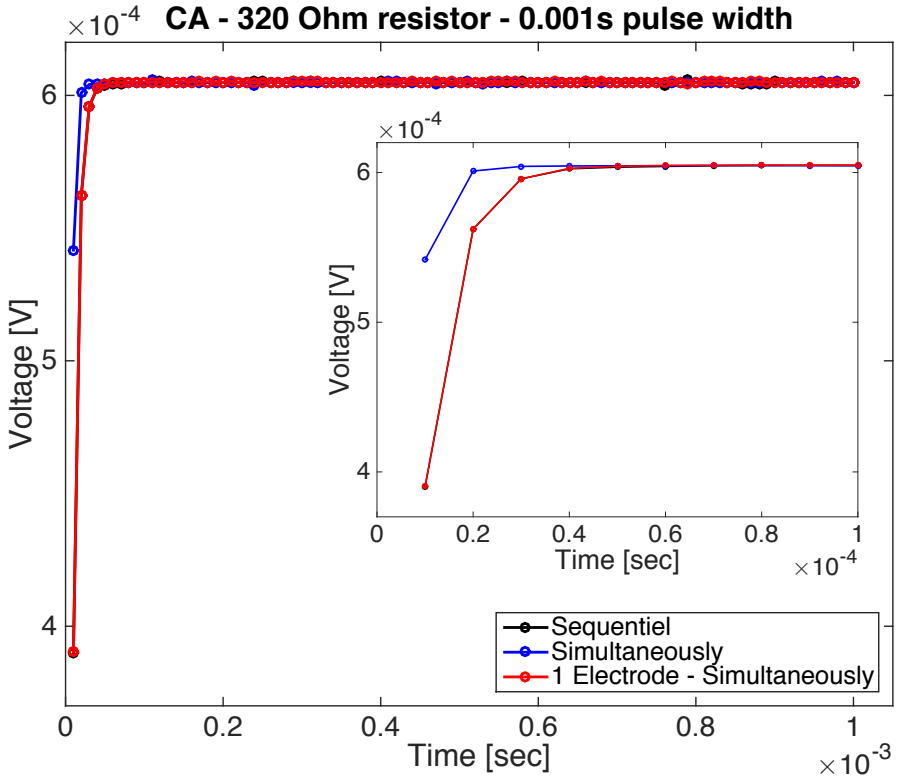

Figure 8.2: Current output from potentiostat software. A 1 ms pulse from -0.2 and 0.2 V is applied to three different configurations.

The current vs. time output from the potentiostat software is plotted in figure 8.2. All three traces have a pulse length of 1 ms. The inset shows a closer look into the first 0.1 ms of the pulse. While the black and red curve are the same, the blue curve has a different

slope and maximum current. The black curve corresponds to case B, where two electrodes are connected and the current is recorded simultaneously.

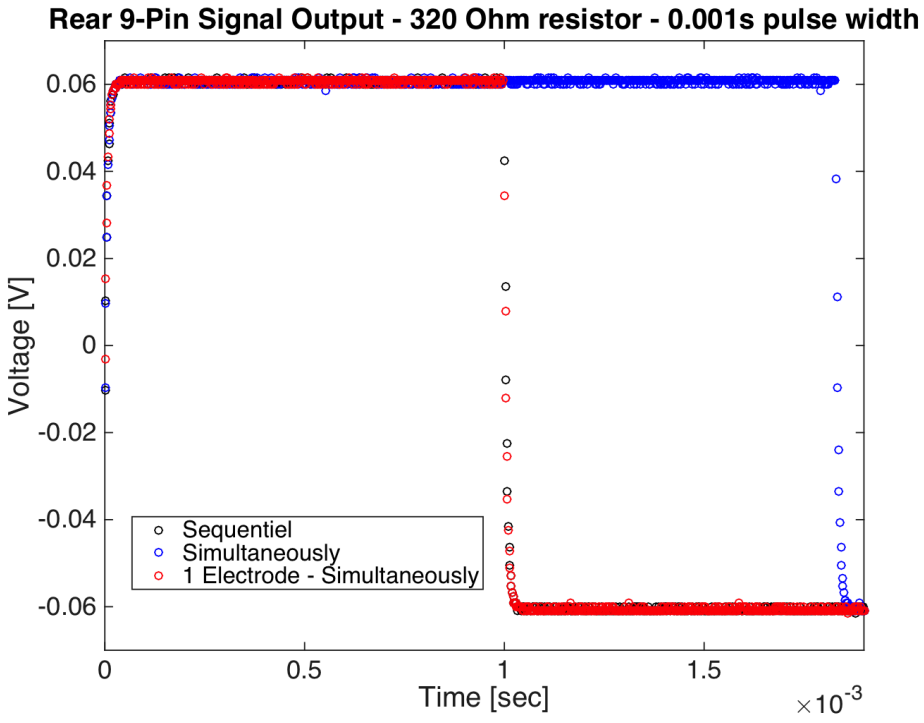

Figure 8.3: Wrong Voltage output from 9-pin connector of potentiostat. A 1 ms pulse from -0.2 and 0.2 V is applied to three different configurations.

The raw voltage signal that is applied to the resistor can be monitored by connecting a potentiostat to the 9-pin rear connector of the potentiostat. The data for case A-C is shown in figure 8.3. Here, we can clearly see that for case B (blue trace), the applied pulse width is around 1.8 times as long as it should be. There was actually a problem in the software, namely if a pulse width of 1 ms or less is applied to two electrodes simultaneously, the software would actually applied a longer pulse and plot the resulting current trace as it would be 1 ms. Therefore, we see a different slope in the software output.

After discussing this error with a technician of CHI Instruments, their were able to replicate this error on their system as well. This meant that this error was probably implemented in all of their systems. Fortunately, once the error was reported a quick resolution was delivered. After a quick software update, this error was fixed. A 1 ms pulse applied to two electrodes simultaneously is shown in figure 8.4. The output was monitored with an oscilloscope as well.

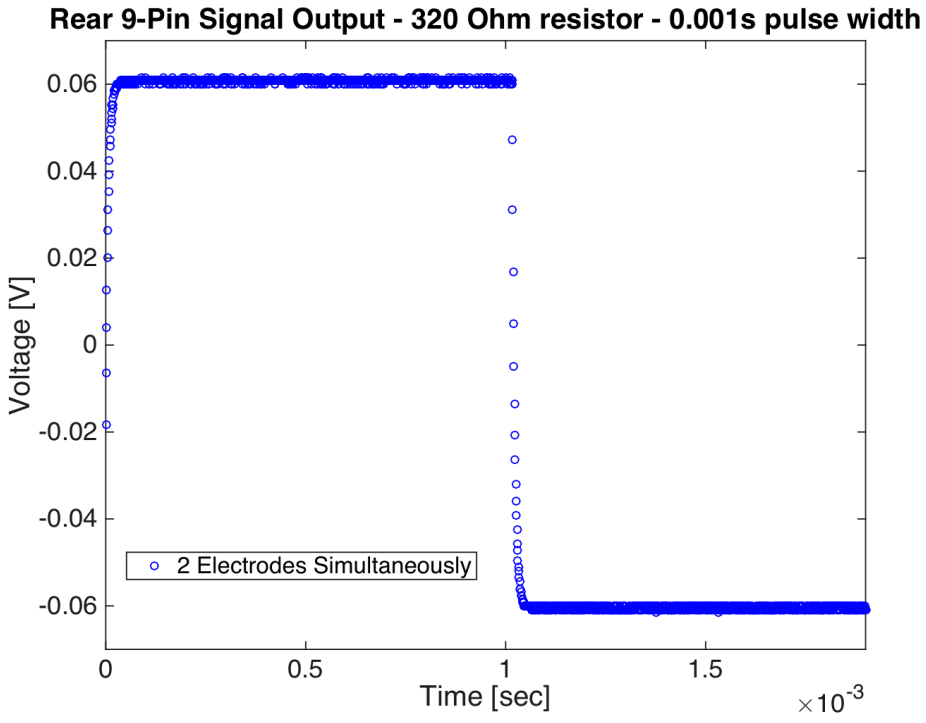

Figure 8.4: Correct Voltage output from 9-pin connector of potentiostat after software update. A 1 ms pulse from -0.2 and 0.2 V is applied to two working electrodes simultaneously.

8.2 A-2: Concentration-Dependent Surface Stress

The correlation of surface stress change of the cantilever as a function of ion concentration is briefly shown here. In figure 8.5 we increased the chloride concentration in our buffer solution Tris HCl 10 mM NaCl (10, 50, 200, 1000 mM). The surface stress response of the cantilever is measured and the applied potential is switched between +200 and -200 mV (vs. Ag/AgCl). The surface stress change amplitude at the switching potential is plotted for each concentration. A Langmuir adsorption curve is fitted to our data. This curve is in line with our findings in chapter 5, that the higher the ion concentration, the larger the surface stress change.

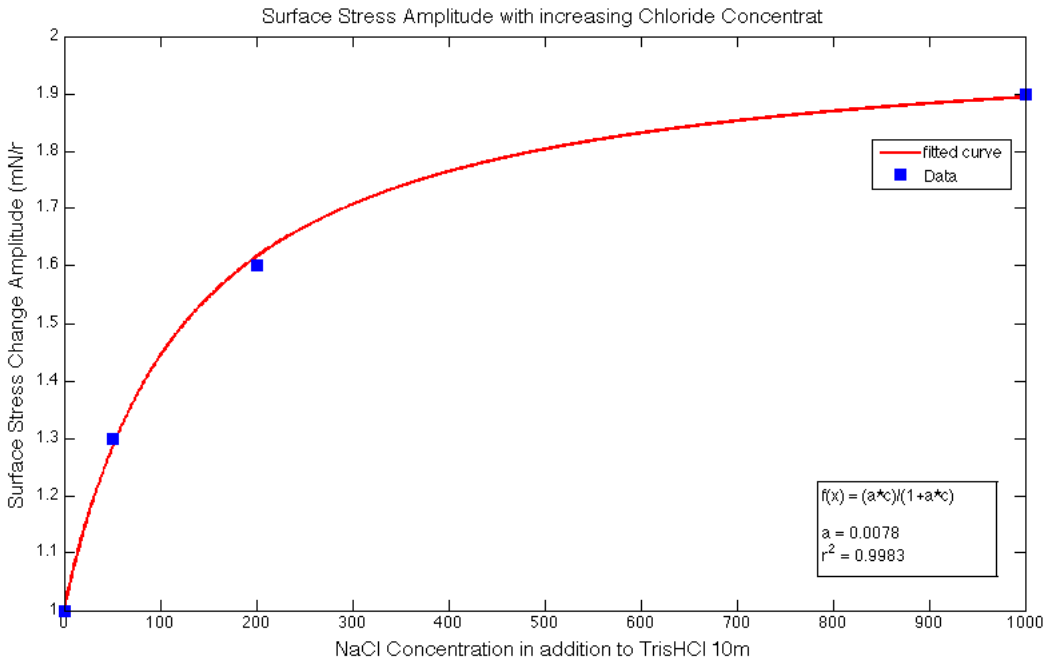

Figure 8.5: Surface stress amplitude for increasing chloride concentration in Tris HCl 10 mM NaCl (10, 50, 200, 1000 mM)

8.3 A-3: Potential-Dependent Surface Stress

The pulse width dependence of the current and surface stress for two different ions has been shown in the previous sections. Next, the potential dependence of the current and stress response is measured. As expected with larger applied potential values, the current as well as the surface stress response increases. For both response and for both ions (perchlorate and chloride), a linear response is observed for potentials between ±0.1 to ± 0.5V.

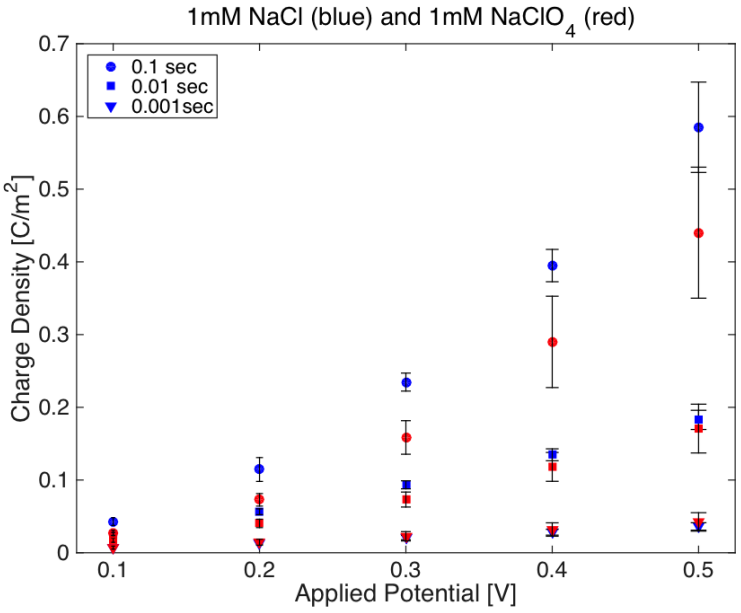

Figure 8.6: Charge density dependence on the applied potential for 1 mM $NaClO_4$ and 1 mM NaCl.

The charge density response is higher for NaCl than for $NaClO_4$ for longer pulses for all tested potentials (figure 8.6). This makes sense, as the charge is proportional to the current ($Q = \int I dt$) and the current is proportional to the voltage ($I = \frac{V}{R}$), therefore the charge is proportional to the applied potential. For shorter potential pulses, the difference between these two ions is not statistically significant anymore. A similar trend is observed for

the surface stress change at increasing applied potentials. However, the difference between $NaClO_4$ and NaCl is more pronounced (figure 8.7). At 0.1 sec (circles), the mean for NaCl shows a two-times increase in surface stress compared to $NaClO_4$ for all potentials. This effect is weakened for shorter pulses until the values for both ions are similar.

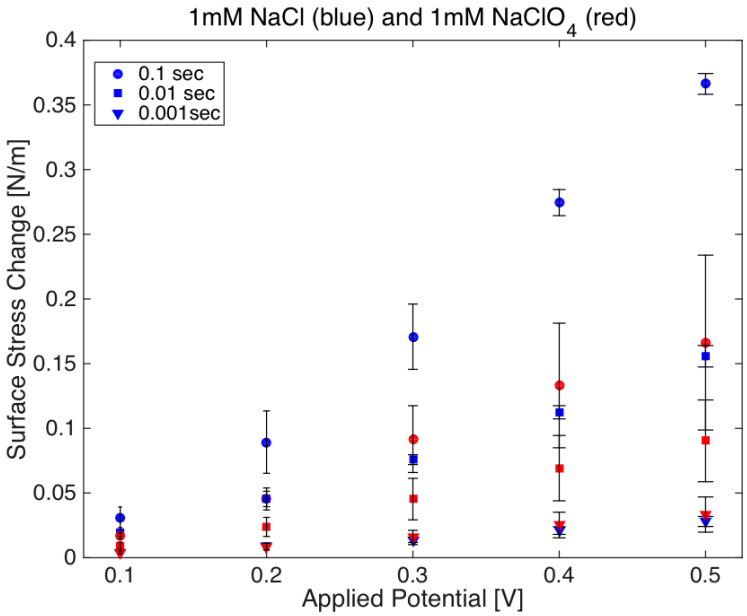

Figure 8.7: Surface stress change dependence on the applied potential for 1 mM $NaClO_4$ and 1 mM NaCl.

Bibliography

[1] Ann-Lauriene Haag, Yoshihiko Nagai, R Bruce Lennox, and Peter Grütter, "Characterization of a gold coated cantilever surface for biosensing applications," EPJ Techniques and Instrumentation **2**, 1–12 (2015).

[2] Axel Warsinke, "Point-of-care testing of proteins," Analytical and Bioanalytical Chemistry **393**, 1393–1405 (2009).

[3] Joseph Wang, "Electrochemical Glucose Biosensors," Chemical Reviews **108**, 814–825 (2008).

[4] D. Grieshaber, R. MacKenzie, J. Voeroes, and E. Reimhult, "Electrochemical biosensors-Sensor principles and architectures," Sensors **8**, 1440–168 (2008).

[5] Michael Seidel and Reinhard Niessner, "Automated analytical microarrays: a critical review," Analytical and Bioanalytical Chemistry **391**, 1521–1544 (2008).

[6] Paul D'Orazio, "Biosensors in clinical chemistry - 2011 update," Clinica Chimica Acta **412**, 1749–1761 (2011).

[7] Celine I.L. Justino, Teresa A. Rocha-Santos, Armando C. Duarte, and Teresa A. Rocha-Santos, "Review of analytical figures of merit of sensors and biosensors in clinical applications," TrAC Trends in Analytical Chemistry **29**, 1172–1183 (2010).

[8] Onur Tigli and Sukru U. Senveli, "Biosensors in the small scale: methods and technology trends," IET Nanobiotechnology **7**, 7–21 (2013).

[9] Michael a. Cullinan, Robert M. Panas, Christopher M. DiBiasio, and Martin L. Culpepper, "Scaling electromechanical sensors down to the nanoscale," Sensors and Actuators A: Physical **187**, 162–173 (2012).

[10] JL Arlett, E B Myers, and M L Roukes, "Comparative advantages of mechanical biosensors." Nature nanotechnology **6**, 203–15 (2011).

[11] Thomas Michels and Ivo W. Rangelow, "Review of scanning probe micromachining and its applications within nanoscience," Microelectronic Engineering **126**, 191–203 (2014).

[12] Simin Mehrabani, Ashley Maker, and Andrea Armani, "Hybrid Integrated Label-Free Chemical and Biological Sensors," Sensors **14**, 5890–5928 (2014).

[13] Javier Tamayo, Priscila M Kosaka, José J Ruz, Álvaro San Paulo, and Montserrat Calleja, "Biosensors based on nanomechanical systems," Chem. Soc. Rev. **42**, 1287–1311 (2013).

[14] Philip S Waggoner and Harold G Craighead, "Micro- and nanomechanical sensors for environmental, chemical, and biological detection," Lab on a Chip **7**, 1238 (2007).

[15] Jürgen Fritz, "Cantilever biosensors." The Analyst **133**, 855–63 (2008).

[16] Thomas Braun, MK Ghatkesar, and Natalija Backmann, "quantitative time-resolved measurement of membrane protein - ligand interactions using microcantilever array sensors," Nature nanotechnology **4**, 179–185 (2009).

[17] Hans Peter Lang, Martin Hegner, and Christoph Gerber, "Cantilever array sensors," Materials Today **8**, 30–36 (2005).

[18] Michel Godin, Vincent Tabard-Cossa, Peter Grutter, and Peter Williams, "Quantitative surface stress measurements using a microcantilever," Applied Physics Letters **79**, 551 (2001).

[19] Nickolay V. Lavrik, Michael J. Sepaniak, and Panos G. Datskos, "Cantilever transducers as a platform for chemical and biological sensors," Review of Scientific Instruments **75**, 2229–2253 (2004).

[20] M S Hanay, S Kelber, a K Naik, D Chi, S Hentz, E C Bullard, E Colinet, L Duraffourg, and ML Roukes, "Single-protein nanomechanical mass spectrometry in real time." Nature nanotechnology **7**, 602–8 (2012).

[21] Oleksiy Svitelskiy, Vince Sauer, Douglass Vick, Kar-Mun Cheng, Ning Liu, Mark R. Freeman, and Wayne K. Hiebert, "Nanoelectromechanical devices in a fluidic environment," Physical Review E **85**, 056313 (2012).

[22] Lu Ding, Christophe Baker, Pascale Senellart, Aristide Lemaitre, Sara Ducci, Giuseppe Leo, and Ivan Favero, "High Frequency GaAs Nano-Optomechanical Disk Resonator," Physical Review Letters **105**, 263903 (2010).

[23] Yi Wen Hu, Yun Feng Xiao, Yong Chun Liu, and Qihuang Gong, "Optomechanical sensing with on-chip microcavities," Frontiers of Physics **8**, 475–490 (2013).

[24] Rüdiger Berger, Emmanuel Delamarche, Hans Peter Lang, Christoph Gerber, James K Gimzewski, and Ernst Meyer, "Surface Stress in the Self-Assembly of Alkanethiols on Gold," Science **276**, 2021–2024 (1997).

[25] Michel Godin, Vincent Tabard-Cossa, Yoichi Miyahara, Tanya Monga, P J Williams, L Y Beaulieu, R Bruce Lennox, and Peter Grutter, "Cantilever-based sensing: the origin of surface stress and optimization strategies." Nanotechnology **21**, 75501 (2010).

[26] G. Y. Chen, T. Thundat, E. A. Wachter, and R. J. Warmack, "Adsorption-induced surface stress and its effects on resonance frequency of microcantilevers," Journal of Applied Physics **77**, 3618–3622 (1995).

[27] D. Ramos, J. Tamayo, J. Mertens, M. Calleja, and A. Zaballos, "Origin of the response of nanomechanical resonators to bacteria adsorption," Journal of Applied Physics **100**, 2004–2007 (2006).

[28] Shengbo Sang, Yuan Zhao, Wendong Zhang, Pengwei Li, Jie Hu, and Gang Li, "Surface stress-based biosensors," Biosensors and Bioelectronics **51**, 124–135 (2014).

[29] Yang-Li Yang, Min-Chieh Chuang, Shyh-Liang Lou, and Joseph Wang, "Thick-film textile-based amperometric sensors and biosensors." The Analyst **135**, 1230–4 (2010).

[30] A. Gupta, D. Akin, and R. Bashir, "Single virus particle mass detection using microresonators with nanoscale thickness," Applied Physics Letters **84**, 1976–1978 (2004).

[31] Kidong Park, Larry J Millet, Namjung Kim, Huan Li, Xiaozhong Jin, Gabriel Popescu, N R Aluru, K Jimmy Hsia, and Rashid Bashir, "Measurement of adherent cell mass and growth," Proceedings of the National Academy of Sciences **107**, 20691–20696 (2010).

[32] K Jensen, Kwanpyo Kim, and a Zettl, "An atomic-resolution nanomechanical mass sensor." Nature nanotechnology **3**, 533–7 (2008).

[33] G. Binnig and C. F. Quate, "Atomic Force Microscope," Physical Review Letters **56**, 930–933 (1986).

[34] Christiane Ziegler, "Cantilever-based biosensors," Analytical and Bioanalytical Chemistry **379**, 946–959 (2004).

[35] Blake N. Johnson and Raj Mutharasan, "Biosensing using dynamic-mode cantilever sensors: A review," Biosensors and Bioelectronics **32**, 1–18 (2012).

[36] L. A. Pinnaduwage, "A microsensor for trinitrotoluene vapour," Nature **425**, 2003–2003 (2003).

[37] Rodolphe Marie, Henriette Jensenius, Jacob Thaysen, Claus B Christensen, and Anja Boisen, "Adsorption kinetics and mechanical properties of thiol-modified DNA-oligos on gold investigated by microcantilever sensors," Ultramicroscopy **91**, 29–36 (2002).

[38] Hui Hou, Xiaojing Bai, Chunyan Xing, Baoping Lu, Jinhui Hao, Xi Ke, Ningyu Gu, Bailin Zhang, and Jilin Tang, "Label-free detection of single-stranded DNA binding protein based on a cantilever array." Talanta **109**, 173–6 (2013).

[39] Jeanne C Stachowiak, Min Yue, Kenneth Castelino, Arup Chakraborty, and Arun Majumdar, "Chemomechanics of Surface Stresses Induced by DNA Hybridization," Langmuir **22**, 263–268 (2006).

[40] KM Hansen, HF Ji, Guanghua Wu, Ram Datar, Richard Cote, Arunava Majumdar, and Thomas Thundat, "Cantilever-based optical deflection assay for discrimination of DNA single-nucleotide mismatches," Analytical Chemistry **73**, 1567–1571 (2001).

[41] M. Álvarez, L G Carrascosa, M Moreno, A Calle, Á. Zaballos, L M Lechuga, C Martínez-A, and J Tamayo, "Nanomechanics of the Formation of DNA Self-Assembled Monolayers and Hybridization on Microcantilevers," Langmuir **20**, 9663–9668 (2004).

[42] Yoshihiko Nagai, Jorge Dulanto Carbajal, John H White, Robert Sladek, Peter Grutter, and R Bruce Lennox, "An Electrochemically Controlled Microcantilever Biosensor," Langmuir **29**, 9951–9957 (2013).

[43] Audrey Sassolas, Béatrice D. Leca-Bouvier, and Loïc J. Blum, "DNA Biosensors and Microarrays," Chemical Reviews **108**, 109–139 (2008).

[44] Johann Mertens, Celia Rogero, Montserrat Calleja, Daniel Ramos, Jose Angel Martín-Gago, Carlos Briones, and Javier Tamayo, "Label-free detection of DNA hybridization based on hydration-induced tension in nucleic acid films," Nature Nanotechnology **3**, 301–307 (2008).

[45] Di Li, Shiping Song, and Chunhai Fan, "Target-Responsive Structural Switching for Nucleic Acid-Based Sensors," Accounts of Chemical Research **43**, 631–641 (2010).

[46] Jeong Hoon Lee, Kyo Seon Hwang, Jaebum Park, Ki Hyun Yoon, Dae Sung Yoon, and Tae Song Kim, "Immunoassay of prostate-specific antigen (PSA) using resonant frequency shift of piezoelectric nanomechanical microcantilever," Biosensors and Bioelectronics **20**, 2157–2162 (2005).

[47] Rupa Mukhopadhyay, Vadim V. Sumbayev, Martin Lorentzen, Jørgen Kjems, Peter A. Andreasen, and Flemming Besenbacher, "Cantilever sensor for nanomechanical detection of specific protein conformations," Nano Letters **5**, 2385–2388 (2005).

[48] Y Arntz, J D Seelig, H P Lang, J Zhang, P Hunziker, J P Ramseyer, E Meyer, M Hegner, and Ch Gerber, "Label-free protein assay based on a nanomechanical cantilever array," Nanotechnology **14**, 86–90 (2002).

[49] Gossett a. Campbell, Marjorie B. Medina, and Raj Mutharasan, "Detection of Staphy-

lococcus enterotoxin B at picogram levels using piezoelectric-excited millimeter-sized cantilever sensors," Sensors and Actuators, B: Chemical **126**, 354–360 (2007).

[50] Thomas Braun, Natalija Backmann, Manuel Vögtli, Alexander Bietsch, Andreas Engel, Hans-Peter Lang, Christoph Gerber, and Martin Hegner, "Conformational Change of Bacteriorhodopsin Quantitatively Monitored by Microcantilever Sensors," Biophysical Journal **90**, 2970–2977 (2006).

[51] Niall Maloney, Gyongyi Lukacs, Jason Jensen, and Martin Hegner, "Nanomechanical sensors for single microbial cell growth monitoring." Nanoscale **6**, 8242–9 (2014).

[52] Luke Johnson, Amit K. Gupta, Azam Ghafoor, Demir Akin, and Rashid Bashir, "Characterization of vaccinia virus particles using microscale silicon cantilever resonators and atomic force microscopy," Sensors and Actuators, B: Chemical **115**, 189–197 (2006).

[53] Harald Ibach, "The role of surface stress in reconstruction, epitaxial growth and stabilization of mesoscopic structures," Surface Science Reports **29**, 195–263 (1997).

[54] H. Ibach, "Adsorbate-induced surface stress," Journal of Vacuum Science & Technology A: Vacuum, Surfaces, and Films **12**, 2240 (1994).

[55] W Haiss, "Surface stress of clean and adsorbate-covered solids," Reports on Progress in Physics **64**, 591–648 (2001).

[56] J.R. Casanova-Moreno and D. Bizzotto, "Frequency response analysis of potential-modulated orientation changes of a DNA self assembled layer using spatially resolved fluorescence measurements." Electrochimica Acta (2014), 10.1016/j.electacta.2014.09.037.

[57] Shana O. Kelley, Jacqueline K. Barton, Nicole M. Jackson, Lee D. McPherson, Aaron B. Potter, Eileen M. Spain, Michael J. Allen, and Michael G. Hill, "Orienting DNA helices on gold using applied electric fields," Langmuir **14**, 6781–6784 (1998).

[58] Laurent Libioulle, Alexander Bietsch, Heinz Schmid, Bruno Michel, and Emmanuel Delamarche, "Contact-Inking Stamps for Microcontact Printing of Alkanethiols on Gold," Langmuir **15**, 300–304 (1999).

[59] S Salomon, T Leïchlé, D Dezest, F Seichepine, S Guillon, C Thibault, C Vieu, and L Nicu, "Arrays of nanoelectromechanical biosensors functionalized by microcontact printing," Nanotechnology **23**, 495501 (2012).

[60] Hua Zhang, Ki-Bum Lee, Zhi Li, and Chad a Mirkin, "Biofunctionalized nanoarrays of inorganic structures prepared by dip-pen nanolithography," Nanotechnology **14**, 1113–1117 (2003).

[61] Alexander Bietsch, Jiayun Zhang, Martin Hegner, Hans Peter Lang, and Christoph Gerber, "Rapid functionalization of cantilever array sensors by inkjet printing," Nanotechnology **15**, 873–880 (2004).

[62] Didier Falconnet, Gabor Csucs, H. Michelle Grandin, and Marcus Textor, "Surface engineering approaches to micropattern surfaces for cell-based assays," Biomaterials **27**, 3044–3063 (2006).

[63] Ulrich Rant, Kenji Arinaga, Shozo Fujita, Naoki Yokoyama, Gerhard Abstreiter, and Marc Tornow, "Dynamic Electrical Switching of DNA Layers on a Metal Surface," Nano Letters **4**, 2441–2445 (2004).

[64] A W Peterson, R J Heaton, and R M Georgiadis, "The effect of surface probe density on DNA hybridization." Nucleic acids research **29**, 5163–5168 (2001).

[65] AJ Bard and LR Faulkner, *Electrochemical Methods - Fundamentals and Applications*, 2nd ed. (John Wiley & Sons, Inc., New York, USA, 2001).

[66] H. Helmholtz, "Ueber einige Gesetze der Vertheilung elektrischer Stroeme in koerperlichen Leitern mit Anwendung auf die thierisch-elektrischen Versuche," in *Annalen der Physik*, Vol. 89 (1853) pp. 211–249.

[67] Otto Stern, "Zur Theorie der Elektrolytischen Doppelschicht," Zeitschrift fur Elektrochemie **30**, 508–516 (1924).

[68] Dominik Kramer, "Dependence of surface stress, surface energy and surface tension on potential and charge," Phys. Chem. Chem. Phys. **10**, 168–177 (2008).

[69] P.R. Couchman and C.R. Davidson, "The Lippmann relation and surface thermodynamics," J. Electroanal. Chem. **85**, 407–409 (1977).

[70] Jacek Lipkowski, Zhichao Shi, Aicheng Chen, Bruno Pettinger, and Christoph Bilger, "Ionic adsorption at the Au(111) electrode," Electrochimica Acta **43**, 2875–2888 (1998).

[71] H. Ibach, Claudia E. Bach, Margret Giesen, and Alexander Grossmann, "Potential-induced stress in the solid-liquid interface: Au(111) and Au(100) in an HClO4 electrolyte," Surface Science **375**, 107–119 (1997).

[72] J Lipkowski, W Schmickler, D.M Kolb, and R Parsons, "Comments on the thermodynamics of solid electrodes," Journal of Electroanalytical Chemistry **452**, 193–197 (1998).

[73] G. G. Stoney, "The Tension of Metallic Films Deposited by Electrolysis," Proceedings of the Royal Society A: Mathematical, Physical and Engineering Sciences **82**, 172–175 (1909).

[74] Ulrich Rant, Kenji Arinaga, Simon Scherer, Erika Pringsheim, Shozo Fujita, Naoki Yokoyama, Marc Tornow, and Gerhard Abstreiter, "Switchable DNA interfaces for the highly sensitive detection of label-free DNA targets." Proceedings of the National Academy of Sciences of the United States of America **104**, 17364–9 (2007).

[75] Ulrich Rant, Kenji Arinaga, Shozo Fujita, Naoki Yokoyama, Gerhard Abstreiter, and Marc Tornow, "Electrical manipulation of oligonucleotides grafted to charged surfaces," Organic & Biomolecular Chemistry **4**, 3448 (2006).

[76] Wolfgang Kaiser and Ulrich Rant, "Conformations of end-tethered DNA molecules on gold surfaces: Influences of applied electric potential, electrolyte screening, and temperature," Journal of the American Chemical Society **132**, 7935–7945 (2010).

[77] Joseph C Genereux and Jacqueline K Barton, "Mechanisms for DNA charge transport." Chemical reviews **110**, 1642–62 (2010).

[78] Joseph C Genereux, Amie K Boal, and Jacqueline K Barton, "DNA-mediated charge transport in redox sensing and signaling." Journal of the American Chemical Society **132**, 891–905 (2010).

[79] Alon A Gorodetsky, Marisa C Buzzeo, and Jacqueline K Barton, "DNA-Mediated Electrochemistry," Bioconjugate Chemistry **19**, 2285–2296 (2008).

[80] "Oligonucleotide. online; accessed on april 3rd, 2016," .

[81] Kara Weber, Lisa Hockett, and Stephen Creager, "Long-Range Electronic Coupling between Ferrocene and Gold in Alkanethiolate-based Monolayers on Electrodes," The Journal of Physical Chemistry B **101**, 8286–8291 (1997).

[82] James P. Collman, Ali Hosseini, Todd a. Eberspacher, and Christopher E D Chidsey, "Selective anodic desorption for assembly of different thiol monolayers on the individual electrodes of an array," Langmuir **25**, 6517–6521 (2009).

[83] Lana L. Norman and Antonella Badia, "Microcantilevers Modified with Ferrocene-Terminated Self-Assembled Monolayers: Effect of Molecular Structure and Electrolyte Anion on the Redox-Induced Surface Stress," The Journal of Physical Chemistry C **115**, 1985–1995 (2011).

[84] Rochus Breuer and Michael Schmittel, "Redox-stable SAMs in water (pH 0-12) from 1,1'-biferrocenylene- terminated thiols on gold," Organometallics **31**, 6642–6651 (2012).

[85] Yasuyuki Yokota, Yoshitada Mino, Yuta Kanai, Toru Utsunomiya, Akihito Imanishi, Matthäus A. Wolak, Rudy Schlaf, and Ken-ichi Fukui, "Comparative Studies of Photoelectron Spectroscopy and Voltammetry of Ferrocene-Terminated Self-Assembled Monolayers Possessing Different Electron-Donating Abilities," The Journal of Physical Chemistry C **118**, 10936–10943 (2014).

[86] Y T Yang, C Callegari, X L Feng, K L Ekinci, and M L Roukes, "Zeptogram-scale nanomechanical mass sensing." Nano letters **6**, 583–6 (2006).

[87] Anja Boisen and Thomas Thundat, "Design & fabrication of cantilever array biosensors," Materials Today **12**, 32–38 (2009).

[88] V Tabard-Cossa, Michel Godin, Ian J. Burgess, Tanya Monga, R. Bruce Lennox, and Peter Grütter, "Microcantilever-Based Sensors : Effect of Morphology, Adhesion, and Cleanliness of the Sensing Surface on Surface Stress," Analytical Chemistry **79**, 8136–8143 (2007).

[89] Wolfgang Haiss, Richard J. Nichols, K Sass, Klaus P. Charle, Jürgen K. Sass, and Klaus P. Charle, "Linear correlation between surface stress and surface charge in anion adsorption on Au(111)," Journal of Electroanalytical Chemistry **452**, 199–202 (1998).

[90] L Y Beaulieu, Michel Godin, Olivier Laroche, Vincent Tabard-Cossa, and Peter Grütter, "A complete analysis of the laser beam deflection systems used in cantilever-based systems." Ultramicroscopy **107**, 422–30 (2007).

[91] L. Y. Beaulieu, Michel Godin, Olivier Laroche, Vincent Tabard-Cossa, and Peter Grutter, "Calibrating laser beam deflection systems for use in atomic force microscopes and cantilever sensors," Applied Physics Letters **88**, 083108 (2006).

[92] Lee M. Fischer, Maria Tenje, Arto R. Heiskanen, Noriyuki Masuda, Jaime Castillo, Anders Bentien, Jenny Émneus, Mogens H. Jakobsen, and Anja Boisen, "Gold cleaning methods for electrochemical detection applications," Microelectronic Engineering **86**, 1282–1285 (2009).

[93] Lawrence Yoon Suk Lee and R Bruce Lennox, "Electrochemical Desorption of n -Alkylthiol SAMs on Polycrystalline Gold: Studies Using A Ferrocenylalkylthiol Probe," Langmuir **23**, 292–296 (2007).

[94] A B Steel, T M Herne, and M J Tarlov, "Electrochemical quantitation of DNA immobilized on gold." Analytical chemistry **70**, 4670–7 (1998).

[95] L M Demers, D S Ginger, S.-J. Park, Z. Li, S.-W. Chung, and Mirkin. C A, "Direct Patterning of Modified Oligonucleotides on Metals and Insulators by Dip-Pen Nanolithography," Science **296**, 1836–1838 (2002).

[96] Fuyuan Ma and RB Lennox, "Potential-assisted deposition of alkanethiols on Au: Con-

trolled preparation of single-and mixed-component SAMs," Langmuir **16**, 6188–6190 (2000).

[97] Christopher M. A. Brett, Slavoj Kresak, Tibor Hianik, and Ana Maria Oliveira Brett, "Studies on Self-Assembled Alkanethiol Monolayers Formed at Applied Potential on Polycrystalline Gold Electrodes," Electroanalysis **15**, 557–565 (2003).

[98] Ž Petrović, M. Metikoš-Huković, and R. Babić, "Potential-assisted assembly of 1-dodecanethiol on polycrystalline gold," Journal of Electroanalytical Chemistry **623**, 54–60 (2008).

[99] Rita Meunier-Prest, Guillaume Legay, Suzanne Raveau, Nicolas Chiffot, and Eric Finot, "Potential-assisted deposition of mixed alkanethiol self-assembled monolayers," Electrochimica Acta **55**, 2712–2720 (2010).

[100] Rihab Sahli, Claire Fave, Noureddine Raouafi, Khaled Boujlel, Bernd Schöllhorn, and Benoiît Limoges, "Switching on/off the chemisorption of thioctic-based self-assembled monolayers on gold by applying a moderate cathodic/anodic potential," Langmuir **29**, 5360–5368 (2013).

[101] Woon Kie Paik, Seunghun Eu, Kanghee Lee, Seungwhan Chon, and Minsok Kim, "Electrochemical reactions in adsorption of organosulfur molecules on gold and silver: Potential dependent adsorption," Langmuir **16**, 10198–10205 (2000).

[102] Seungwhan Chon and Woon-kie Paik, "Adsorption of self-assembling sulfur compounds through electrochemical reactions: Effects of potential, acid and oxidizing agents," Physical Chemistry Chemical Physics **3**, 3405–3410 (2001).

[103] Chuan-Jian Zhong and Marc D Porter, "Fine structure in the voltammetric desorption

curves of alkanethiolate monolayers chemisorbed at gold," Journal of Electroanalytical Chemistry **425**, 147–153 (1997).

[104] Chuan-Jian Zhong, Jerzy Zak, and Marc D. Porter, "Voltammetric reductive desorption characteristics of alkanethiolate monolayers at single crystal Au(111) and (110) electrode surfaces," Journal of Electroanalytical Chemistry **421**, 9–13 (1997).

[105] Toshikazu Kawaguchi, Hiroaki Yasuda, Katsuaki Shimazu, and Marc D. Porter, "Electrochemical quartz crystal microbalance investigation of the reductive desorption of self-assembled monolayers of alkanethiols and mercaptoalkanoic acids on Au," Langmuir **16**, 9830–9840 (2000).

[106] Jeff L. Shepherd, Arnold Kell, Emily Chung, Chad W. Sinclar, Mark S. Workentin, and Dan Bizzotto, "Selective Reductive Desorption of a SAM-Coated Gold Electrode Revealed Using Fluorescence Microscopy," Journal of the American Chemical Society **126**, 8329–8335 (2004).

[107] Eugene H J Wong, Georgia L. May, and C. Paul Wilde, "Oxidative desorption of thiols as a route to controlled formation of binary self assembled monolayer surfaces," Electrochimica Acta **109**, 67–74 (2013).

[108] Rebecca Y. Lai, Sang Ho Lee, H. T. Soh, Kevin W. Plaxco, and Alan J. Heeger, "Differential labeling of closely spaced biosensor electrodes via electrochemical lithography," Langmuir **22**, 1932–1936 (2006).

[109] Francesco Ricci, Rebecca Y Lai, Alan J Heeger, Kevin W Plaxco, and James J Sumner, "Effect of Molecular Crowding on the Response of an Electrochemical DNA Sensor," Langmuir **23**, 6827–6834 (2007).

[110] Kristin B. Cederquist and Christine D. Keating, "Hybridization efficiency of molecular beacons bound to gold nanowires: Effect of surface coverage and target length," Langmuir **26**, 18273–18280 (2010).

[111] Kenneth Castelino, Balaji Kannan, and Arun Majumdar, "Characterization of grafting density and binding efficiency of DNA and proteins on gold surfaces," Langmuir **21**, 1956–1961 (2005).

[112] Chimica Fisica, Universith Milano, and Petrii O. A. Trasatti, S., "Real Surface Area Measurements in Electrochemistry," Pure and Applied Chemistry **63**, 711–734 (1991).

[113] Christopher E D Chidsey, Carolyn R Bertozzi, T M Putvinski, and a M Mujsce, "Coadsorption of ferrocene-terminated and unsubstituted alkanethiols on gold: electroactive self-assembled monolayers," Journal of the American Chemical Society **112**, 4301–4306 (1990).

[114] Gary K. Rowe, Michael T. Carter, John N. Richardson, and Royce W. Murray, "Consequences of Kinetic Dispersion on the Electrochemistry of an Adsorbed Redox-Active Monolayer," Langmuir **11**, 1797–1806 (1995).

[115] Ilwhan Oh, Joohong Kye, and Seongpil Hwang, "In situ real time electrochemical measurement of kinetics of thiol adsorption on gold using microelectrode," International Journal of Electrochemical Science **6**, 5125–5133 (2011).

[116] H. Ibach, "Stress in densely packed adsorbate layers and stress at the solid-liquid interface - is the stress due to repulsive interactions between the adsorbed species?" Electrochimica Acta **45**, 575–581 (1999).

[117] Yoshitaka Umeno, Christian Elsässer, Bernd Meyer, Peter Gumbsch, M Nothacker,

Jörg Weissmüller, and F Evers, "Ab initio study of surface stress response to charging," Europhysics Letters (EPL) **78**, 13001 (2007), arXiv:0702441 [cond-mat] .

[118] R. N. Viswanath, D. Kramer, and J. Weissmüller, "Variation of the surface stress-charge coefficient of platinum with electrolyte concentration," Langmuir **21**, 4604–4609 (2005).

[119] R. N. Viswanath, D. Kramer, and J. Weissmüller, "Adsorbate effects on the surface stress-charge response of platinum electrodes," Electrochimica Acta **53**, 2757–2767 (2008).

[120] J Weissmüller, R N Viswanath, D Kramer, P Zimmer, R Würschum, and H Gleiter, "Charge-induced reversible strain in a metal," Science **300**, 312–315 (2003).

[121] C. Friesen, N. Dimitrov, R. C. Cammarata, and K. Sieradzki, "Surface stress and electrocapillarity of solid electrodes," Langmuir **17**, 807–815 (2001).

[122] Qibo Deng, Daniel-Hendrik Gosslar, Maxim Smetanin, and Jörg Weissmüller, "Electrocapillary coupling at rough surfaces," Phys. Chem. Chem. Phys. **17**, 11725–11731 (2015).

[123] Qibo Deng and Jorg Weissmuller, "Electrocapillary coupling during electrosorption," Langmuir **30**, 10522–10530 (2014).

[124] R Morrow, D R McKenzie, and M M M Bilek, "The time-dependent development of electric double-layers in saline solutions," Journal of Physics D: Applied Physics **39**, 937–943 (2006).

[125] R. Morrow and D. R. McKenzie, "The time-dependent development of electric double-layers in pure water at metal electrodes: the effect of an applied voltage on the local

pH," Proceedings of the Royal Society A: Mathematical, Physical and Engineering Sciences **468**, 18–34 (2012).

[126] R Morrow and N Sato, "The discharge current induced by the motion of charged particles in time-dependent electric fields; Sato's equation extended," Journal of Physics D: Applied Physics **32**, L20–L22 (1999).

[127] W R Fawcett, "Charge distribution effects in the solution chemistry of polyatomic ions," Condensed Matter Physics **8**, 413–424 (2005).

[128] William M. Haynes, *Handbook of Chemistry and Physics*, 96th ed., edited by William M. Haynes (Crc Press Llc, 2015) pp. 5–77.

[129] Aleksandar Vacic, Jason M Criscione, Nitin K Rajan, Eric Stern, Tarek M Fahmy, and Mark a Reed, "Determination of Molecular Configuration by Debye Length Modulation," Journal of the American Chemical Society **133**, 13886–13889 (2011).

[130] TM Herne and MJ Tarlov, "Characterization of DNA probes immobilized on gold surfaces," Journal of the American Chemical Society **7863**, 8916–8920 (1997).

[131] Muslum Ilgu and Marit Nilsen-Hamilton, "Aptamers in analytics," The Analyst **141**, 1551–1568 (2016).

[132] Arica A. Lubin and Kevin W. Plaxco, "Folding-Based Electrochemical Biosensors: The Case for Responsive Nucleic Acid Architectures," Accounts of Chemical Research **43**, 496–505 (2010).

[133] R A Sperling and W J Parak, "Surface modification, functionalization and bioconjugation of colloidal inorganic nanoparticles," Philosophical Transactions of the Royal Society A: Mathematical, Physical and Engineering Sciences **368**, 1333–1383 (2010).

[134] H Grönbeck, Alessandro Curioni, and Wanda Andreoni, "Thiols and disulfides on the Au (111) surface: The headgroup-gold interaction," Journal of the American ... , 3839–3842 (2000).

[135] Boyang Hu and Guohua Tao, "Molecular dynamics simulations on lithium diffusion in LiFePO 4 : the effect of anti-site defects," J. Mater. Chem. A **3**, 20399–20407 (2015).

[136] Aleksandar Vacic, Jason M. Criscione, Nitin K. Rajan, Eric Stern, Tarek M. Fahmy, and Mark A. Reed, "Determination of molecular configuration by debye length modulation," Journal of the American Chemical Society **133**, 13886–13889 (2011).

[137] Andrew T. Catherine, Stephanie N. Shishido, Gregg A. Robbins-Welty, and Amy Diegelman-Parente, "Rational design of a structure-switching DNA aptamer for potassium ions," FEBS Open Bio **4**, 788–795 (2014).